ENGINEERING DESIGN AND MATHEMATICAL SIMULATION OF MECHANO-INSTRUCTIVE COLLAGEN SCAFFOLDS FOR TREATMENT OF DIFFICULT-TO-HEAL WOUNDS

by

David Oleh Sohutskay

A Dissertation

Submitted to the Faculty of Purdue University

In Partial Fulfillment of the Requirements for the degree of

Doctor of Philosophy

Weldon School of Biomedical Engineering

West Lafayette, Indiana

May 2021

THE PURDUE UNIVERSITY GRADUATE SCHOOL
STATEMENT OF COMMITTEE APPROVAL

Dr. Sherry L. Voytik-Harbin, Chair
Weldon School of Biomedical Engineering

Dr. Adrian Buganza Tepole
Department of Mechanical Engineering

Dr. Luis Solorio
Weldon School of Biomedical Engineering

Dr. Dan F. Spandau
Department of Dermatology, Indiana University School of Medicine

Dr. Sunil S. Tholpady
Department of Surgery, Indiana University School of Medicine

Dr. Matthew J. Turner
Department of Dermatology, Indiana University School of Medicine

Approved by:
Dr. Andrew O. Brightman

Dedicated to my family for their support and love over the years, to my friends and colleagues, and to everyone who helped me along the way.

And to a better future through science, mathematics, and medicine.

ACKNOWLEDGMENTS

This work would not have been possible without the broad network of mentors, coworkers, family, and friends. There are many that I would like to thank here. First, I would like to thank my advisor, Dr. Sherry Voytik-Harbin, for her mentorship and guidance during my time at Purdue. Thank you for believing in me and supporting my passion in tissue engineering. I am so thankful to have had the opportunity to work in your lab. From our early morning meetings in MJIS troubleshooting cell culture to the many Zoom meetings throughout the pandemic. Sherry is an inspiration and I have always appreciated our shared interest in collagen, the best protein.

Thanks to Dr. Adrian Buganza Tepole for your mentorship as well. I remember first seeing your seminar as a new faculty member and being amazed by the complexity and accuracy of the models you developed. Your excitement about mathematical modeling and our new collaborations inspired my own. I have appreciated your support throughout the project with theory, coding, and writing. Thank you for giving me the tools to succeed.

Thanks to Dr. Sunil Tholpady; your surgical experience and guidance was invaluable to the development of our animal model. I also appreciate the unique perspective you had on many topics, such as applications of our work, physician needs, and a perspective on the industry and competing technologies. I enjoyed our conversations about research in medicine and your physician-scientist career advice as well.

Thanks to Dr. Luis Solorio for your expertise and excitement regarding bioengineering research. I have enjoyed our conversations about my thesis work and your own work in tissue engineering. You have always provided insightful questions and considerations during my presentations, and I enjoyed working in the next lab over to your students.

Thanks to Dr. Dan Spandau for your helpful biological perspective. Though the project has undergone some changes over the years, I appreciate your help with epithelial cell culture, understanding skin biology, and the analysis of our in vivo results. Your knowledge in biomedical science among my committee of mostly engineers was always appreciated.

Thanks to Dr. Matt Turner for your clinical mentorship. Your perspectives on the medical applications of our work as well as your scientific method suggestions have been very helpful. I appreciate your enthusiasm and willingness to help. I am looking forward to returning to medicine and your continued career advice.

I appreciate the comradery and help from all the members of the Harbin lab, past, present, and future. Your friendship and teamwork helped to make this work a reality. Dr. Catherine Whittington, Dr. Rucha Joshi, Dr. Sarah Brookes, Dr. Kevin Blum, Dr. Clarissa Stephens, Will Hoggatt, Lauren Watkins, Rachel Morrison, Stephanie Thiede, Xiaohong Tan, Evan Surma, John Nicholas, and Ajay Nachiappan. Thanks especially to Dr. Nimisha Bajaj for sharing her enthusiasm for mathematical modeling. To Daniel Romary, Madeline McLaughlin, Mahera Husain, I am looking forward to joining you back at the Indiana University School of Medicine soon. I would like to add special thanks to Dr. Kevin Buno, my fellow Buckeye and partner on the animal wound healing studies. Chapter 3 of this thesis is in equal part your accomplishment. In addition, special thanks to Dr. TJ Puls, who also worked with me on Chapter 2. I also want to thank the undergraduates that have helped contribute to this thesis work, especially Zach Harbin, Muira Fontaine, and Parker Van Emmerick. I hope your time in the Purdue Summer Undergraduate Research Fellowship program and beyond was valuable. You are well on your way to great futures.

No research could be completed without collaborators. Thanks to Dr. Merv Yoder and Dr. Riyi Shi – even though I was unable to have either of you as a thesis advisor I appreciated the rotations I completed in your laboratories. Thanks to the Purdue Weldon School of Biomedical Engineering faculty and staff, Dr. Andrew Brightman, Sandy May, Tammy Siemers, for their support. Thanks to Dr. Taeyoon Kim and Dr. Eric Naumann, whose courses in biomechanics helped to initiate my own interest in collagen biophysics and computational modeling. Thanks to Carol Dowell, Samantha Nier, Melissa Bible, Tina Cleary for their training and assistance in our animal experiments. Thanks to Bill Schonlein, Norvin, Susan Hardy, and Kirk Foster, Asem Aboelzahab, Rucha Joshi, Carla Brady and Pam Lamb.

To the Medical Scientist Training Program students and directors, I will be forever grateful. To Dr. Maureen Harrington and Dr. Raghu Mirmira for believing in me and accepting me to the program, and to the new directors who will be taking their place. Thank you as well to all of the students, especially Freddy Damen, Thao Trinh, Sara Ibrahim, Jennifer Martynowicz, Megan Bernath, and Brian Grice for your friendship over the years. Thanks to Jan and all the other faculty and staff involved in the program, and all members of the Indiana University School of Medicine. The knowledge I gained during the first two years of medical school was immensely helpful during my PhD, and I am looking forward to returning.

Thanks to my undergraduate research advisors Dr. Jessica Winter, Dr. Carlos Castro, Dr. Hooman Sadri-Ardekani, Dr. Anthony Atala, and Dr. Zachary Weil, and all of my professors at Ohio State. Without each of you I would not be where I am today. You taught me the foundations of science.

I would like to thank my funding sources. The Indiana/Purdue Physician/Engineer Training Program which ensured my funding throughout medical and graduate school. Again, to Sherry and Adrian, for supporting my research with their resources. This project was supported by the Indiana Clinical Translational Sciences Institute TL1 Fellowship (NIH CTSI UL1TR002529), Interdisciplinary Bioengineering Training in Diabetes Research Program (NIH NIDDK T32 DK101001), and Indiana Medical Scientist/Engineering Training Program (MSTP; NIGMS T32 GM077229). This work was also supported by the National Science Foundation (NSF CMMI 1911346). Thanks to the Purdue Graduate Student Government and Indiana University School of Medicine for awarding travel grants for the presentation of this work at various conferences, and to the Purdue Biomedship program for the exposure to biomedical entrepreneurship and startups.

Finally, I would like to thank and dedicate this to my parents Joe Sohutskay and Vera Miller, my siblings Nicholas and Alexandra Sohutskay, my grandparents, aunts and uncles, cousins, and all other family and friends. Thanks to Sierra Kneifel for your love and support in finishing this thesis and grad school. I appreciate you so much. Finally, I would like to dedicate this to my grandmother Sofia Sochockyj, who passed away before this work was finished.

TABLE OF CONTENTS

LIST OF TABLES

LIST OF FIGURES

LIST OF ABBREVIATIONS

EDC	1-ethyl-3-(3-dimethylaminopropyl)-carbodiimide hydrochloride
3D	3-dimensional
DAB	3,3'-diaminobenzidine
ADAMTS2	A Disinegrin and Metalloproteinase with Thrombospondin Motifs 2
AGE	Advanced glycation end product
α-SMA	Alpha smooth muscle actin
ASTM	American Society of Testing and Materials
RGD	Arginine-glycine-aspartic acid
AFM	Atomic force microscopy
CD	Cluster of differentiation
CMP	Collagen mimetic peptide
Cryo-SEM	Cryogenic scanning electron microscopy
dECM	Decellularized extracellular matrix
DHT	Dehydrothermal
DNA	Deoxyribonucleic acid
DDR	Discoidin domain receptor
ECM	Extracellular matrix
FGF	Fibroblast growth factor
FDA	Food and Drug Administration
GelMA	Gelatin methacrylate
GAG	Glycosaminoglycan
HHL	Histidinyl-hydroxylysino-norleucine
LAIR1	Leukocyte-associated immunoglobulin-like receptor 1
LOX	Lysyl oxidase
NHS	N-hydroxysuccinimide
OI	Osteogenesis imperfecta
PBS	Phosphate-buffered saline
RAGE	Receptor for advanced glycation end products
rhBMP-2	Recombinant human bone morphogenetic protein

rhCOL	Recombinant human collagen
RNA	Ribonucleic acid
SIS	Small intestine submucosa
TGF-β	Transforming growth factor beta
UV	Ultraviolet
VEGF	Vascular endothelial growth factor

LIST OF SYMBOLS

$\boldsymbol{a}_0$	Principal collagen alignment vector
$\boldsymbol{A}$	Structural tensor
b	Von Mises distribution concentration parameter
c	Cytokine density
$\boldsymbol{C}$	Right Cauchy-Green Deformation Tensor
$\boldsymbol{C}^e$	Elastic Right Cauchy-Green Deformation Tensor
$\boldsymbol{C}^p$	Plastic Right Cauchy-Green Deformation Tensor
$\boldsymbol{D}$	Diffusion coefficient
$\mathcal{D}$	Statistical data
E_t	Tensile modulus
$\boldsymbol{F}$	Deformation gradient
G'	Storage modulus
G''	Loss modulus
I_1	First invariant of the stress tensor
I_2	Second invariant of the stress tensor
I_3	Third invariant of the stress tensor
J	Jacobian of deformation (total volume change)
J^e	Elastic Jacobian (elastic volume change)
J^p	Plastic Jacobian (plastic volume change)
$\mathcal{J}$	Simulated total integrated contraction
$\mathcal{J}^m$	Experimental total integrated contraction
k_0	Linear stiffness
k_f	Collagen fiber stiffness

k_v	Incompressibility parameter
k_2	Collagen fiber nonlinearity
$\boldsymbol{n}_0$	Out-of-plane orthogonal alignment vector
p^m	Probability of fiber alignment
$\boldsymbol{s}_0$	In-plane orthogonal alignment vector
UTS	Ultimate tensile strength
$\boldsymbol{\beta}$	Biochemical parameters
Γ	Boundary (tissue interface or surface)
ϵ	Statistical model error
ε_f	Failure strain
$\boldsymbol{\theta}$	Statistical model parameters
$\boldsymbol{\Theta}$	Local structural parameters
κ	Collagen dispersion
$\boldsymbol{\lambda}$	Principal stretch (eigenvector)
$\boldsymbol{\lambda}^e$	Elastic stretch
$\boldsymbol{\lambda}^p$	Plastic stretch
λ^m	Experimental measured stretch
μ_a	Principle angle
ρ	Cell density
σ^m	Experimental measured stress
$\boldsymbol{\sigma}^{pas}$	Passive Stress
$\boldsymbol{\sigma}^{act}$	**A**ctive Stress
$\boldsymbol{\sigma}^{tot}$	Total stress
φ	Collagen density
φ^m	Measured collagen density

ϕ	Collagen density (normalized)
$\boldsymbol{\Psi}$	Strain energy density
Ω^s	Skin domain
Ω^w	Wound domain

ABSTRACT

Wounds of the skin, especially those that are large and breach multiple tissue layers, remain a major burden to those that they affect as well as our healthcare system. Because these tissue defects supersede the body's natural healing capacity, normal skin anatomy and functional integrity is not restored in an orderly and timely fashion, leading to devastating consequences such as long healing times, pain, infection, scarring, and loss of mobility and function owing to contracture. As a result, there exists a need for better therapies that can rapidly and reliably restore skin cosmesis and function. Given that the collagen extracellular matrix of the dermis is a vital component to skin mechanobiology and wound healing, our skin restoration strategy focused on defining how specific collagen microstructure features contribute to the multi-scale properties and healing response of dermal replacement scaffolds. In this thesis, we first define the history of collagen biomaterials, their biochemistry and biomechanical properties, and engineering techniques for fabrication of scaffolds. We then hypothesize that collagen fibril density and architecture are important design considerations for mechano-instructive dermal regeneration scaffolds. To test this, we used self-assembling type I collagen polymer (oligomer), together with a controlled plastic compression molding technique to create scaffolds with varied microstructural and mechanical features. The dermal replacement scaffolds were then evaluated in full-thickness skin wounds in rats and compared to no-fill control, autograft rat skin, and a commercial collagen dressing. Increasing fibril content of oligomer scaffolds inhibited wound contraction and decreased myofibroblast marker expression. Cellular and vascular infiltration of scaffolds over the 14-day period varied with the graded density and orientation of fibrils. To extend and enhance prototype development and testing we developed a finite element growth model of wound healing, incorporating experimental measures of scaffold structure and mechanical properties and in-vivo healing outcomes. Model constitutive equations were calibrated to our experimental data with a Bayesian fitting. We demonstrated the ability of the model to match experimental findings and create new predictions. A perturbation analysis showed that wound contraction was most sensitive to collagen density and fiber stiffness, suggesting these are important design features of scaffolds. Collectively, these results will forward the multi-scale design and fabrication of mechano-instructive dermal scaffolds that promote skin regeneration while simultaneously reducing wound contraction. This work bridges experimental and computational tools, highlighting the increasing

role of mathematical models in engineered tissue replacement design and their potential to contribute to more personalized wound therapies.

1. INTRODUCTION

1.1 Background and Significance

1.1.1 Problem: Significance and Scope of Cutaneous Wounds

Injuries to the skin are some of the most common medical problems experienced. Loss of skin barrier function can lead to rapid infection, fluid and heat loss, and death. Fortunately, most do not need intervention, but those that do place a high burden on patients and physicians. More than 6.5 million patients in the United States suffer from chronic wounds[1]. In addition, acute injuries such as burns lead to 40,000 hospitalizations and can be lethal due to their size, causing 3,400 deaths each year[2]. A single moderate burn case can cost more than $200,000[3]. Wounds can cause loss of mobility from lower limb amputation or joint contracture. In addition, the cosmetic impacts of cutaneous wounds are unique. Wounds can have a negative effect on quality of life by causing embarrassment or social isolation. Up to 1-2% of the population may experience a chronic wound during their lifetime[4]. Traditionally, wounds are treated on an escalating scale from simple bandaging and antibiotics to surgical skin grafts. A newer alternative is that of biologically-active dermal replacement scaffolds. These scaffolds are constructed using natural or synthetic biomaterials and have emerged as FDA-approved therapies for difficult-to-heal wounds that have failed standard therapy[5, 6]. Although these products have gained traction in a large market, they are still limited by poor mechanical properties, susceptibility to proteases, and poor biocompatibility due to the use of exogenous crosslinkers. Because of this, most treatments take multiple applications and many weeks to be effective in closing a wound. The development of a low-cost, effective therapy for difficult-to-heal wounds has great potential in reducing severe consequences of wounds such as serious infections, amputations, scarring, and death. In this following section, we provide a brief review of cutaneous injury and the role of engineered skin substitutes in therapy.

Wounds Healing Physiology and Pathology

Classical wound healing (Figure 1.1) progresses through overlapping phases of hemostasis, inflammation, proliferation, and remodeling[7].

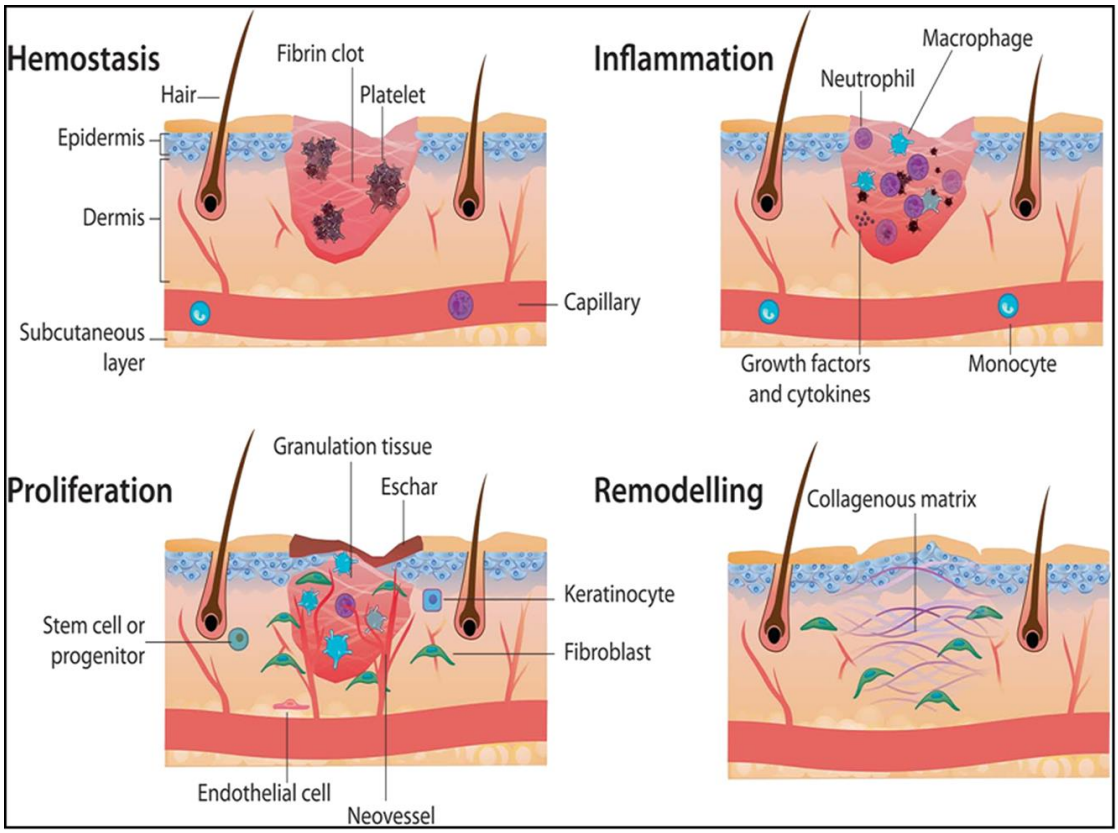

Figure 1.1: Phases of wound healing. First, a clot is formed to stop bleeding. Platelets degranulate and release growth factors and cytokines which attract inflammatory cells. Fibroblasts, endothelial cells, and keratinocytes proliferate and produce granulation tissue. Finally, the wound matrix is remodeled over a long period of time, leaving behind a dense and aligned scar. Reproduced with permission from [8, 9].

Initial hemostasis occurs due to the activity of platelets and the coagulation cascade. This process serves primarily to stop blood loss, however as platelets degranulate they also release inflammatory and mitogenic factors. Together with the damage- and pathogen-associated molecular patterns (DAMPs and PAMPs), these initiate the later phases of the wound healing response. During the subsequent inflammatory phase there is sequential infiltration by granulocytes, lymphocytes, and monocytes. As the inflammatory cells replicate, they remove damaged tissue and sources of infection. Next, the granulation phase begins. Fibroblasts lay down collagen to restore the lost extracellular matrix. Under the influence of cytokines and mechanical forces, they also differentiate into myofibroblasts and contract the newly deposited matrix. At the same time, keratinocytes migrate over the newly deposited matrix to close the surface wound, and

endothelial cells proliferate to form new blood vessels. At the conclusion of this stage, cells begin to undergo apoptosis, and the wound settles to an almost-equilibrium state. Over the continuing months to years the collagen will continue to remodel, however, the tissue will likely never reach its original configuration. Acute wounds are often able to achieve closure. However, even closed wounds lose form and function. Healed acute injuries typically lead to scarring – a process characterized by contracture and excess collagen deposition and alignment. Contracted wounds lose adnexal structures such as hair follicles, nerves, and sweat glands. Scars that occur over large portions of the body or over extensor surfaces may restrict motion, or worse split open when put under excess pressure. For more detailed reviews of wound healing pathophysiology see [10, 11].

Difficult-to-Heal Wounds

Within a normal wound, healing progresses through predictable phases of inflammation, migration, proliferation, matrix deposition, and finally tissue remodeling. In contrast to minor wounds which heal rapidly, difficult-to-heal wounds may develop due to severe acute trauma or mechanical, metabolic, or ischemic abnormalities. Interruptions in any of these may result in development of a difficult-to-heal wound, which may remain unhealed for weeks, or heal with significant scarring[11]. Volumetric loss of large portions of the dermis and epidermis is associated with immune dysfunction, hypothermia, fluid and protein loss. In ulcers, ischemia and mechanical stress contribute to tissue disruption,[12] while increased inflammation and proteolytic activity in ulcers causes an imbalance of scaffold production and degradation by host cells[13]. Expression of MMPs is generally higher in ulcers than normal wounds, while expression of tissue inhibitor of metalloproteinases (TIMPs) is lower, leading to a net loss of extracellular matrix[14]. This imbalance in the production of ECM and its turnover leads to chronicity. Similarly, diabetic ulcers that express higher levels of cytokines such as tumor necrosis factor-α (TNF-α) and monocyte chemoattractant protein-1 (MCP-1) fail to heal at high rates, likely due to a pro-inflammatory phenotype which promotes tissue destruction and inhibits cellular ingrowth.[15] And finally, due to the persistent open wound, a significant portion of ulcers become infected and are even more likely to require intensive care or lower extremity amputation.[16]

Extracellular Matrix Biomechanics and Mechanobiology

The ECM of skin is primarily comprised of collagen, a fibrous protein which provides the primary tensile strength of tissues. More recently, however, there has been increasing interest in the hierarchical multiscale communication from cells to tissues that collagen facilitates[17]. This mechanobiological signaling is now known to be fundamental to wound healing in all tissues. Integrins – which serve as direct linkages between the ECM and cellular cytoskeleton – activate many downstream messengers during wound healing and tissue homeostasis including focal adhesion kinase (FAK)[18], Rho-GTPases, and YAP/TAZ[19, 20]. These signals are particularly important in the fibroblast to myofibroblast transition (Figure 1.2), a key cellular event in the process of wound healing as myofibroblasts display increased contractile and collagen-remodeling behavior.

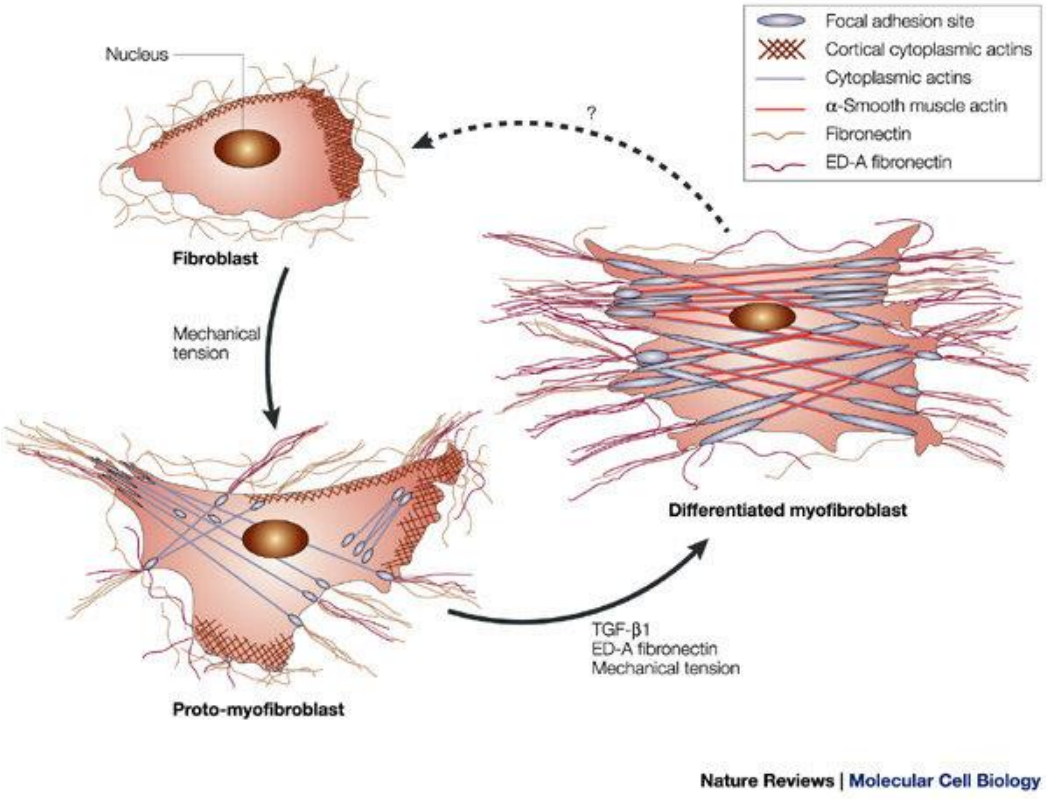

Figure 1.2. Fibroblast differentiation to myofibroblasts is driven by both mechanical and chemical signals. Fibroblasts under strain become proto-myofibroblasts, then under the influence of TGF-β become myofibroblasts. This process demonstrates a strong dependence of cell phenotype on extracellular matrix mechanical properties. Reproduced with permission from [21].

Despite these advances, the exact role of collagen/cell mechanosignaling in wound repair and tissue regeneration is still being elucidated.

1.1.2 Need: Treatments

There is a need for treatments that can rapidly close wounds and restore appearance and function to the skin, including mobility, sensation, and barrier function. Here we will briefly describe the state-of-the-art before continuing into a discussion of opportunities for new therapies.

Conventional Therapy

The scope and magnitude of therapy required for cutaneous wounds varies significantly depending on etiology. As wounds become more severe, therapy is escalated to avoid the development of complications[22]. Conventional treatment is supportive in nature. All wounds are treated with bandaging, antibiotics, and offloading. Wounds may be debrided to improve healing. Perhaps the most important treatment is controlling the process that led to wound development. However, success rates of standard care are low for severe wounds.[23] As wounds become more difficult-to-manage, additional therapies are needed. Hospitalization for inpatient therapy can be important in delivery of supportive care as well as intensive treatments such as skin grafts. Advanced supportive care can include intravenous antibiotics, parenteral nutrition, and respiratory support. Although full-thickness skin grafts (FTSG) are generally more successful in engraftment and scar reduction, the most typical skin grafts are split-thickness skin grafts (STSG) due to donor site limitations. Ultimately, the costs of hospitalization are great, so a reduction in wounds that reach this stage or alternative therapies would be beneficial to both patients and healthcare providers[1]. Finally, tissue engineered dermal substitutes have emerged as late therapies for both chronic refractory wounds or severe difficult-to-heal acute wounds. These are discussed in further detail in the following section.

Tissue Engineered Dermal Substitutes

For difficult-to-heal wounds, biologic wound dressings have become an alternative to skin grafts. Many products are composed of complete decellularized ECM – a natural choice as it contains the assembled structure of skin or similar tissues. However, these products have some

limitations in their variability and possible immunogenicity due to cellular debris[24]. Moreover, it is unknown if the full dermal structure is necessary or optimal for skin regeneration. Other clinically approved dermal replacements such as the Integra product line use collagen – the most prevalent biomolecule in skin and the body in general – as a base material[25-27]. But unlike collagen in the body, which is constructed from molecular building blocks with endogenous crosslinks, collagen biomaterials used for wound healing represent chemically processed decellularized tissue in sheet or particulate form, or contain denatured protein (gelatin).[28] The addition of these components changes many biological and physical properties of grafts. There are many limitations to these current products including poor mechanical stability, extended production times, and high risk of treatment failure. Exogenous crosslinking is often applied to improve strength and resist rapid proteolytic degradation, but these methods decrease material biocompatibility, leading to chronic inflammation.[29] More complex scaffolds may incorporate growth factors, MMP inhibitors, or cells, but these can be expensive and difficult to implement clinically[30, 31].

The requirements for a scaffold to both promote integration as well as maintain integrity and hydration are often empirically determined. The optimal mechanical criteria for recellularization are largely unknown. A 2016 Cochrane Review found these scaffolds are generally superior to traditional therapy, but few studies have shown a decrease in lower extremity amputation, and the risk reduction is low.[32] Even in success, these products are primarily thought to act as sacrificial scaffolds or growth factor depots that are degraded and replaced by granulation tissue rather than as functional tissue replacements.[33] Development of a novel wound therapy that can rapidly generate functional replacement tissue will require development of materials that can be rapidly colonized by cells without structural failure or rejection by host cells.

1.1.3 Research Gap

In this section we briefly discuss the limitations of current skin grafts in additional detail, our proposed solution, and the innovation of our approach.

Limitations of Current Products

Engineered dermal substitutes have emerged as treatments for both acute and chronic wounds, initially to combat the cost and scarcity of skin grafts. In systematic reviews, an average of 43-58% of engineered scaffold treated wounds heal completely[25, 34]. In addition, at present the focus of these therapies is on wound closure and repair so to avoid dehiscence and recurrence. There has been little success in regenerating the complex architecture of skin including adnexal structures. Although collagen is the preeminent material choice for engineered dermal replacements, approaches to date have largely used decellularized tissue products, including those derived from dermis. However, these are potentially immunogenic and have a single architecture which cannot be modulated the way assembled materials can. As an alternative, the Integra product is an engineered dermal substitute containing collagen in an insoluble sponge format, which are crosslinked for increased stability. This was a significant landmark in the use of engineering design criteria in tissue engineering. Whereas the initial criteria for the dermal regeneration template were pore size, chemical composition, ligand density, and degradation rate[35-37], new research suggests the importance of additional features such as a highly connected collagen network architecture, tensile mechanical properties, and unmodified protein chemistries[38-40]. To address these limitations, we propose a new engineered dermal substitute developed using a new biomaterial, collagen Oligomer, which is mechanically stable and can be fabricated into multiple mechanical and geometric design configurations.

In addition, we propose the development of a mathematical model for predicting dermal replacement therapy outcomes. The clear importance of fibrous tissue mechanobiology also suggests a need for better computational models of wound healing. These models can be used to make predictions regarding biological mechanisms of pathology or be used in personalized medicine to optimize individual patient therapy. The mathematical modeling of growth, and tissue engineering in vitro and in situ is currently one of the largest open problems in continuum modeling[41]. Gaps in the current understanding of healing include a detailed understanding of how scaffold properties (initial ECM, growth factor, and cell conditions) as well as mechanical loads determine biological and material transport leading to either closure and homeostasis of a chronic wound versus degrading and reopening. To this end, many mathematical models have been developed to explain experimental wound healing and develop predictions for optimizing therapy (Figure 1.3). Continuum models have been developed for wound healing demonstrating the flux

of collagen/ECM, fibroblasts/cells, blood vessels, cytokines, and the development of mechanical properties[42-44]. More models focus on acute than chronic healing, and many considering healing by contraction of the surrounding tissue. Some detailed reviews tabulate conservation and mechanical models[44-47]. Important historical models include the reaction-diffusion models such as [48] which have given rise to contraction models which include a balance of linear momentum such as [49, 50], generally to show matrix contraction over time. More recent models include further complexity [51, 52], but there are no current models that explicitly consider dermal replacement therapies.

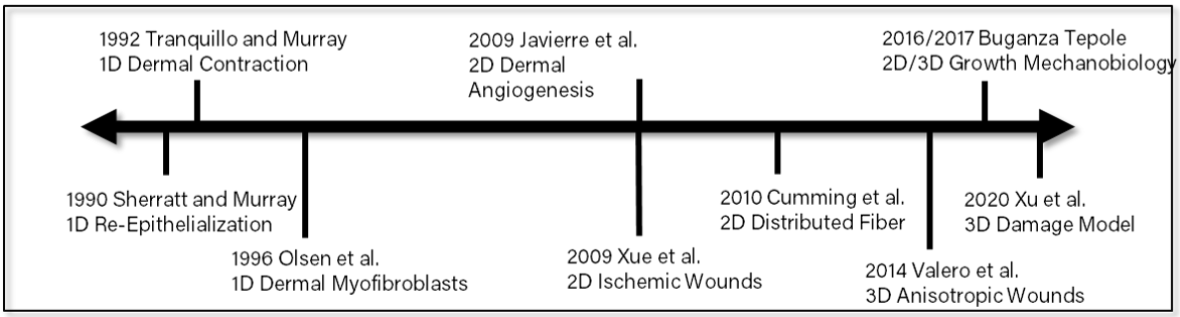

Figure 1.3. Timeline of wound healing models. Early models focused on reaction-diffusion -based descriptions of recellularization. Since then, focus has expanded on extracellular matrix biomechanics and mechanobiology culminating in new 3D models of complex wounds with cell/cytokine/collagen interactions and plastic remodeling.

1.1.4 Solution

Innovation

Collagen is relatively unique among proteins in that it undergoes hierarchical self-assembly both in the body and in vitro. It is the dominant biomaterial composing most tissues, but molecular forms have historically been isolated by acetic acid solubilization (telocollagen) or pepsin digestion (atelocollagen) – methods which yield solutions that vary in purity and solubility and have limited in-vitro self-assembly capacity. Recently, our lab isolated and purified a novel crosslinked molecular subdomain of collagen from porcine skin, which we refer to as Oligomer[38, 39]. Unlike monomeric collagens, which represent individual collagen molecules, Oligomer represents aggregates of collagen molecules held together covalently by a natural intermolecular crosslink. This subdomain is soluble in dilute acid and exhibits self-assembly when brought to

physiologic pH and ionic strength, forming fibrillar scaffolds with features similar to those found in the body's tissues. In the body, mature collagen intermolecular crosslinks formed by lysyl oxidase (LOX) during collagen fibril formation provide the collagen scaffold of tissues with improved resistance to both mechanical forces as well as endogenous proteases.[53] Similarly, the presence of intermolecular crosslinks within oligomer brings enhanced self-assembly kinetics, improved mechanical integrity because of increased interfibrillar connectivity, and increased resistance to proteolysis. This unique property enables fabrication of a broad array of collagen scaffolds with systematically varied physical parameters (Figure 1.4).[40]

We have developed and applied a protocol (ASTM International Standard F3089-14) for standardization this material. Using advanced fabrication techniques such as plastic compression we are able to create dense constructs that approximate the mechanics of normal dermis.[54] We have applied this material to a number of *in vitro* and *in vivo* systems including therapeutic vasculogenesis,[55] treatment for muscle and cartilage loss,[56, 57] and tissue reinforcement[58]. During these experiments, we have consistently identified long-term persistence (months) of the material, with a complete lack of inflammation or foreign body response. We believe this high biocompatibility is due to the fact that our material is completely composed of purified, highly conserved collagen protein. Additionally, the fibrils formed by Oligomer retain their inherent mechanochemical biosignaling capacity and are reinforced by endogenous crosslinks – not chemically treated. Oligomer supports a rapid assembly from liquid to a semi-solid fibrillar collagen scaffold within minutes at physiologic conditions. The resulting highly connected, D-banded fibrillar scaffolds resemble native tissue and are amenable to scalable manufacturing procedures, addition of cells and/or therapeutic agents (antibiotics and growth factors). Oligomer matrices exhibit improved mechanical properties (stiffness and strength) and proteolytic resistance in vitro. Based on this understanding, our approach involved mechanical control of an Oligomeric collagen engineered dermal substitute to probe wound phenotypic response. We applied a controlled confined compression biofabrication technique to Oligomeric collagen to create samples with varied fibril density and microstructure (Figure 1.4).

Here we propose the use of Oligomer as a dermal replacement in the treatment of wounds. We developed a dermal replacement scaffold with customizable biophysical properties to modulate recellularization and tissue remodeling. The main outcome of is the preliminary design of a low-cost customizable scaffold that can improve wound healing outcomes. These results will

provide valuable evidence for the design of future studies in humans. To further enhance the design and testing of restorative dermal scaffolds we implemented a mathematical mechanobiology model of in situ dermal replacement for wound therapy using a continuum mechanics framework. Mathematical models have been developed to study skin biophysics wound healing, but rarely applied to therapeutic tissue replacements[59, 60]. When they are, they can be used to make predictions regarding therapeutic efficacy and optimize design[61, 62]. With this background, we propose the application of this in silico model to in situ dermal replacement with an engineered collagen scaffold. The long-term goal of this research is to produce a mechanically-defined engineered dermal replacement to reduce morbidity and mortality of difficult-to-heal wounds.

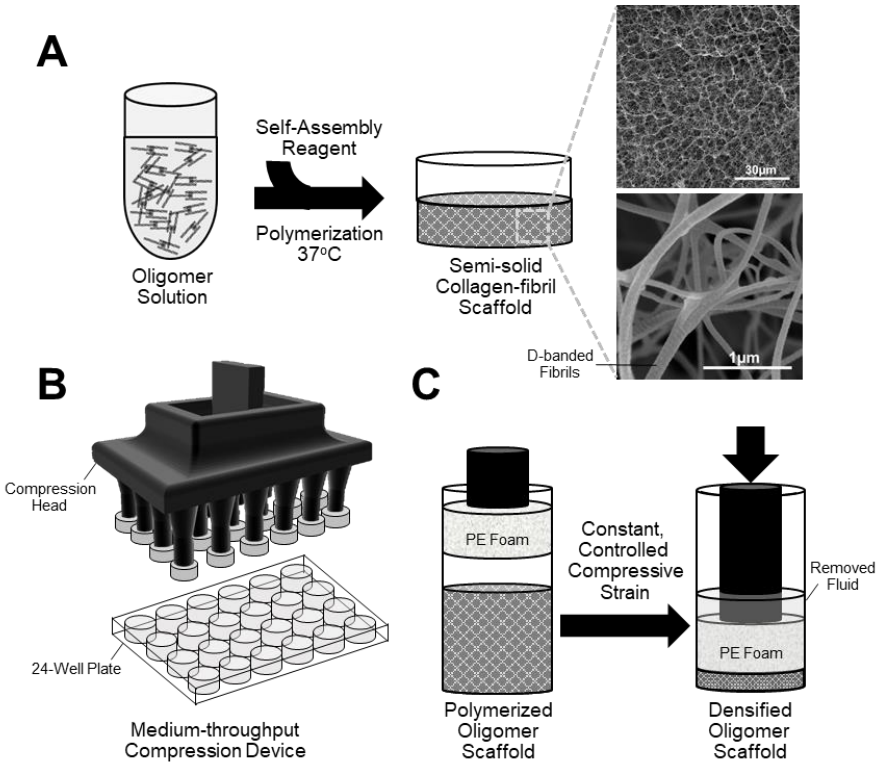

Figure 1.4. Diagram demonstrating the fabrication process of collagen oligomer scaffolds. (A) Oligomer is polymerized from a liquid to solid form with a native fibrillar architecture. (B,C) A plastic compression protocol can be used to create scaffolds of varied density and microarchitecture.

1.2 Organization of Thesis

The work contained in this thesis spans the molecular, micro-, and macro-scale engineering of collagen biomaterials for difficult-to-heal wounds. We discuss the basic science of collagen, *in vitro* mechanical and structural analysis, *in vivo* animal testing, and *in silico* computational studies.

Much of the content in this introductory Chapter 1 is restated from a Qualifying Literature Assessment and Preliminary Examination also submitted as requirements of this Doctor of Philosophy degree. Following this, the thesis is framed in three main sections.

In Chapter 2, we review collagen-based biomaterials and their biochemical and biomechanical properties. This review defines many important features of collagen and fabrication techniques used in tissue engineering to set the stage for our experimental studies. Naturally, our perspective draws heavily from work in the biochemistry and engineering of collagen oligomer developed by members of the Harbin lab.

In Chapter 3, an *in vivo* dermal replacement model is presented, which was published in the journal *Regenerative Medicine*. We fabricated oligomer scaffolds with varied mechanical properties and tested them in a full-thickness rodent skin wound model.

In Chapter 4, we use data from our animal studies together with a mathematical theory of wound healing to develop a predictive model for contractile wounds. The goal of this chapter is to use experimental data to inform a continuum model of wound healing in the setting of treatment with an engineered dermal replacement. We consider the mechanical deformations and their impact on the ECM using the multiplicative decomposition approach to growth modeling, together with a diffusion-reaction based approach to recellularization. Our focus is primarily on the fibroblast system during wound healing and the effects of the collagen network structure. With this information, the outcomes of therapy can be predicted, and used to improve engineering design.

Finally, in Chapter 5 we conclude with a discussion of the significance of our findings and plans for additional work. The proposed project will advance the ability to heal chronic wounds including diabetic, pressure, arterial, and venous ulcers. This work is a significant improvement over state-of-the-art by providing a one-step therapy that replaces damaged tissue. Not only will this design help patients and physicians, it will also provide valuable information regarding the impact of extracellular matrix mechanobiology on dermal cell phenotype. Furthermore,

researchers in the tissue engineering field will benefit from the use of our in vivo and in silico model development in future work to develop replacement tissues for different applications.

1.3 References

1. Sen CK, Gordillo GM, Roy S, Kirsner R, Lambert L, Hunt TK, Gottrup F, Gurtner GC, Longaker MT. Human skin wounds: a major and snowballing threat to public health and the economy. Wound Repair Regen. 2009;17(6):763-71.
2. Sander EA, Lynch KA, Boyce ST. Development of the mechanical properties of engineered skin substitutes after grafting to full-thickness wounds. J Biomech Eng. 2014;136(5):051008.
3. Rowan MP, Cancio LC, Elster EA, Burmeister DM, Rose LF, Natesan S, Chan RK, Christy RJ, Chung KK. Burn wound healing and treatment: review and advancements. Critical Care. 2015;19(1):243.
4. Gottrup F. A specialized wound-healing center concept: importance of a multidisciplinary department structure and surgical treatment facilities in the treatment of chronic wounds. Amer J Surgery. 2004;187(5):S38-S43.
5. MacNeil S. Progress and opportunities for tissue-engineered skin. Nature. 2007;445(7130):874-80.
6. MacNeil S. Biomaterials for tissue engineering of skin. Materials Today. 2008;11(5):26-35.
7. Bunman S, Dumavibhat N, Chatthanawaree W, Intalapaporn S, Thuwachaosuan T, Thongchuan C. Burn Wound Healing: Pathophysiology and Current Managementof Burn Injury. Bangkok Med J. 2017;13(2).
8. Nour S, Baheiraei N, Imani R, Khodaei M, Alizadeh A, Rabiee N, Moazzeni SM. A review of accelerated wound healing approaches: biomaterial- assisted tissue remodeling. J Mater Sci Mater Med. 2019;30(10):120.
9. Lisovsky A, Chamberlain MD, Wells LA, Sefton MV. Cell Interactions with Vascular Regenerative MAA-Based Materials in the Context of Wound Healing. Adv Healthc Mater. 2015;4(16):2375-87.
10. Gurtner GC, Werner S, Barrandon Y, Longaker MT. Wound repair and regeneration. Nature. 2008;453(7193):314-21.

11. Eming SA, Martin P, Tomic-Canic M. Wound repair and regeneration: mechanisms, signaling, and translation. Sci Transl Med. 2014;6(265):265sr6.
12. Clayton W, Elasy TA. A Review of the Pathophysiology, Classification, and Treatment of Foot Ulcers in Diabetic Patients. Clin Diabetes. 2009;27(2):52-8.
13. Liu Y, Min D, Bolton T, Nube V, Twigg SM, Yue DK, McLennan SV. Increased matrix metalloproteinase-9 predicts poor wound healing in diabetic foot ulcers. Diabetes Care. 2009;32(1):117-9.
14. Lobmann R, Ambrosch A, Schultz G, Waldmann K, Schiweck S, Lehnert H. Expression of matrix-metalloproteinases and their inhibitors in the wounds of diabetic and non-diabetic patients. Diabetologia. 2002;45(7):1011-6.
15. Dinh T, Tecilazich F, Kafanas A, Doupis J, Gnardellis C, Leal E, Tellechea A, Pradhan L, Lyons TE, Giurini JM, Veves A. Mechanisms involved in the development and healing of diabetic foot ulceration. Diabetes. 2012;61(11):2937-47.
16. Alexiadou K, Doupis J. Management of diabetic foot ulcers. Diabetes Ther. 2012;3(1):4.
17. Evans ND, Oreffo RO, Healy E, Thurner PJ, Man YH. Epithelial mechanobiology, skin wound healing, and the stem cell niche. J Mech Behav Biomed Mater. 2013;28:397-409.
18. Greenberg RS, Bernstein AM, Benezra M, Gelman IH, Taliana L, Masur SK. FAK-dependent regulation of myofibroblast differentiation. FASEB J. 2006;20(7):1006-8.
19. Lee MJ, Byun MR, Furutani-Seiki M, Hong JH, Jung HS. YAP and TAZ regulate skin wound healing. J Invest Dermatol. 2014;134(2):518-25.
20. Elbediwy A, Vincent-Mistiaen ZI, Spencer-Dene B, Stone RK, Boeing S, Wculek SK, Cordero J, Tan EH, Ridgway R, Brunton VG, Sahai E, Gerhardt H, Behrens A, Malanchi I, Sansom OJ, Thompson BJ. Integrin signalling regulates YAP and TAZ to control skin homeostasis. Development. 2016;143(10):1674-87.
21. Tomasek JJ, Gabbiani G, Hinz B, Chaponnier C, Brown RA. Myofibroblasts and mechano-regulation of connective tissue remodelling. Nat Rev Mol Cell Biol. 2002;3(5):349-63.
22. Nunan R, Harding KG, Martin P. Clinical challenges of chronic wounds: searching for an optimal animal model to recapitulate their complexity. Dis Model Mech. 2014;7(11):1205-13.
23. Markova A, Mostow EN. US skin disease assessment: ulcer and wound care. Dermatol Clin. 2012;30(1):107-11, ix.

24. Badylak SF, Gilbert TW. Immune response to biologic scaffold materials. Semin Immunol. 2008;20(2):109-16.
25. Holmes C, Wrobel JS, Maceachern MP, Boles BR. Collagen-based wound dressings for the treatment of diabetes-related foot ulcers: a systematic review. Diabetes Metab Syndr Obes. 2013;6:17-29.
26. Yannas I, Tzeranis D, Harley B, So P. Biologically active collagen-based scaffolds: advances in processing and characterization. Phil Trans R Soc Lond A. 2010;368(1917):2123-39.
27. Yannas IV, Tzeranis D, So PT. Surface biology of collagen scaffold explains blocking of wound contraction and regeneration of skin and peripheral nerves. Biomed Mater. 2015;11(1):014106.
28. Brett D. A Review of Collagen and Collagen-based Wound Dressings. Wounds. 2008;20(12):347-56.
29. Valentin JE, Stewart-Akers AM, Gilbert TW, Badylak SF. Macrophage participation in the degradation and remodeling of extracellular matrix scaffolds. Tissue Eng A. 2009;15(7):1687-94.
30. Supp DM, Boyce ST. Engineered skin substitutes: practices and potentials. Clin Dermatol. 2005;23(4):403-12.
31. Griffiths M, Ojeh N, Livingstone R, Price R, Navsaria H. Survival of Apligraf in acute human wounds. Tissue Eng. 2004;10(7-8):1180-95.
32. Santema TB, Poyck PP, Ubbink DT. Skin grafting and tissue replacement for treating foot ulcers in people with diabetes. Cochrane Database Syst Rev. 2016;2:CD011255.
33. Macri L, Clark RA. Tissue engineering for cutaneous wounds: selecting the proper time and space for growth factors, cells and the extracellular matrix. Skin Pharmacol Physiol. 2009;22(2):83-93.
34. Felder III JM, Goyal SS, Attinger CE. A systematic review of skin substitutes for foot ulcers. Plast Reconstr Surg. 2012;130(1):145-64.
35. Dagalakis N, Flink J, Stasikelis P, Burke JF, Yannas IV. Design of an artificial skin. Part III. Control of pore structure. J Biomed Mater Res. 1980;14(4):511-28.
36. Yannas IV, Burke JF. Design of an artificial skin. I. Basic design principles. J Biomed Mater Res. 1980;14(1):65-81.

37. Yannas IV, Burke JF, Gordon PL, Huang C, Rubenstein RH. Design of an artificial skin. II. Control of chemical composition. J Biomed Mater Res. 1980;14(2):107-32.
38. Bailey JL, Critser PJ, Whittington C, Kuske JL, Yoder MC, Voytik-Harbin SL. Collagen oligomers modulate physical and biological properties of three-dimensional self-assembled matrices. Biopolymers. 2011;95(2):77-93.
39. Critser PJ, Kreger ST, Voytik-Harbin SL, Yoder MC. Collagen matrix physical properties modulate endothelial colony forming cell-derived vessels in vivo. Microvasc Res. 2010;80(1):23-30.
40. Kreger ST, Bell BJ, Bailey J, Stites E, Kuske J, Waisner B, Voytik-Harbin SL. Polymerization and matrix physical properties as important design considerations for soluble collagen formulations. Biopolymers. 2010;93(8):690-707.
41. Ateshian G, Humphrey J. Continuum mixture models of biological growth and remodeling: past successes and future opportunities. Annu Rev Biomed Eng. 2012;14:97-111.
42. Vermolen F, Javierre E. A finite-element model for healing of cutaneous wounds combining contraction, angiogenesis and closure. J Math Biol. 2012;65(5):967-96.
43. Valero C, Javierre E, Garcia-Aznar JM, Gomez-Benito MJ. A cell-regulatory mechanism involving feedback between contraction and tissue formation guides wound healing progression. PLoS One. 2014;9(3):e92774.
44. Valero C, Javierre E, García-Aznar J, Menzel A, Gomez-Benito M. Challenges in the modeling of wound healing mechanisms in soft biological tissues. Ann Biomed Eng. 2015;43(7):1654-65.
45. Jorgensen SN, Sanders JR. Mathematical models of wound healing and closure: a comprehensive review. Med Biol Eng Comput. 2016;54(9):1297-316.
46. Weihs D, Gefen A, Vermolen FJ. Review on experiment-based two-and three-dimensional models for wound healing. Interface Focus. 2016;6(5):20160038.
47. Ud-Din S, Bayat A. Non-animal models of wound healing in cutaneous repair: In silico, in vitro, ex vivo, and in vivo models of wounds and scars in human skin. Wound Repair Regen. 2017;25(2):164-76.
48. Sherratt JA, Murray JD. Models of epidermal wound healing. Proc R Soc Lond B. 1990;241(1300):29-36.

49. Tranquillo RT, Murray J. Continuum model of fibroblast-driven wound contraction: inflammation-mediation. J Theor Biol. 1992;158(2):135-72.
50. Olsen L, Sherratt JA, Maini PK. A mechanochemical model for adult dermal wound contraction and the permanence of the contracted tissue displacement profile. J Theor Biol. 1995;177(2):113-28.
51. Buganza Tepole A, Kuhl E. Computational modeling of chemo-bio-mechanical coupling: a systems-biology approach toward wound healing. Comput Methods Biomech Biomed Engin. 2016;19(1):13-30.
52. Tepole AB. Computational systems mechanobiology of wound healing. Comp Meth App Mech Eng. 2017;314:46-70.
53. van der Slot-Verhoeven AJ, van Dura EA, Attema J, Blauw B, Degroot J, Huizinga TW, Zuurmond AM, Bank RA. The type of collagen cross-link determines the reversibility of experimental skin fibrosis. Biochim Biophys Acta. 2005;1740(1):60-7.
54. Blum KM, Novak T, Watkins L, Neu CP, Wallace JM, Bart ZR, Voytik-Harbin SL. Acellular and cellular high-density, collagen-fibril constructs with suprafibrillar organization. Biomater Sci. 2016;4(4):711-23.
55. Whittington CF, Yoder MC, Voytik-Harbin SL. Collagen-polymer guidance of vessel network formation and stabilization by endothelial colony forming cells in vitro. Macromol Biosci. 2013;13(9):1135-49.
56. Zhang H, Voytik-Harbin S, Brookes S, Zhang L, Wallace J, Parker N, Halum S. Use of autologous adipose-derived mesenchymal stem cells for creation of laryngeal cartilage. Laryngoscope. 2018;128(4):E123-E9.
57. Brookes S, Voytik-Harbin S, Zhang H, Halum S. Three-dimensional tissue-engineered skeletal muscle for laryngeal reconstruction. Laryngoscope. 2018;128(3):603-9.
58. Yrineo AA, Adelsperger AR, Durkes AC, Distasi MR, Voytik-Harbin SL, Murphy MP, Goergen CJ. Murine ultrasound-guided transabdominal para-aortic injections of self-assembling type I collagen oligomers. J Control Release. 2017;249:53-62.
59. Limbert G. Mathematical and computational modelling of skin biophysics: a review. Proc Math Phys Eng Sci. 2017;473(2203):20170257.
60. Benítez JM, Montáns FJ. The mechanical behavior of skin: Structures and models for the finite element analysis. Computers & Structures. 2017;190:75-107.

61. Flegg JA, Byrne HM, McElwain DL. Mathematical model of hyperbaric oxygen therapy applied to chronic diabetic wounds. Bull Math Biol. 2010;72(7):1867-91.
62. Szafron JM, B. Ramachandra A, Breuer CK, Marsden AL, Humphrey JD. Optimization of tissue engineered vascular graft design using computational modeling. Tissue Eng. 2019(ja).

2. COLLAGEN SELF-ASSEMBLY: BIOPHYSICS AND BIOSIGNALING FOR ADVANCED TISSUE GENERATION

This chapter is reproduced with permission from:

Sohutskay, David O., Theodore J. Puls, and Sherry L. Voytik-Harbin. "Collagen self-assembly: biophysics and biosignaling for advanced tissue generation." *Multi-scale Extracellular Matrix Mechanics and Mechanobiology*. Springer, Cham, 2020. 203-245.

Abstract

Type I collagen is the predominant protein in the body and the extracellular matrix, where it gives rise to the vast diversity of tissue form and function. Within the extracellular matrix, this natural polymer exists as the fibrillar scaffolding that not only dictates tissue-specific structure and mechanical properties but also interacts with cells and other biomolecules to orchestrate complex processes associated with tissue development, homeostasis, and repair. For this reason, the hierarchical self-assembly of collagen molecules and their inherent biochemical and biophysical signaling capacity have been a long-standing subject of study across multiple disciplines, including structural biochemistry, biomechanics, biomaterials and tissue engineering, computational modeling, and medicine. This review works to capture some of the major discoveries and innovative technologies related to the supramolecular assembly of collagen in vivo and vitro, with a focus on motivating their integration and application for advanced tissue fabrication and regenerative medicine therapies.

Keywords

collagen, biomaterials, biomechanics, mechanobiology, tissue fabrication

2.1 Tissue Engineering and Regenerative Medicine: The Goal and Challenge

The fields of tissue engineering and regenerative medicine, which operate at the interface of engineering and life sciences, have evolved over the last three decades with the goal of restoring damaged or dysfunctional tissues and organs through the development of biological substitutes and/or the promotion of tissue regeneration. Miniaturized in-vitro human tissue systems are also highly sought after as an alternative to animals for cosmetic and chemical toxicity testing, high-throughput/high-content drug screening, and basic research. One foundational element of such

efforts has been development of biomaterials that recreate the extracellular matrix (ECM) component of tissues. The ECM constitutes non-living material produced and secreted by cells within which they are distributed and organized. It represents a composite material, largely composed of an insoluble collagen-fibril scaffold surrounded by an interstitial fluid phase, giving tissues both poroelastic and viscoelastic properties[1]. More specifically, applied deformation to the composite will intrinsically lead to fluid flow that homogenizes scaffold pore pressure. At the same time, the composite will undergo viscoelastic deformation, exhibiting both viscous (liquid) and elastic (solid) characteristics[2]. ECM is found in all tissues and organs, providing not only the essential physical structure that organizes and supports cellular constituents but also crucial biochemical and biomechanical signaling required for tissue morphogenesis, homeostasis, and remodeling. In fact, a dynamic and reciprocal dialogue exists between cells and their surrounding ECM, such that multi-scale tissue architecture and function are integrated[3]. As such, the ability to recapitulate this natural scaffold and dynamic cell-ECM interactions has been a focused effort of tissue engineering and regenerative medicine even prior to the formal definition of these fields.

When tissue engineering emerged as a new field in the early 1990s, emphasis was placed on the use of synthetic polymers for development of porous scaffolds to mimic the structural features of ECM[4]. Synthetic materials received preference over natural polymers, such as collagen, largely owing to advantages associated with cost, batch-to-batch reproducibility, mechanical stability, as well as amenability to customization, processing, and scale-up manufacturing. Furthermore, at the time, medical devices containing candidate synthetic materials had already received FDA-approval, documenting their biocompatibility and paving the way for translation into the clinic. To date, extensive effort has been invested in the design and manufacturing of synthetic biomaterials that are biocompatible (non-toxic to cells) and possess the structural and mechanical properties of a target tissue. Another fundamental design criteria was that the biomaterial should be biodegradable, allowing host cells to progressively deposit site-appropriate replacement tissue over time[5-7]. However, in recent times, concerns have been raised regarding the immune-mediated, foreign-body responses elicited by synthetic materials[8,9] as well as their lack of biological signaling capacity[10,11]. As a result, design criteria for next-generation biomaterials are changing, moving away from merely providing bulk structure and mechanical properties to strategies that guide biological processes underlying tissue regeneration[11-13].

Despite this initial focus on synthetics, others targeted the use of natural materials, including intact ECMs prepared from various tissues and their component molecules (e.g., collagen, fibrin, glycosaminoglycans). Here, the goal was to capitalize on the biological signaling capacity inherent to these molecules and their assemblies for purposes of inducing site-appropriate tissue regeneration. Interestingly, evaluation of the present-day tissue engineering and regenerative medicine market, shows that biologically-derived materials (e.g., decellularized tissues) and natural polymers, specifically type I collagen, account for the majority of translated technologies[14]. Within this context, this chapter focuses on type I collagen and its use for tissue engineering and regenerative medicine applications. We start by providing a historical overview of milestone discoveries related to collagen biochemistry and collagen-based biomaterials, highlighting their impact on research and medicine. The next section describes what is known regarding the biosynthesis and hierarchical self-assembly of type I collagen as it occurs within the body. This is followed by a brief description of collagen biomechanics and the more recent discovery of collagen's participation in mechanobiology signaling, which collectively have contributed new and important design criteria for cell-instructive biomaterials. We then rigorously define and compare various collagen preparations, lending support to the notion that "all collagens or collagen-containing materials are not alike." We then hone in on collagen advancements and applications that support next-generation, multi-scale design and custom fabrication of collagen scaffolds and tissues. Finally, we conclude with a look to the future, where this natural polymer interfaces with other tissue engineering and regeneration advancements, including stem cells (adult, induced pluripotent), computational modeling, and advanced manufacturing, to address today's challenges and unmet clinical needs.

2.2 Collagen Biomaterials: The History

Scientific inquiry and applications of collagen as a tool and in medicine date back millennia. Figure 2.1 provides a timeline, outlining some of the major milestones in the development and application of collagen biomaterials. The word collagen is Greek, from the roots κόλλα- (glue) and -γέν (to make), so called because the first application of denatured collagen (gelatin) was as an adhesive for wood furnishings[15]. The first medical application of collagen as an implantable biomaterial was likely "catgut" suture, which was documented as early as 150 A.D. by Galen of Pergamon [16,17]. Despite the moniker, these collagenous threads were typically

formed from decellularized sheep intestine, not cats. Although catgut sutures were used for centuries, it wasn't until the late 19th century that their production was perfected, with the development of chromic acid-based sterilization procedures by Lister and MacEwen[18,19]. Catgut persisted into modern use, though largely supplanted by resorbable synthetic products due to their ease of manufacturing and sterilization. Despite the common usage of collagen over this early time period, it's unique structure as a semiflexible, triple helical rod was not determined until the 1950s. Ramachandran and others used fiber diffraction analysis and model building, together with early amino acid composition and sequence data, to elucidate that the three component polypeptide chains, each in an extended left-handed polyproline II-helix conformation, were supercoiled in a right-handed manner about a common axis[20].

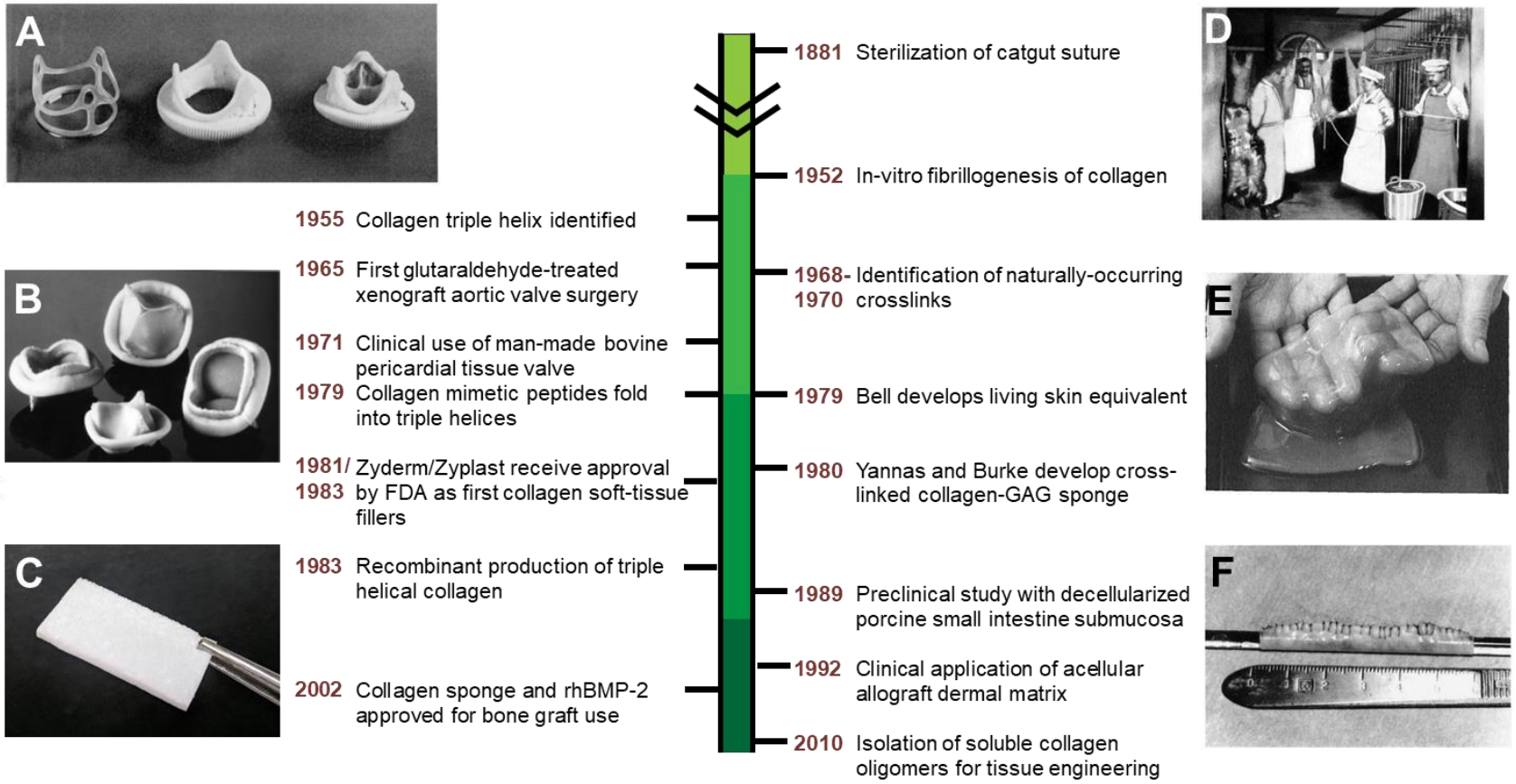

Figure 2.1: Timeline of key developments in the history of collagen biomaterials. A. Assembly and reinforcement of glutaraldehyde-treated aortic valve xenograft onto supports (reprinted with permission from Zudhi et al., 1974). B. Man-made bioprosthetic valves prepared from glutaraldehyde-treated bovine pericardial tissue (reprinted with permission from Society for Cardiothoracic Surgery in Great Britain and Ireland). C. Freeze-dried collagen-glycosaminoglycan sponge. D. Processing and sterilization of catgut sutures using the Kuhn procedure (reprinted with permission from Dietz et al., 2007). E. Living-skin equivalent prepared from fibroblast-contracted collagen matrix (reprinted with permission from Bell et al., 1983). F. Vascular graft fashioned from decellularized small intestine submucosa (reprinted with permission from Badylak et al, 1989).

In the mid-1960's, another historical milestone was reached for collagen biomaterials—the use of biological tissue valves derived from porcine or bovine sources. The very first xenograft (porcine) aortic valve replacement in a human patient was performed in 1965 by Carpentier and his team[21]. It was later discovered that stent reinforcements and treatment of these valves with exogenous glutaraldehyde crosslinking reduced their antigenicity and degradation, dramatically improving clinical success rates[22,23]. The first clinical use of an "engineered" or man-made heart valve followed in 1971, when Marian Ion Ionescu introduced the novel concept of constructing heart valves by attaching glutaraldehyde-treated bovine pericardium to a support frame[24]. This application of a replenishable collagen tissue source for valve design and manufacturing has contributed significantly to the evolution of the heart valve industry. Today, innovative, non-invasive trans-catheter approaches involving stented pericardial tissue are paving the way for expanded valve applications and patient populations, including children[25].

More widespread use of collagen for tissue-engineered medical products came with the isolation and decellularization of porcine small intestine submucosa (SIS), developed at Purdue University in the late 1980s[26]. Here, the design strategy was to remove all cellular components while maintaining the complex molecular composition, architecture, and mechanical properties, and biological activity inherent to the naturally-occurring ECM. With a focus on inducing tissue regeneration, SIS became one of the first major tissue engineering industry success stories[27,28], with Cook Biotech continuing to expand its portfolio of wound management and surgical reconstruction products based on this technology. Today, a number of decellularized tissue products populate the market, including those derived from multiple animal tissue sources (porcine and bovine small intestine, dermis, and urinary bladder) as well as human tissue sources (dermis and placenta). It is notable that AlloDerm, produced by LifeCell, was the first decellularized human dermal tissue on the market, receiving initial FDA approval in 1992 for treatment of burns[29].

As an alternative to these top-down approaches to tissue design, others have applied bottom-up strategies, focused on applications of purified collagen in both insoluble fibrillar and soluble, fibril-forming (self-assembling) formats. Improvements in biotechnology and development of scalable extraction procedures, such as those developed by Miller and Rhodes[30], facilitated large-scale production of high-purity collagens, paving the way for their use in tissue engineering and medicine. One of the first and most successful products created from insoluble

fibrillar collagen was the "collagen-glycosaminoglycan membrane," which was initially developed by Yannas and Burke for management of skin wounds[31-33]. These scaffolds were created by freeze drying a viscous slurry of purified bovine hide particulate and chondroitin 6-sulfate from shark cartilage followed by chemical crosslinking. Design criteria including pore size, mechanical properties, and degradation (resorption) rate were modulated, with the goal of retarding wound contraction while carefully controlling host cell infiltration and tissue deposition. This technology was acquired by Integra, which successfully entered the burn market with the first dermal regeneration template in 1995. Integra's tissue-engineered products have become a significant commercial success with many applications, including burns, diabetic ulcers, and dental wounds. One might argue this is, in large part, owing to the design control afforded by their fabrication process.

Insoluble fibrillar collagen also served as the starting material for injectable soft tissue fillers products that reached popularity for cosmetic applications in the late twentieth century[34]. More specifically, Zyderm and its chemically cross-linked counterpart Zyplast consisted of insoluble bovine dermal collagen dispersed in phosphate-buffered saline, which contained lidocaine as a local anesthetic. Because these injectable collagens required multiple injections and chemical crosslinking to enhance their stability in vivo, they are no longer on the market and have been superseded by hyaluronic acid products[35]. Lyophilized collagen sponges, again which comprise insoluble fibrillar collagen, have also been used as drug or growth factor carriers. One particular example of a mainstay collagen-based drug delivery device is InFuse bone graft, which received approval in the early 2000s. This product involves the application of recombinant human bone morphogenetic protein 2 to a lyophilized collagen sponge prior to implantation into bone defects[36,37].

Some of the first descriptions of in-vitro collagen self-assembly, also referred to as fibrillogenesis or polymerization, came in 1952 by Gross and Schmitt as well as Jackson and Fessler in 1955[38,39]. Collagen self-assembly refers to the spontaneous and precise multi-scale aggregation of collagen molecules to form longitudinal staggered arrays, giving rise to insoluble fibrous networks with a characteristic banding pattern. Additional details regarding this process as it occurs in vivo and in vitro can be found in Sections 3.2 and 6.1, respectively.

Although some earlier studies identified the ability of cells to interface with collagen, it was Bell and co-workers, in 1979, who reported that human dermal fibroblasts encapsulated within a

reconstituted collagen matrix reorganized the fibrous scaffold into a "dermal equivalent" following culture in vitro[40]. This landmark discovery, which came at the infancy of tissue engineering, eventually gave rise to Apligraf, the first "living" dermal-epidermal skin product[41]. Apligraf was produced by culturing human keratinocytes on the surface of the contracted collagen-fibroblast dermal layer. It received initial FDA approval in 1998 and remains on the market to date with indications for venous leg and diabetic foot ulcers that are not responding to conventional therapy.

Although self-assembling collagens have received considerable attention for development of 3D in-vitro tissue systems, tissue-engineered constructs, and drug delivery vehicles, translation into medically useful products has been limited to date. There have been and continue to be numerous commercial products consisting of collagen that can be solubilized in dilute acid or comes as solutions in dilute acid for research or cell culture applications. These formulations represent single collagen molecules (monomeric collagen) extracted and purified from various tissue sources; however, little focus is often given to self-assembly as a functional and standardizable collagen property[42]. As a result, significant product-to-product and lot-to-lot variation exists in the time required for collagen self-assembly (polymerization kinetics) as well as the physical properties (microstructure and mechanical properties) of self-assembled construct[42,43]. Other persistent challenges of monomeric collagens include long polymerization times (>30 minutes), low mechanical integrity of formed constructs, and rapid degradation following culture in vitro and/or implantation in vivo[44].

Increased attention on self-assembling collagens came in the late 1990s and early 2000s, with the emergence of recombinant collagens, collagen mimetic peptides, and oligomeric collagen. Advancements in recombinant technology and peptide synthesis facilitated the pursuit of recombinant human collagen (rhCOL) and synthetic collagen-mimetic peptides (CMPs) as potential alternative collagen sources[45]. Today, rhCOL has been produced in plant, insect, yeast, and bacterial systems which co-express the necessary enzymes to create stable collagen triple helices; however, only a subset of these can self-assemble into fibrils[45,46]. The first report of tissue-derived oligomeric collagen for tissue engineering applications came in 2010[47,42]. Unlike monomeric collagens, oligomers represented aggregates of collagen molecules (e.g., trimers) that retained their natural intermolecular crosslinks[48]. Published work shows that oligomers overcome many of the limitations of conventional monomeric formulations, with rapid

polymerization, dramatically improved mechanical integrity, and resistance to proteolytic degradation both in vitro and in vivo (See Sections 6.1 and 6.2 for specific details).

Collagen has a storied history as the preeminent biomaterial of the body and medicine. The current landscape has led to a variety of collagen formats and formulations, which are routinely categorized as crosslinked tissues, decellularized ECMs, insoluble fibrillar collagens, and self-assembling collagens. There exists great promise and potential at the interface of self-assembling collagens, bioinspired multi-scale tissue design, and scalable manufacturing processes for advanced tissue design and fabrication. Additionally, unraveling the mechanisms by which this natural polymer guides fundamental cell behaviors through biochemical and biophysical signaling will continue to inspire approaches to promote tissue regeneration.

2.3 Hierarchical Design of Collagen In Vivo

Understanding the unique hierarchical organization of type I collagen and its associated physical properties, interactions with other biomolecules, and metabolism (turnover) is fundamental to its use in the fabrication of next-generation biomaterials and tissue-engineered medical products. As the most prevalent protein, collagen is widely distributed throughout the body, where it is found in load-bearing tissues (e.g., skin, bone, tendon, cartilage, and blood vessels), organs (e.g., bladder, stomach, and intestine), and other connective tissues (e.g., pericardium, fat, and placenta). Collagen molecules are produced by cells and deposited within the extracellular space, where they self-assemble in a multi-scale fashion to give rise to the fibrillar scaffold of the tissue ECM. As shown in Figure 2.2, this supramolecular assembly involves several aggregation steps: first from single polypeptide chains to a stable triple helical molecule, then to microfibrils, fibrils, and fibers, and finally to macro-scale tissues. Although its primary sequence is identical across tissues, posttranscriptional modifications and formation of intermolecular cross-links contribute to diversification of collagen building blocks, ECM collagen-fibril networks, and therefore tissue-specific form and function[49,50].

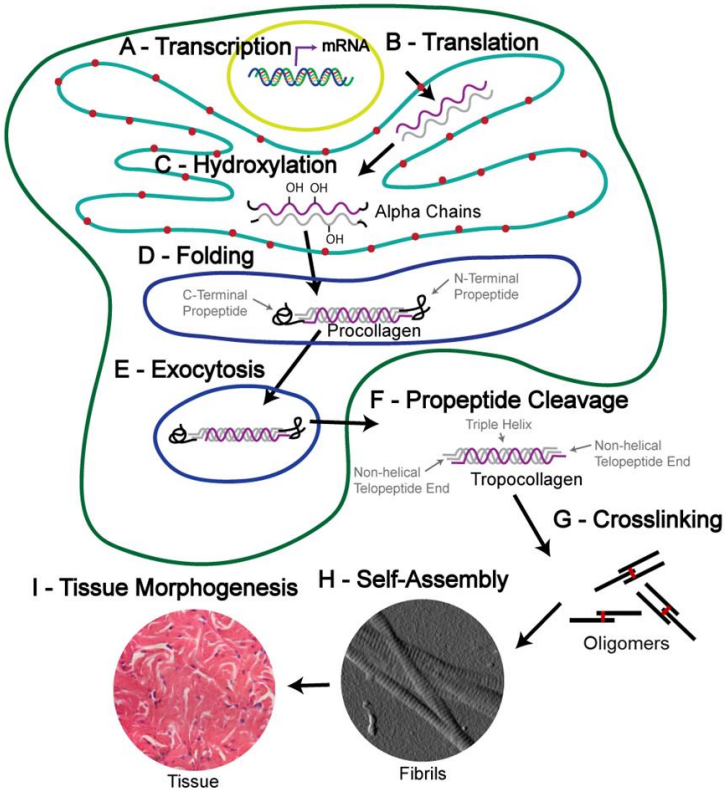

Figure 2.2: Multi-scale assembly of collagen as occurs in vivo. (A) Collagen genes are transcribed from DNA into RNA. (B) Translation of component polypeptide alpha chains by ribosomes and translocation into the rough endoplasmic reticulum. (C) Hydroxylation of alpha chains by lysyl hydroxylases. (D) Folding of trimeric procollagen molecule. (E) Transfer of procollagen to Golgi for additional post-translational modification and packaging for exocytosis. (F) Enzymatic cleavage of propeptide ends yielding tropocollagen molecules. (G) Crosslinking of tropocollagen molecules by lysyl oxidases to form oligomers. (H) Self-assemble of collagen molecules into D-banded fibrils. (I). Fibrils merge to form fibers and networks, giving rise to complete complex tissues architecture.

2.3.1 Biosynthesis of Collagen

The biosynthesis and folding of collagen as it occurs within the cell has been the topic of extensive study since the 1950s. It represents a highly complex process involving various post-translation events, including hydroxylation, glycosylation, trimerization, and cross-linking, so only the fundamentals are covered here. For more comprehensive coverage, the reader is referred to recent reviews[51-53]. Type I collagen is a trimeric protein composed of two α1 and one α2 polypeptide chains. Each of these chains contains the hallmark Gly-X-Y repeat, where X and Y can be any amino acid but are usually proline and hydroxyproline, respectively. This repeating

sequence results in the formation of left-handed helices by component polypeptide chains, the interaction of which results in an overall right-handed triple helical structure. The full-length, processed tropocollagen molecule, which represents the fundamental building block of tissues, is approximately 300nm in length and about 1.5nm in diameter. Mutations in any of the component α chains, particularly ones that cause problems with folding and cross-linking, have significant consequences on tissue architecture and function, such as the heritable disease osteogenesis imperfecta (OI), a potentially lethal brittle bone disease[54].

As outlined in Figure 2.2, synthesis begins with transcription and translation of individual soluble protocollagen chains. Within the endoplasmic reticulum, protocollagen α chains are strategically hydroxylated on proline and lysine residues by specific hydroxylase enzymes. These hydroxylation reactions are important not only for protein folding, but also for downstream intra- and inter-molecular crosslinking. Processed polypeptides then fold and assemble into the procollagen molecule, which contains a central triple-helical region, flanked by non-helical telopeptide and propeptide domains on each end. Terminal propeptides, most notably the one found at the carboxy terminus, and the Gly-X-Y repeats, are critical to proper protein folding[53,55]. This folding and trimerization process is further assisted by molecular chaperones and enzymes[56,57]. Additional post-translational processing of procollagen molecules includes the addition of carbohydrate moieties prior to translocation to the Golgi apparatus, where modification of N-linked oligosaccharides is known to occur.

Secretion of procollagen from cells is similar to that of other extracellular proteins, where molecules passing through the Golgi are packaged into secretory vesicles prior to moving to the cell surface for release by exocytosis. After secretion, amino- and carboxy-terminal propeptides are cleaved by multiple C- and N- terminal proteinases. This conversion is critical for proper self-assembly of fibrils, since tropocollagen has a drastically decreased critical aggregation concentration[53]. In fact, defects in N-terminal proteinase ADAMTS2 (“a disintegrin and a metalloproteinase with thrombospondin repeats”) have been shown to lead to the dermatosparaxis variant of Ehlers-Danlos syndrome, which is characterized by fragile, hyperextensible soft tissues[54].

2.3.2 In-vivo Collagen Self-Assembly and Crosslinking

In contrast to the intracellular biosynthetic pathways described above, the precise mechanisms underlying collagen fibril assembly and tissue-specific organization are less well defined. Various models have been proposed to describe the progressive assembly of micro-fibrils, fibrils, fibers, and fiber bundles; however, significant mechanistic gaps that lack corroborating experimental evidence remain. There is, however, strong support suggesting that molecular aggregation begins within secretory vesicles, with the rest of the assembly process occurring exterior to the cell[53]. An important element of collagen assembly and stabilization is the formation of crosslinks, catalyzed by members of the lysyl oxidase (LOX) family. It is here where divergent theories exist, with lysyl oxidase often portrayed as a "welding" mechanism for already assembled collagen fibers. However, the isolation and properties of soluble collagen oligomers, representing stable cross-linked collagen molecules (e.g., trimers), together with what appears as a strategic tissue-specific distribution of crosslink chemistries (Figure 2.3) challenges this notion[50]. Furthermore, it has been documented experimentally, that LOX is unable to penetrate the fibril surface, despite the presence of crosslinking throughout the fibril.[58] Based upon these findings and our experience with collagen oligomers, we are a proponent of the theory where collagen assembles as prefibrillar aggregates of staggered monomers, with LOX binding and catalyzing the formation of oligomers[58]. In turn, these early oligomer precursors serve as nucleation sites and direct the progressive molecular packing and assembly that ultimately gives rise to tissue-specific ECMs.

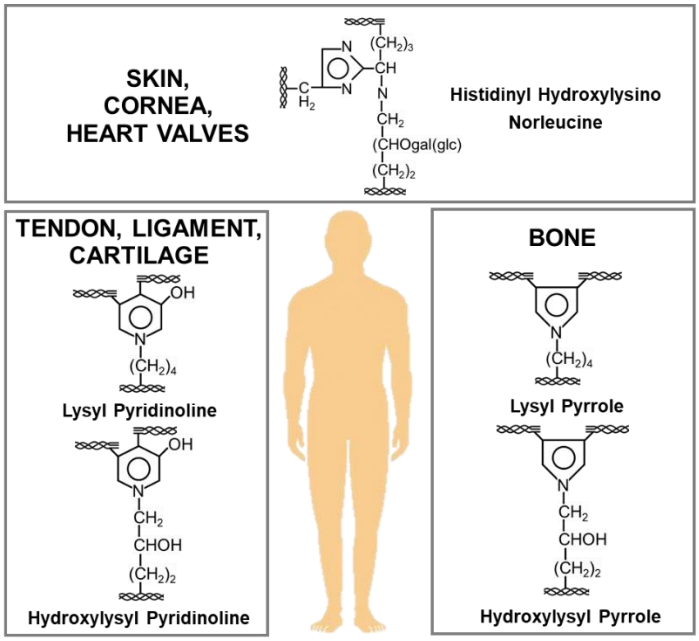

Figure 2.3: Structures of mature, trivalent collagen intermolecular crosslinks and their associated tissue-specific distribution (based on Eyre and Wu, 2005).

Naturally-occurring intra- and inter-molecular collagen crosslinks, which impart mechanical strength to collagen assemblies, have been extensively studied since the 1960s. These bonds form not only between collagen molecules of the same type in homopolymeric fibrils but also between different types of collagen molecules that give rise to heteromeric structures[50]. The significant contribution of different crosslinks chemistries in tissue-specific structure and function can be gleaned by analyzing their distribution (Figure 2.3), where crosslink number and type appear to be associated with mechanical loading and collagen turnover[59,50]. Furthermore, these cross-link chemistries, like the primary sequence of collagen, are well conserved across species. Finally, evidence that cross-link content is a critical determinant of collagen fibril ultrastructure, ECM microstructure, and tissue mechanical properties is derived from numerous hereditable diseases as well as in-vitro and in-vivo studies where specific cross-linking enzymes (e.g., lysyl oxidase or lysyl hydroxylase) are selectively inhibited or genetically knocked out[60-62]. Our own in-vitro work with purified soluble oligomers shows the profound effect of these cross-linked collagen building blocks on the supramolecular assembly, including assembly kinetics, fibril-fibril associations, scaffold mechanical properties and persistence (resistance to proteolytic

degradation), and modulation of fundamental cellular processes, such as vessel morphogenesis and tumor cell invasion.60

The bulk of research defining the basic pathways of collagen crosslinking was performed over 3 decades ago, with the identification of new crosslink chemistries and their implications continuing today. For detailed reviews, see [50,63,64]. In brief, major collagen crosslinks are derived from the oxidative deamination of ε-amino groups of specific lysine and hydroxylysines by LOX within non-triple helical telopeptides regions of the molecules. In turn, the resulting aldehydes react with lysine or hydroxylysine residues within the central triple-helical region of adjacent molecules to form intermediate divalent cross-links of the aldol, hydroxyaldol, or ketoimmine varieties. Upon maturation, these divalent crosslinks convert into more stable trivalent crosslinks such as the histidine derivative histidinyl-hydroxylysino-norleucine (HHL) which is prominent in skin and hydroxylysyl pyrrole which is prevalent in bone.

2.3.3 Supramolecular Collagen Assemblies

The supramolecular assembly of collagen is not random but ordered, and much of the process is inherent to the post-translationally modified molecule itself. While residual propeptides have an inhibitory effect on fibril formation, telopeptides are required for proper molecular registry and alignment[65]. The generally accepted Petruska model of collagen fibril structure is a repeated lattice, where collagen molecules are present in a head-to-tail quarter staggered array generating a characteristic banding pattern with 67nm D-spacing (Figure 2.2). While this general value of D-spacing is most commonly found in the literature, there is ample evidence suggesting that a distribution of values occurs throughout tissues, and may vary with age as observed with estrogen depletion in osteoporosis[66,67]. Additionally, atomic force microscopy, x-ray diffraction, and crystallography studies have elucidated more complex 3D structures within fibrils, including polar ends, tilted or twisted molecules, and crystalline and disordered regions[68-70]. Oligomers may serve to nucleate formation of branch sites or connections between fibrils during self-assembly, providing an additional mechanism of stabilization[71]. In turn, these fibrils and their networks merge as well as entangle with each other to form larger composite structures such as fibers, bundles or fibrils, and lamellae. Tissues contain an array of higher-order collagen network structures that might be recreated in tissue engineering to give rise to improved functional outcomes. For example, skin is well-known for its anisotropic basket weave structure that

contributes to its multiaxial tensile strength[72-74]. Tendons are composed of criss-crossing fibers densely bundled in parallel, making them ideally suited for their load-bearing function[75]. Other unique structures include the orthogonal lattice of the cornea[76] and the parallel lamellae in osteons of bone[77].

The high conservation of collagen's primary sequence and crosslink chemistries across species illustrate their importance as determinants of tissue form and function[50]. Collagen molecules also contain many critical functional domains (motifs) that allow adhesion of cells, binding to other ECM molecules and growth factors, and control of proteolytic degradation. In fact, one fundamental reason why synthetic polymers have failed to displace collagen as a leading tissue engineering material is because of the immense biological activity held in its multifunctional domains. A comprehensive summary and diagram of these various domains has been provided by Sweeney and co-workers.[78] Reciprocal binding interactions between collagen, growth factors, heparin, fibronectin, and other matrix components lends further stability, fluid retention, and biological signaling capacity to the ECM.[79] Collagen is recognized by several cell surface receptors including integrins, DDR receptor tyrosine kinases, glycoprotein VI for platelet adhesion, and inhibitory immune receptor LAIR-1.[80] Of these, integrins are exquisitely mechanosensitive and a prime target for tissue engineering and regeneration design.

2.4 Biomechanics and Mechanobiology of Collagen

Energy storage, transmission, and dissipation are some of the key mechanical functions provided by ECMs, contributing to bulk tissue mechanical properties as well as guiding cellular behavior through mechanochemical transduction. The hierarchical structure of collagen lends itself to both experimental and computational approaches for deciphering structure-function relationships at the various size scales as well as determining how forces are transmitted between the matrix and resident cells.

2.4.1 Scaffold and Tissue Biomechanics

To date, measurements of mechanical properties have been made on single molecules, individual collagen fibrils, collagen fibers, as well as native and engineered collagen tissues, with atomic force microscopy (AFM) serving as an important tool at the smaller size scales[81-83].

From these efforts, the elastic modulus, which provides a measure of rigidity or stiffness, and the fracture strength for a single tropocollagen molecule, has been estimated at 6-7GPa and 11GPa, respectively, supporting its role as a "rigid rod"[84]. As we move up size scales, the mechanical properties of fibrils, fibers, and tissues are somewhat less and largely a function of their nano- and micro-structural organization.

The diversity of tissue mechanical properties is a manifestation and optimization of collagen structure on its various size scales. In general, collagenous tissues exhibit a characteristic non-linear stress-strain behavior with characteristic strain-stiffening, where the network becomes more rigid with increased deformation[85]. The small strain region, also known as the toe region, corresponds to removal of crimp, both at the molecular and fibrillar levels. The following phase of mechanical testing is a linear region, where the stiffness of collagen fibrils increases considerably with extension. This region has been associated with stretching of collagen triple helices or of the crosslinks between helices, implying a side-by-side gliding of neighboring molecules. Finally, at failure, a disruption of component fibrils occurs. It is well established that initial loading curves for collagenous tissues are different from subsequent loadings, therefore conventionally tissues are "preconditioned" via application of several loading and unloading cycles prior to measurement of mechanical properties. Preconditioning assists in reducing the contributions weak bonds/entanglements and the subsequent reorientation of component fibrils[86,87]. The stress-strain response is also sensitive to strain rate, a characteristic of viscoelastic materials. Other behaviors exhibited by tissues and other viscoelastic materials include hysteresis—time-based dependence of a material's output on its history, stress-relaxation—decrease in stress in response to a persistent strain (deformation), and creep—tendency to deform in response to a persistent stress[88-90].

Experimental studies on intact tissues and engineered collagen-fibril constructs as well as computational simulations indicate that key determinants of tissue viscoelastic and poroelastic properties include intrinsic stiffness of the constituent fibrils, interfiber connectivity (branching, bundling), fibril/fiber dimensions (length and diameter), and interactions between insoluble collagen fibrils, other ECM components, and the surrounding interstitial fluid. For example, when fibrils are aligned in parallel to the applied force, constructs fail at lower strain but higher stress values than those with more random fibril organizations. With aligned fibrils, low levels of deformation are required for their recruitment and reorganization in the axis of extension, where

they are able to bear load. By contrast, with randomly organized fibrils, higher deformation levels are required for fibril reorganization and not all fibrils are positioned to bear load due to bending or buckling. In addition, while fibril diameter and length certainly contribute to bulk mechanical properties, fibril connectivity is likely the most important determinant, with native and engineered tissues with increased fibril connectivity (branching) and stronger fibril-fibril associations (bundling) able to store increased elastic energy. Supporting this notion we find Young's modulus values for tendon, where fibrils and fibers are parallel aligned are 43-1600 MPa, while reported values are 21-39 MPa for dermis with its basket weave construction and 0.6-3.5 MPa for artery and vein with their layered laminae[91]. The high tear-resistance of skin also has been attributed to unique features of collagen networks, namely fibril straightening and reorientation, elastic stretching and interfibrillar sliding, which redistribute stresses and do not allow tear propagation[92]. While these molecular level events associated with preyield deformation of tissues are fairly well established, those that occur from the yield point to tissue failure (post yield) are less well defined. A number of studies on the overloading of tendon have documented fibril dissociation into their fine subfibrillar components[93,94], while others report events associated with molecular unfolding[95,96].

2.5 Mechanobiology and Functional Tissue Engineering

Since the early days of tissue engineering, significant focus has been placed creating constructs that matched the physical characteristics of natural tissues, such as geometry and structure, or the mechanical measures, such as Young's modulus (stiffness) or failure strength. However, with the advent of mechanobiology, it is now recognized that cells can sense and respond to mechanical cues at the molecular and micro-scale levels, just as easily as they do chemical ones. Now, tissue design has shifted from simply mimicking the physical properties (e.g., architecture, mechanical properties) of tissue to focusing on creating biomaterials that provide the correct mechanochemical signals to direct cell phenotype and function as well as tissue morphogenesis[97]. This viewpoint was formalized as "functional tissue engineering" in 2000 by a United States National Committee on Biomechanics subcommittee. Their main goal was to increase awareness of the importance of engineered tissue biomechanics by identifying criteria for mechanical requirements and encouraging tissue engineers to incorporate biomechanics into their design process.[98] This encourages a more multi-scale design approach to tissue engineering and

regeneration strategies, which is more focused on guiding the cell response, including therapeutic cell populations within the construct as well as host cells. This perspective is further bolstered by advancements in the stem cell area, where plentiful numbers of multi-potential cell populations can be harvested directly from tissues (e.g., fat, bone marrow, blood) or developed from induced pluripotent stem cells, which are created by reprogramming skin or blood cells into an embryonic-like pluripotent state.

When approaching tissue fabrication, whether in the body or man-made, it is important to understand how hierarchical collagen construction contributes to not only tissue-level mechanical properties but also transmission of loads across size scales to cells and vice versa. Biophysical cues such as those originating from the ECM microstructure and mechanical properties are now recognized as major signaling sources, regulating growth and differentiation of cells[99]. It's important to note that this transmission of biophysical signals is a two-way street, evoked by the contractile machinery of resident cells or by loads applied externally. This exchange of biophysical information is further facilitated by the physical connectivity between cells and collagen fibrils, which in large part is mediated through specific cell surface receptor proteins known as integrins. It was Donald Ingber that first depicted the dynamic force balance that exists between cells and their ECM using the popular tensegrity model, where cytoskeleton and ECM form a single, tensionally integrated structural system[100]. It is at this interface where specific design criteria and constraints for advanced tissue fabrication continue to emerge. While certainly a difficult task, sophisticated methods designed to probe biophysical and biomolecular responses of living cells within tissues continue to assist in elucidation of the mechanochemical signaling that occurs from tissue level through the ECM to the cell nucleus.

2.6 Collagens as a Natural Polymer for Custom Tissue Fabrication

Because type I collagen is one of most commonly used biomaterials in both research and clinical settings, there exists a wide variety of formulations, as alluded to in Sections 1 and 2. Most collagen-based products used clinically represent processed intact tissues (e.g., decellularized tissues) or insoluble fibrillar collagen (e.g. sponge, particulate) in various formats, with only a few products prepared from self-assembling collagens. This section focuses on advancements related to self-assembling collagen formulations and their potential for multi-scale tissue design. We begin with molecular and micro-level design control, identifying how specific collagen building blocks,

assembly conditions, and exogenous crosslinking affect the microstructure of engineered biomaterials and tissues. This is followed by a description of higher-level fabrication and manufacturing techniques for controlling macro-scale properties, including 3D geometry and physical properties (e.g., mechanical strength and stiffness). Special emphasis is placed on the cellular response, whether in vitro or in vivo, documenting its dependence upon multiple size scale features, extending from molecular to macroscopic.

2.6.1 Micro-Scale Design Control

The first fundamental level of design control for collagen materials resides at the molecular level. Molecular level features largely determine the achievable range of chemical, biological, and physical attributes of resulting scaffolds and tissue constructs; however, user control at this level is often overlooked.

2.6.2 Molecular Building Blocks

The molecular make-up, structure, and self-assembly capacity of various collagen building blocks are summarized in Table 1, where extraction, processing and reconstitution techniques are known to be a source of variation. Insoluble fibrillar collagen, which is the starting material for many freeze-dried collagen and collagen-glycosaminoglycan sponge products, represents a particulate of undissociated collagen fibers isolated and purified from comminuted tissues. While this form of collagen does not self-assemble or offer molecular and fibril-microstructure control, it does aggregate to form a viscous gel or slurry when swollen in acid or hydrated in phosphate buffered saline, which has proven useful for various medical applications. As documented by Yannas and Burke and others, insoluble fibrillar collagen supports cell adhesion and offers design control of larger scale material features such as particulate content, porosity, and resorption rate[33,31,32].

Table 1. Summary of collagen building block characteristics and their associated level of design control for engineered biomaterials and tissues.

Building Block	Molecular Composition, Structure, and Self-assembly Capacity	Design Control
Fibrillar Collagen	• Insoluble • Collagen fiber particulate processed and purified from comminuted tissues • Does not exhibit self-assembly	• Macrolevel
Atelocollagen	• Soluble • Tropocollagen molecule devoid of telopeptide ends • Exhibits fibril assembly with modified or no D-banding • Contains collagen functional domains	• Microlevel • Macrolevel
Telocollagen	• Soluble • Telopeptide ends allow for formation of D-banded fibrils • Contains collagen functional domains	• Microlevel • Macrolevel
Oligomer	• Soluble • Aggregates of tropocollagen molecules (e.g., trimers) that retain natural intermolecular crosslink • Exhibits fibril and suprafibrillar assembly with D-banding and high fibril-fibril connectivity or branching • Contains collagen functional domains	• Microlevel • Macrolevel
Recombinant	• Soluble • Recombinant human procollagen • Post-translational modification requires co-expression of relevant enzymes • Endopeptidase treatment yields self-assembling atelocollagen • Contains collagen functional domains	• Molecular • Microlevel • Macrolevel
Collagen Mimetic Peptides	• Soluble • Peptides (~30-60 amino acids) containing repeats of helical region sequences • Self-assembly into helices and fibers largely driven by electrostatic interactions • Lack collagen functional domains	• Molecular • Microlevel • Macrolevel

Unlike fibrillar collagen, other collagen building blocks do have the capacity to self-assemble or form fibrils in vitro, providing control over molecular and fibril microstructure features. The ability of relatively pure collagen molecules to spontaneously form fibrils when brought to physiologic conditions (pH and ionic strength) and warmed was first reported by Gross in the 1950s and has since been the subject of extensive research[101,38]. Collagen is routinely extracted and purified from various tissue sources (rat tail tendon or calf skin) using either dilute acid or enzymatic digestion (pepsin), yielding a solution composed predominantly of single molecules (monomers)[43]. Historically, cross-linked oligomers and insoluble molecular aggregates that accompanied monomers were viewed as undesirable by-products, especially for studies focused on collagen molecule structure and fibril assembly[102]. In fact, enzymatic digestion, secondary purification strategies, or young or lathrytic animals were routinely used to minimize or eliminate these components[103,30,104,105]. Acetic acid extraction followed by salt precipitation is one of the most common approaches used to generate telocollagen, which represent full length tropocollagen molecules with telopeptide regions intact[106]. The addition of pepsin to the extraction mixture increases yield but causes cleavage of telopeptide regions, giving rise to atelocollagen[107]. More recently, a sodium citrate extraction process was applied to porcine dermis, generating a high fraction of soluble oligomeric collagen for biomaterials development[42,48]. Oligomers represent aggregates of individual collagen molecules (e.g., trimers) that retain their natural intermolecular crosslinks.

Monomeric collagens, specifically telocollagen and atelocollagen, continue to be the most commonly used self-assembling collagens because of their relatively facile extraction and commercial availability. However, the shortcomings of these preparations are well established and commonly cited by users, including lot-to-lot variability in purity and self-assembly capacity, long polymerization times (often >30 minutes), lack of user control, low mechanical strength, and poor stability in vitro and in vivo[42,43,108]. When comparing telocollagen and atelocollagen, it has been shown that telopeptide preservation is important for the thermal stability of the collagen triple helix and the organized arrangement of collagen molecules into fibrils[109,51]. The loss of the telopeptide regions in atelocollagen significantly hinders and slows assembly kinetics, resulting in less organized fibrils that vary in size and lack natural D-banding pattern[110,107,111]. This difference in molecular chemistry and fibril microstructure also affects matrix physical properties

and proteolytic resistance, with atelocollagen generating weaker (i.e., Young's modulus and yield strength) constructs that are more prone to rapid dissolution and proteolytic degradation[112,42].

Oligomers, a more recently-discovered collagen building block, appear to play a critical role in collagen self-assembly, both in vitro and in vivo. Over the past decade, oligomer preparations have proven to be quite robust and reproducible, exhibiting rapid polymerization (<1 minute at 37^{o}C) and generating distinct fibril microstructures compared to telocollagen and atelocollagen formulations[48,42,113]. Since oligomers retain intermolecular crosslinks, they exhibit a higher average molecular weight compared to monomers and a distinct protein and peptide banding pattern[48,42]. In addition, the presence of cross-linked oligomers induces fibrillar as well as suprafibrillar assembly, resulting in networks with high fibril-fibril connectivity and branching. These higher-order assembly properties support formation of collagen scaffolds that not only retain their shape but exhibit a much broader range of physical properties and slow turnover (Figure 2.4)[111,42,113]. In particular, collagen oligomer scaffolds demonstrate significantly increased shear, tensile, and compressive moduli compared to their monomeric counterparts (Figure 2.4C-E). Since these parameters increase linearly or quadratically with oligomer concentration, differences become even greater at high concentration. The improved stability and mechanical integrity exhibited by oligomer effectively eliminates the need for exogenous crosslinking, which is routinely applied to constructs produced from monomeric collagens[85,114].

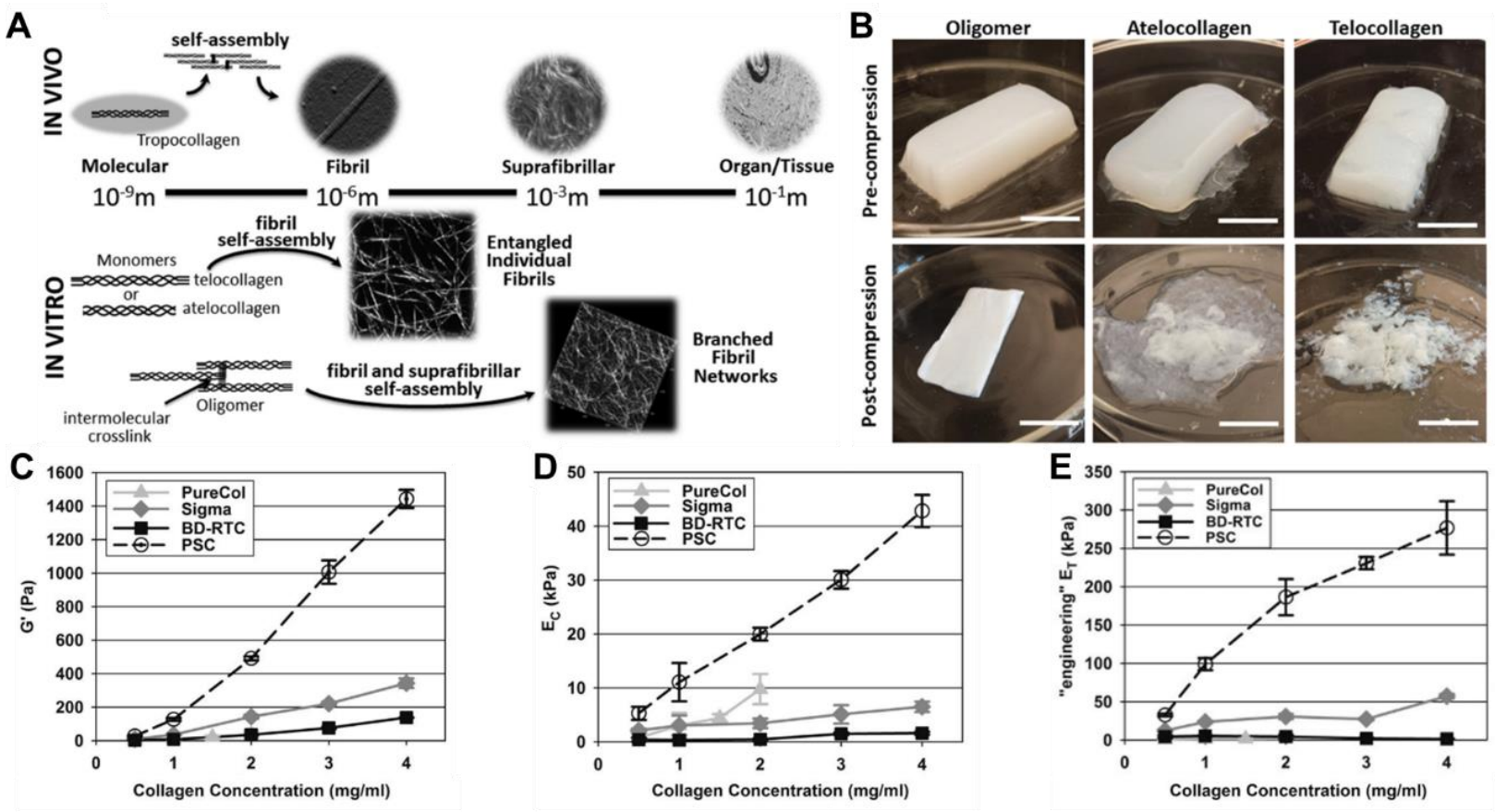

Figure 2.4. Self-assembly of collagen and comparison of different collagen formulations. A. Hierarchical, multi-scale assembly of type I collagen as occurs in vivo and in vitro with polymerizable monomer (atelocollagen and telocollagen) and oligomer formulations. (Reprinted with permission from Blum et al., 2016) B. Representative images of oligomer, atelocollagen, and telocollagen constructs before (3.5 mg/mL) and after (24.5 mg/mL) confined compression (86% strain or 7×), demonstrating differences in shape retention and mechanical properties. Scale bars = 2 mm. (Reprinted with permission from Blum et al., 2016) C.-E. Comparison of mechanical properties, including C) shear storage modulus (G'), unconfined compressive modulus (Ec), and tensile modulus (ET), for oligomer (PSC) and commercial atelocollagen (PureCol) and telocollagen (Sigma, BD-RTC) formulations. (Reprinted with permission from Kreger et al., 2010).

Other approaches for generating purified collagen molecule preparations, especially human, include recombinant technology or peptide synthesis. Production of collagen molecules and peptides via these techniques supports design control at the molecular level (Figure 2.5A), which is especially useful for elucidating relationships between specific molecular motifs/domains and functional properties.[115] To date, researchers have successfully genetically modified mammalian, bacterial, and plant systems to produce recombinant human procollagen, from which self-assembling collagen formulations can be derived[116-119]. One of the challenges associated with recombinant collagen production has been the ability to introduce and co-express various genes involved in collagen post-translational modifications, including prolyl-4-hydroxylase and lysyl hydroxylase, which are necessary for triple-helix stabilization.[120] To date, a number of groups have overcome this obstacle, successfully generating stable procollagen triple helices.[121-125] Since procollagen molecules are unable to undergo self-assembly due to the presence of propeptide ends, endopeptidase treatment (e.g., pepsin, ficin) is routinely applied to yield fibril-forming recombinant human atelocollagens.[115,126] At present, atelocollagen produced recombinantly yields thinner fibrils with less mechanical integrity than their tissue-derived counterparts (Figure 2.5B).[127] Researchers focused on recombinant collagen development for biomedical applications continue to work to scale their processes to support more cost-effective, large-scale production.[115,121]

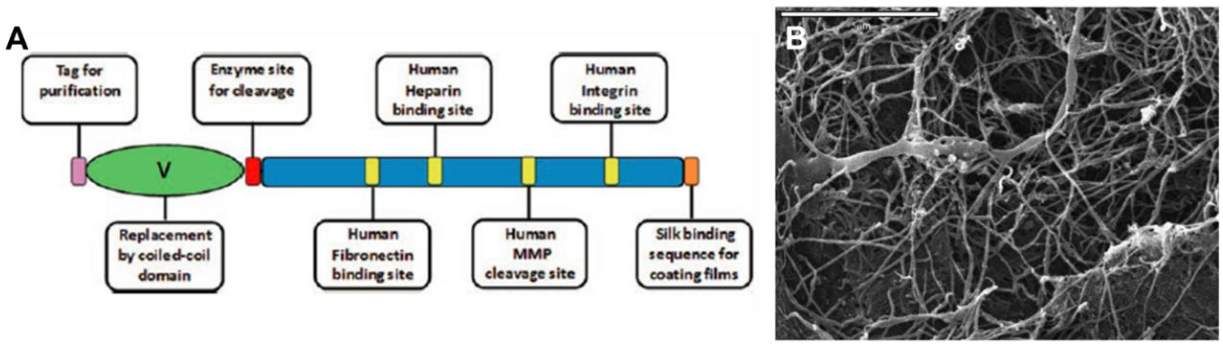

Figure 2.5. Examples of the utility of recombinant collagens. A. Schematic representation of recombinant bacterial collagen construct, showing examples of possible sequence manipulations. (Reprinted with permission from Brodsky and Ramshaw, 2017) B. Scanning electron microscopy of fibrils formed from purified recombinant human atelocollagen produced in tobacco plants. Scale bar = 5μm (Reprinted with permission from Stein et al., 2009)

Collagen mimetic peptides (CMPs) produced using synthetic chemistry methods are another means of achieving molecular-level design control.[128] Relatively short sequences, roughly 30 amino acids in length, are synthesized with the goal of forming homo- or hetero-trimeric collagen helices, which in turn self-assemble into fibrils. The majority of sequences consist of amino acid triplet repeats found within the helical region of collagen, capitalizing on electrostatic forces to drive molecular assembly. While a number of groups have created CMPs that generate fibrils, creating peptides that mimic the various levels of collagen supramolecular assembly, including staggered alignment, has been a challenging.[123] In 2009, Chaikof, Conticello and co-workers reported a CMP that, in part, formed fibrils with a regular D-spacing pattern; however, the periodicity was about 18nm rather than the characteristic 67nm observed in native collagen fibrils (Figure 2.6A)[125]. Building off this work, O'Leary and colleagues prepared a new CMP, where arginine residues were replaced with lysine and glutamate residues were replaced with aspartate, to give the sequence (Pro-Lys-Gly)4(Pro-Hyp-Gly)4(Asp-Hyp-Gly)4[129]. These CMPs showed improved fibril- and hydrogel-forming characteristics, giving rise to shape-retaining gels as shown in Figure 2.6B. Finally, although functional domains, such as integrin binding sequences (e.g. GFOGER), can be engineered into CMPs, size constraints inherent to peptide synthesis (about 60 amino acids or less) preclude the inclusion of all functional collagen domains, thereby limiting overall biosignaling capacity[130].

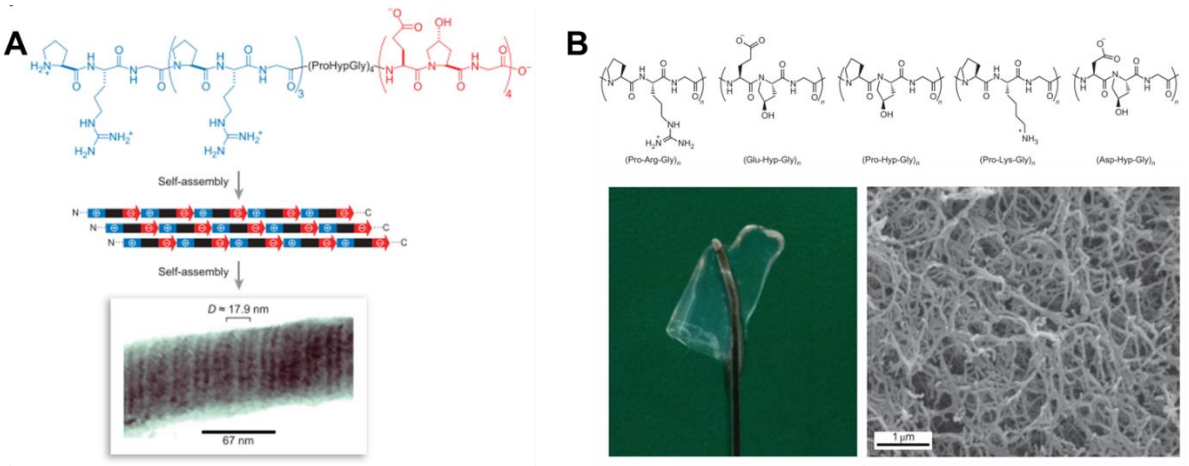

Figure 2.6. Notable examples of self-assembling CMPs. A. Schematic of CMP and associated Coulombic forces between cationic and anionic blocks that yield self-assembled fibrils. Transmission electron microscopy image of CMP fibril shows D-periodicity with D=17.9nm. Natural type I collagen has D□67nm. (Reprinted with permission from Shoulders and Raines, 2009). B. Chemical structure of the common amino-acid triplets used to generate CMPs. Photo and scanning electron microscopy image show shape-retaining fibrillar gel (1%) formed following self-assembly of CMPs consisting of $(Pro\text{-}Lys\text{-}Gly)_4(Pro\text{-}Hyp\text{-}Gly)_4(Asp\text{-}Hyp\text{-}Gly)_4$. (Reprinted with permission from O'Leary et al., 2011)

2.6.3 6.1.2 Polymerization Conditions

In addition to the various collagen building blocks described above, there are a wide variety of external means by which collagen self-assembly can be modulated to create hydrogels, matrices, and scaffolds with distinct structural and physical properties. This section summarizes various conditions, such as concentration, pH, temperature, and ionic strength, that have been used to modulate collagen assembly kinetics and outcomes. These conditions can be carefully controlled to modulate fibril density, fiber length, fibril diameter, fibril-fibril associations (e.g., branching), and pore size, all of which, in turn, determine functional physical properties, including strength, stiffness, fluid and mass transport, and proteolytic degradation. When cells are encapsulated in these self-assembled collagen matrices, they quickly adhere to the collagen fibrils, sensing and responding to differences in microstructure mechanical properties[131-133]. Through this mechanotransduction signaling, fundamental cell behavior is modulated, including cell-induced matrix contraction and remodeling, morphogenesis, proliferation, migration, and differentiation. Additionally, these microstructure features dictate how external mechanical loads are transmitted from the construct or macro-level to resident cells[134].

A landmark study by Wood and Keech in 1960 showed that increasing collagen concentration or temperature, and decreasing pH and ionic strength, accelerated the formation of individual collagen fibrils[135]. Additionally, they reported that higher temperatures, increased pH, and lower ionic strengths yielded thinner fibrils; however, no correlation was made between structural and mechanical properties of resulting fibrils was provided[135]. The effects of temperature, pH, and ionic strength on fibril assembly of telocollagen have been confirmed by many, and studies have expanded to include more detailed mechanical characterization[136-140]. In addition to the effects on self-assembly kinetics, increasing the temperature or pH of the reaction results in decreased pore size and fibril diameter, which have been shown to increase compressive, tensile, and shear storage moduli[136-139]. The effect of ionic strength on matrix mechanics seems to be dependent on pH and temperature, thus making distinctive trends difficult to decipher[138].

Collagen concentration is another primary means by which many researchers vary matrix mechanics, since increasing collagen concentration leads to increased fibril density which increases matrix stiffness (compressive, tensile and shear)[42,131,136]. In attempts to independently control collagen fibril density and matrix stiffness, many have created composite systems, sometimes termed interpenetrating networks, composed of mixtures such as gelatin and collagen[141], alginate and collagen[142], polyethylene glycol and collagen[143]. Whittington and co-workers identified another approach for independently controlling fibril density and matrix stiffness which did not rely on non-collagenous agents. Here, the total content and ratio of type I collagen oligomers to monomers were used to independently vary fibril density and the extent of fibril-fibril branching, both of which are known determinants of in-vivo ECM stiffness[71,144].

Another way in which researchers have attempted to gain design control of collagen self-assembly is motivated by the fact that collagen fibrillogenesis and assembly in vivo is guided by other collagenous and non-collagenous proteins and proteoglycans of the ECM. For example, fibronectin and collagen assembly in vivo are known to be reciprocally dependent such that interruption of one decreases the other.[145] However, early experimental evidence from Brokaw and co-workers suggested that in vitro, the addition of fibronectin only affected collagen self-assembly kinetics, with no changes in the resulting microstructure.[146] On the other hand, it has also been shown that co-polymerization of fibronectin with collagen increases the tensile strength of formed matrices, supporting the notion that fibronectin affects collagen fibril organization and microstructure[147]. Type V collagen also affects in-vivo collagen assembly, where it is thought

to serve as a nucleation site and loss-of-function mutations are embryonic lethal characterized by lack of collagen fibril formation in the mesenchyme.[145] While type I collagen can self-assemble in vitro without type V collagen, Birk et al. showed that the presence of collagen V during in vitro self-assembly yielded heterotypic fibrils with decreased diameter and altered D-periodicity.[148] More recently, Piechocka et al. demonstrated that these relatively minor changes in microstructure caused drastic decreases in shear storage modulus.[149] These authors propose that this discrepancy between in-vitro results and in-vivo mechanisms may be due to the fact that the type V collagen used in vitro is pepsin treated and lacks the N-propeptide region which is present during in-vivo ECM assembly. One final example demonstrating how other ECM components guides collagen assembly and mechanics involves dermatan sulfate (DS)- and chondroitin sulfate (CS) GAGs, along with CS-proteoglycan and DS-proteoglycan (decorin). Interestingly, it has been reported that addition of glycosaminoglycans does not significantly affect microstructure or tensile strength, while addition the respective proteoglycans enhances tensile strength due to a decrease in fibril diameter and inhibition of fibril aggregation[150-152]. Collectively, these studies highlight the impact of other ECM components on the hierarchical organization of collagen. Discrepancies between in vivo and in vitro results, as well as between studies reveal the sensitive nature of these reactions and their dependence of specific molecular features and reaction conditions. Continued elucidation of mechanisms underlying supramolecular collagen assembly both in vivo and in vitro will continue to inspire tissue engineering and regeneration design strategies.

2.6.4 Exogenous Crosslinking

Mechanical integrity, metabolic turnover, and degradation resistance are properties afforded to in-vivo collagen assemblies, in part, by the formation of natural intra- and inter-molecular crosslinks as described in Section 3.2. These natural crosslinks are controlled via post-translational modifications and enzymatic reactions that occur within and outside the cell, respectively, making them difficult to recreate in vitro[50]. The application of oligomeric collagen allows tissue-engineered constructs to capture some of the performance characteristics imparted by natural intermolecular crosslinks. However, for materials produced from insoluble fibrillar collagen or self-assembling monomeric collagens, the development and application of exogenous

physical and chemical crosslinking is commonplace to improve mechanical properties and proteolytic resistance[153].

Glutaraldehyde is one of the most commonly employed chemical crosslinking agents[154]. It is well established that glutaraldehyde enhances collagenous material stiffness, strength, and resistance to proteolytic degradation through formation of intramolecular and intermolecular crosslinks by non-specifically reacting with lysine and hydroxylysine residues on collagen[155]. Despites its widespread use, glutaraldehyde is far from ideal as its crosslinks are transient and release of glutaraldehyde monomers over time which is cytotoxic[153,156]. Additionally, calcification of glutaraldehyde cross-linked tissues upon implantation remains a challenge[157,158].

Dehydrothermal treatment (DHT) and ultraviolet (UV) radiation have been examined as alternatives to glutaraldehyde since the 1980s[156,159]. DHT and UV crosslinking methods are thought to be advantageous because they do not introduce any exogenous toxic chemicals; however, these treatments are been shown to induce partial denaturation or fragmentation of collagen[153]. Carbodiimide treatment is another technique used to form amide-type bonds within collagen. Here, the only by-product is urea, which can be washed away after crosslinking.[153] The combination of 1-ethyl-3-(3-dimethylaminopropyl)-carbodiimide hydrochloride with N-hydroxysuccinimide (EDC/NHS) is the most commonly used strategy and has been applied both during and after self-assembly of monomeric collagen to enhance scaffold strength[160]. Interestingly, when EDC crosslinking was applied to scaffolds created from oligomeric collagen, it did not enhance the mechanical properties thus suggesting that the presence of the natural intermolecular crosslink outweighs the effect of these unnatural chemistries[161]. It is important to note that owing to their non-specificity and cytotoxicity, the majority of exogenous crosslinking strategies are incompatible with self-assembled collagen constructs formed in the presence of cells.

Enzymatically crosslinking collagen with lysyl oxidase and transglutaminase or generating advanced glycation end-products (AGE) with sugars such as ribose are crosslinking strategies that appear to be more compatible with cells, however they only modestly improve mechanical strength and are reported to be cost-prohibitive for large/clinical scale applications[153,162]. Despite being non-cytotoxic in the short term, non-enzymatic glycation, as occurs during ageing and pathological processes such as diabetes, has been linked to reactive oxygen species production and cellular inflammation via the receptor for advanced glycation end products (RAGE) pathways, suggesting

this method of crosslinking may be suboptimal for many engineered products intended to for permanent tissue replacements[163]. Finally, genipin, a plant-derived chemical used in traditional Chinese medicine is another collagen crosslinker that has been shown to be cell-compatible at low concentrations[162,164]. However, genipin turns cross-linked collagenous materials blue and upon in-vivo implantation induces inflammation and an associated foreign body response, although the extent is reduced compared to glutaraldehyde[165,166].

Collectively, molecular and microscale features, including molecular composition, endogenous or exogenous crosslinking, and fibril ultrastructure and architecture, are important considerations when designing next-generation tissue engineering and regenerative medicine strategies. This is especially true when working to promote a regenerative phenotype since cells naturally interface with collagen at these levels and can readily detect and respond to changes at these size scales.

2.7 Meso- and Macro-scale Design Control

The ECM component of tissues has a complex construction with spatial gradients, anisotropies, and higher-order structures. By contrast, the majority of constructs formed by encapsulation of cells within self-assembling collagens in vitro represent isotropic random fibril networks, and are often limited in concentration or fibril density due to the solubility and phase behavior of collagen. For accurate recreation of tissues, the density and spatial organization of the collagen-fibril ECM is an important design consideration. Historically, these meso-scale features have been difficult to control, making the engineering of functional tissue replacements challenging. Recent years have seen the rise of process engineering and manufacturing techniques to address these challenges.

2.7.1 Compression

Initial efforts to convert polymerized collagen-fibril matrices into constructs with tissue-like histology and consistency relied on the remodeling properties of cells to densify or compact surrounding collagen fibrils. More specifically, collagen-fibril matrices seeded with fibroblasts and cultured up to 2 weeks yielded contracted or condensed dermal-like tissue equivalents[41]. Seeding keratinocytes on the surface of these dermal equivalents resulted in the formation of a

multilayered epidermis, yielding a tissue-engineered living skin, which ultimately was produced by Organogenesis and gained FDA approval in 1998 for management of diabetic ulcers and hard-to-heal venous ulcers. Persistent drawbacks to this product include its costly manufacturing process, limited shelf-life (5-10 days) and the slight risk of disease transmission, all of which are due to the requirement of allogeneic cells to contract and further mature the ECM and finished product[167].

In 2005, Brown described a process designed to "engineer tissue-like constructs without cell participation." This "cell-independent" approach involved polymerization of monomeric collagen in the presence or absence of cells followed by plastic compression (PC) in an unconfined format and/or capillary fluid flow into absorbent layers to reduce the interstitial fluid content[168]. Here, low-loads (50-60 g or 1.1 kPa) are applied to the top surface of a collagen matrix to achieve significant fluid reduction (approximately 85-99.8% compressive strain) through a supporting nylon mesh (Figure 2.7A). The resulting densified collagen sheets, which measure 20-200μm in thickness are still fragile, requiring spiraling and multiple compressions to facilitate handling and further mechanical testing. Tensile strength and modulus values of 0.6 ± 0.11 MPa and 1.5 ± 0.36 MPa, respectively, have been supported with 85% viability of encapsulated cells[169]. Additional compression of spiraled constructs improves mechanical integrity but reduces cellular viability[169,170]. This technology contributed to development of the RAFT 3D Cell Culture System by TAP Biosystems (now part of Sartorius Stedim Biotech Group), which applies their patented absorber technology to monomeric rat tail collagen to create densified tissue constructs for research applications.

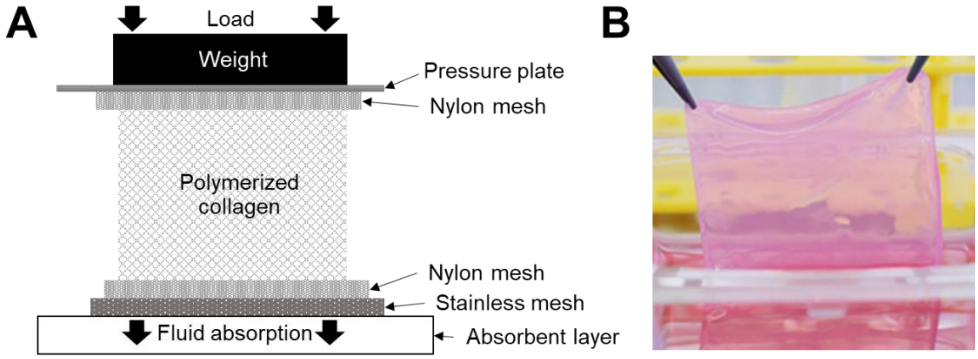

Figure 2.7. Densification of collagen-fibril constructs through plastic deformation achieved with unconfined compression and absorption. A. Plastic compression is achieved by applying known weights to low-density collagen-fibril matrices to achieve fluid reduction through a supporting nylon mesh into an absorbent layer (based on Brown et al., 2005). B. Dermo-epidermal skin substitute produced by densification of monomeric type I collagen in the presence of human dermal fibroblasts. Seven days following culture the collagen-fibroblast construct was seeded with human keratinocytes. (Reprinted with permission from Braziulis et al, 2012)

An adaptation of this PC technology was reported by Reichmann's group for generation of an autologous tissue-engineered skin. This work involved custom-fabrication of a large (7x7cm) compression chamber, fashioned to support weights on top and absorbent filter paper on the bottom[171]. This device was used to cast square polymerized collagen matrices containing human dermal fibroblasts, which in turn were compressed to 0.5-0.6 mm thickness and then transferred to culture dishes. Following 7 days of culture and maturation in vitro, a high density of keratinocytes was applied and cultured for an additional 7 days. To date, analyses of histological outcomes as well as gene expression of relevant dermal and epidermal markers have been conducted[172,171]; however, mechanical properties testing has yet to be reported. This tissue-engineered autologous dermo-epidermal skin graft, referred to as denovoSkin (Figure 2.7B), has obtained orphan drug designation as a treatment for burns by Swissmedic, European Medicine Agency, and the FDA. Reports indicate that this product can be safely and conveniently handled by surgeons, and matures into high quality skin in animal models as well as recently performed clinical studies[172].

Expanded efforts on this front, include work by Voytik-Harbin and collaborators where scalable plastic compression processes have been applied to type I oligomeric collagen, providing increased versatility in product design and geometry as well as predictive meso-scale control[173,111]. As mentioned previously, type I oligomeric collagen exhibits not only fibrillar

but also suprafibrillar assembly, yielding highly interconnected collagen-fibril scaffolds with substantially improved proteolytic resistance and mechanical integrity compared to standard monomeric collagens. In this work, plastic compression was applied in a confined, rather than an unconfined, format to increase fibril density via controlled fluid removal (Figure 2.8A). Interestingly, this approach was not applicable to monomeric matrices due to the inability of the resultant fibril microstructure to sustain or support associated compressive and fluid shear forces[111]. This fabrication process provided control of the final solid fibril content (fibril density) of the compressed construct through modulation of starting volume and concentration of the oligomer solution together with the applied compressive strain[173]. Additionally, strain rate was used to control steepness of fibril density gradient, and placement of porous polyethylene foam and associated porous-solid boundary conditions defined high-order spatial fibril organization (e.g., alignment). Finite element analysis confirmed this process to be dependent upon the fluid flow induced during compression, with steepness of gradient formation dependent on strain rate[173]. These early findings support the notion that controlled, plastic compression together with computational models could be used for predictive design and scalable manufacture of a diverse array of precision-tuned tissue constructs. To date, this fabrication method has been applied for the development of cartilage constructs for laryngeal reconstruction[174,175], articular cartilage constructs with continuous fibril density gradients that recapitulate the different histological zones in native cartilage (Figure 2.8C)[173], acellular and cellular dermal replacements (Figure 2.8B)[111], as well as in-vitro model of cardiac fibrosis[176].

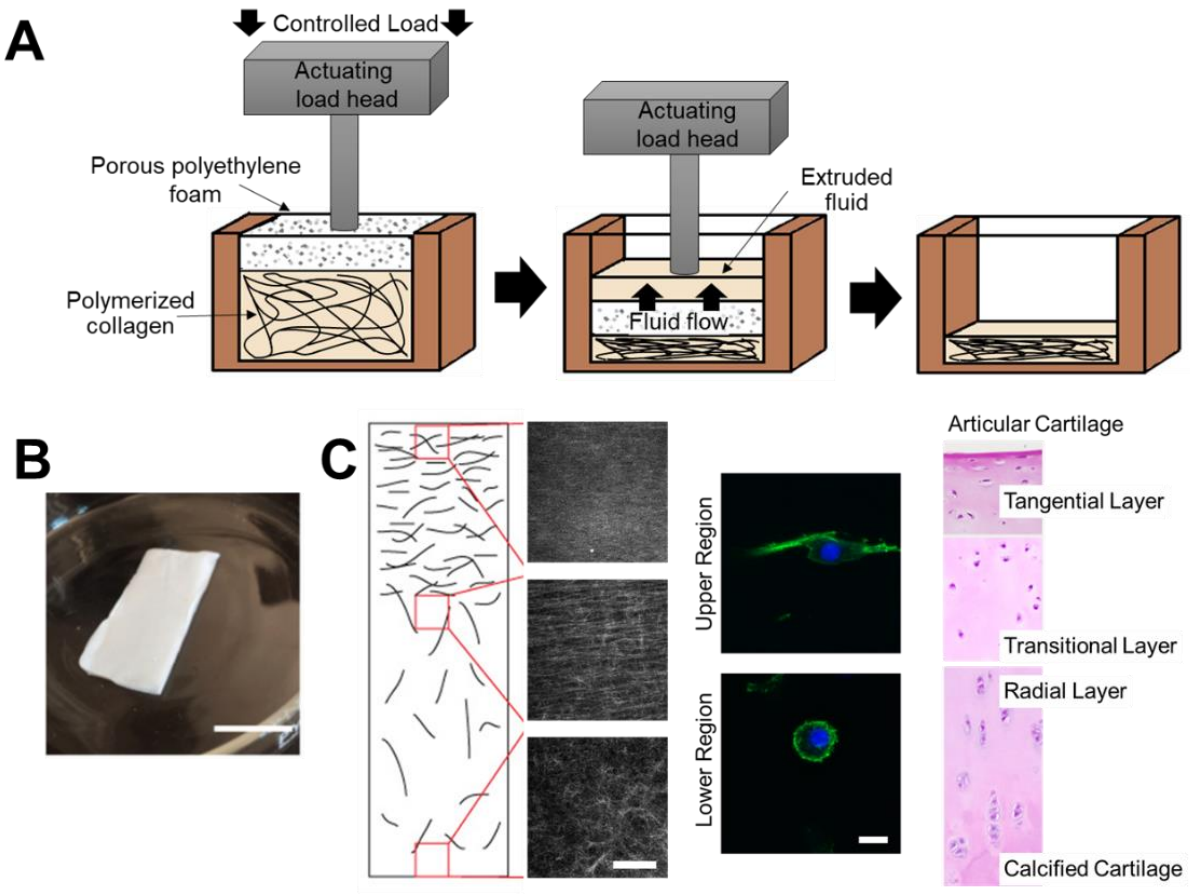

Figure 2.8. Controlled confined compression for fabrication of acellular and cellular constructs with and without continuous structural gradients A. Schematic depicting controlled confined compression process for densification of collagen-fibril constructs. A low-density collagen-fibril matrix is formed in a mold and then compressed at a controlled strain rate to achieve a specified strain. Fluid flow is directed through the porous boundary. (Adapted from Blum et al., 2016) B. Densified sheet formed via controlled confined compression of type I oligomeric collagen. Scale bar = 2mm. (Reprinted with permission by Blum et al., 2016) C. Gradient densification of collagen-fibril matrices as achieved via controlled confined compression. Type I oligomer matrices were compressed with a porous platen, directing fluid flow through an upper porous boundary condition. Confocal reflection microscopy revealed a gradient in fibril density, with a high density of fibrils aligned parallel to the construct surface near the top progressing to a low-density region of randomly organized fibrils near the bottom. Scale bar = 100μm (Reprinted with permission from Novak et al., 2016). Encapsulated cells responded to their local microenvironment as a result of densification, as detected 1 week with confocal microscopy (green=F-actin; blue=nucleus). Cells in the high-density region developed a spindle shape and were oriented parallel to the fibrils, while cells in the low-density regions displayed a more rounded morphology. Scale bar = 10μm. Such gradients in collagen microstructure and cell morphology/phenotype are reminiscent of the gradient layers found in articular cartilage.

2.7.2 Electrospinning

Electrospinning is a fiber-forming process that applies a large electric field between a polymer solution reservoir and a collection plate to form polymer fibers with nanometer-scale diameters. More specifically, when a sufficiently high voltage is applied to a liquid polymer droplet, the body of liquid becomes charged, and electrostatic repulsion counteracts the surface tension and the droplet is stretched. At a critical point a stream of liquid erupts from the surface forming a fiber. This fiber elongates and thins, and the solvent evaporates, as it moves towards the grounded collector where it is deposited. Published work on the electrospinning of collagen dates back nearly two decades[177-179]. In this case, materials are designed to mimic the geometry (e.g., diameter) of collagen fibrils or fibers found in vivo within the extracellular matrix. Since that time a large number of design variables including solvents, molecular make-up of collagen, collagen concentration and viscosity, applied electric field, flow rates, collection distance, and collection strategies (plates, rotating mandrels) have been explored[180,177]. At present, this technique has been used to generate collagen-based scaffolds of varying geometries (tubes, mats) and architectures (randomly oriented, aligned, high porosity, low porosity) for various tissue applications including bone[181], nerve[182], blood vessel[183,184], and skin[185,186]. For more details, the readers are encouraged to see DeFrates et al.[187]. A major limitation associated with present-day electrospinning is its requirement for volatile solvents (e.g., fluoroalcohols), which denature the native structure of collagen yielding gelatin. Furthermore, resulting materials lack collagen fiber ultrastructure (axial periodicity and D-banding) and therefore display altered biological and physical properties compared to native collagen assemblies. To address these issues, electrospinning of collagen is routinely performed in the presence of other synthetic (polycaprolactone, poly(lactic-co-glycolic acid)) or natural (elastin) polymers or in conjunction with physical or chemical crosslinking (e.g., N-(3-dimethylaminopropyl)-N'-ethylcarbodiimide hydrochloride and NHS, and glutaraldehyde) to improve mechanical integrity.

To overcome the persistent challenges associated with the electrospinning of collagen, alternative manufacturing processes are continued to be developed for creation of collagen fibers. For example, Polk and co-workers[188] described volatilization of collagen using a high-speed compressed air jet such as that produced by a common airbrush. This process which they termed pneumatospinning was used to form non-woven meshes of randomly organized and aligned fibrils, approximately 200nm in diameter. Interestingly, pneumatospun and electrospun fibers formed

from acetic acid showed similarity in size, strength, and cytocompatibility. However, like electrospun fibers, pneumatospun fibers were not stable in aqueous media in absence of chemical crosslinking.

2.7.3 3D Bioprinting

In the early 1990s, 3D printing emerged as an additive manufacturing technique for production of 3D objects based on computer-assisted design[189]. With advantages of mass production and fine tuning of spatial-dimensional properties, this process has been adapted for purposes of developing functional tissues and organ constructs. Such constructs are being fashioned for use as in-vitro model systems for basic research or drug screening[190,191], delivery of pharmaceutical agents (genes, drugs) or cells[192,193], and tissue-engineered medical products for tissue replacement or reconstruction[194]. Bioprinting involves sequential layer-by-layer deposition of biomaterials in the presence and absence of specific cell populations in predetermined spatial-dimensional patterns with millimeter or nanometer scale resolution. In this way, porosity, permeability and mechanical properties, and cell-cell and cell-ECM associations within the construct may be controlled. Of the various 3D printing technologies, direct ink writing and inkjet printing have received the most widespread use for bioprinting applications. For direct ink writing, high viscosity hydrogels in the presence or absence of cells are extruded to obtain 3D structures with or without a carrier. By contrast, inkjet bioprinting applies low viscous solutions or suspensions as droplets.

A critical component of bioprinting are the “bioinks”, which typically are polymeric materials that are used to deposit cells and/or serve as the extracellular scaffold. Ideally, bioink materials need to exhibit i) good printability, ii) biocompatibility for maintaining cell viability without eliciting immune reactions, iii) cell-friendly curability, iv) mechanical stability with shape retainability, v) predictive biodegradability including mechanism (hydrolysis or proteolytic degradation) and kinetics, and vi) predictable material-cell interface with ability to promote fundamental cellular behaviors (adhesion and remodeling, migration, proliferation, differentiation) and processes (morphogenesis)[195]. While bioink materials used to date satisfy a subset of these design requirements, bioink development and characterization remains a high-priority activity, together with optimization of the bioink-bioprinter interface[196].

To date a number of synthetic, nature-derived, and natural biomaterials have been used for a myriad of bioprinting activities and have been the subject of recent comprehensive reviews[195-197]. Here, we focus on the application of various collagen-based formulations, especially those that exhibit self-assembly. As stated previously, the use of collagen is advantageous because of its inherent biocompatibility and biosignaling capacity. However, a persistent limitation with conventional monomeric collagens has been their poor mechanical properties and long polymerization times, contributing to poor shape retaining properties and printing resolution. To circumvent these problems, collagen and its denatured counterpart gelatin have been modified by introducing new functional groups or used in conjunction with other biomaterials.

Gelatin methacryloyl (GelMA) represents one of the most popular bioinks, offering fast polymerization, good biocompatibility as well as tunable mechanical properties (for recent reviews see [198]). GelMA is a chemically-modified version of gelatin that exhibits photopolymerization (gelation) upon exposure to light irradiation in the presence of photoinitiators. Gelatin is distinct from native collagen in that it represents a mixture of collagen peptides and single-stranded polypeptide chains produced by collagen hydrolysis. Although it retains arginine-glycine-aspartic acid (RGD) sequences that promote cell attachment as well as target sequences for matrix metalloproteases, it does not maintain collagen's native triple helical structure and therefore inherent fibril-forming capacity. Introduction of methacryloyl groups confers to gelatin the capacity to be photocrosslinked with the assistance of photoinitiators and exposure to light. Many physical parameters of GelMA hydrogels, such as mechanical properties, pore sizes, degradation rates, and swell ratio can be readily tailored by changing the degree of methacryloyl substitution, GelMA prepolymer concentration, initiator concentration, and light exposure time[199,200].

More recently, tissue- and organ-derived decellularized ECMs (dECMs), that retain collagen's fibril-forming capacity, have been gaining increased use as bioinks for 3D bioprinting applications[201]. Traditionally, decellularized ECMs derived from a various allogeneic and xenogeneic tissue sources, namely skin, urinary bladder, small intestinal, and pericardium have been used clinically (surgical mesh, wound management), recent studies have focused on their use for tissue-specific 3D bioprinting applications[202,203]. Creation of dECM bioinks involves application of various decellularization methods to remove cells from tissues and organs. The resulting decellularized tissues are then exposed to acid-treatment in the presence or absence of pepsin, yielding a complex mixture of self-assembling collagen as well as other ECM components

(glycosaminoglycans, proteoglycans, growth factors, fibronectin). It is noteworthy that that dECM composition can vary widely and is dependent upon decellularization and solubilization protocols employed. Furthermore, removal of cells and their associated components is essential so to avoid elicitation of immune-mediated responses when used in vivo[204]. At present, most of these dECM inks form soft hydrogels, therefore the use of exogenous crosslinking in commonplace. To date dECM bioinks have been derived from various tissues and organs including heart, liver, fat, cartilage, skeletal muscle, skin, and vascular tissue. For a more comprehensive review of dECM bioink use in 3D bioprinting see [205].

2.7.4 Extrusion, Electrochemical Processes, and Magnetic Fields

One of the first applications of flow to induce preferential alignment of collagen fibrils was provided by Elsdale and Bard in 1972[206]. This method, referred to as the "draining method", involved pipetting polymerizable collagen into a dish and placing the dish at an incline to achieve gravity-induced flow and aligned bundles of fibrillar collagen. These findings have been extended to more scalable, industrial processes such as extrusion. Extrusion is formally defined as the act or process of shaping a material by forcing it through a die. In the late 1980s and early 1990s, Kato and co-workers described a scalable process for collagen fiber production that involved extrusion of acid-swollen dispersions of insoluble fibrillar collagen through polyethylene tubing into a phosphate-based buffer reservoir to induce gelation (Figure 2.9A)[207,208]. The resultant fibers were then transferred to isopropyl alcohol followed by air drying under tension. Chemical and physical crosslinking resulted in fibers with ultimate tensile strength values that were comparable to those for rat tail tendon fibers (24-66 MPa). When fashioned and implanted as tendon and ligaments, implants showed inflammatory reactions, degradation profiles, and neotissue formation that varied with type of crosslinking[209-212]. More recently, a similar approach was applied to soluble telocollagen and atelocollagen formulations, yielding "strings" of flow-aligned collagen fibrils (Figure 2.9B)[213,214]. Although this process could be applied to yield a wide variety of geometries and patterns, including sheets, meshes, and tubes, functional mechanical properties for tissue engineering applications have yet to be achieved.

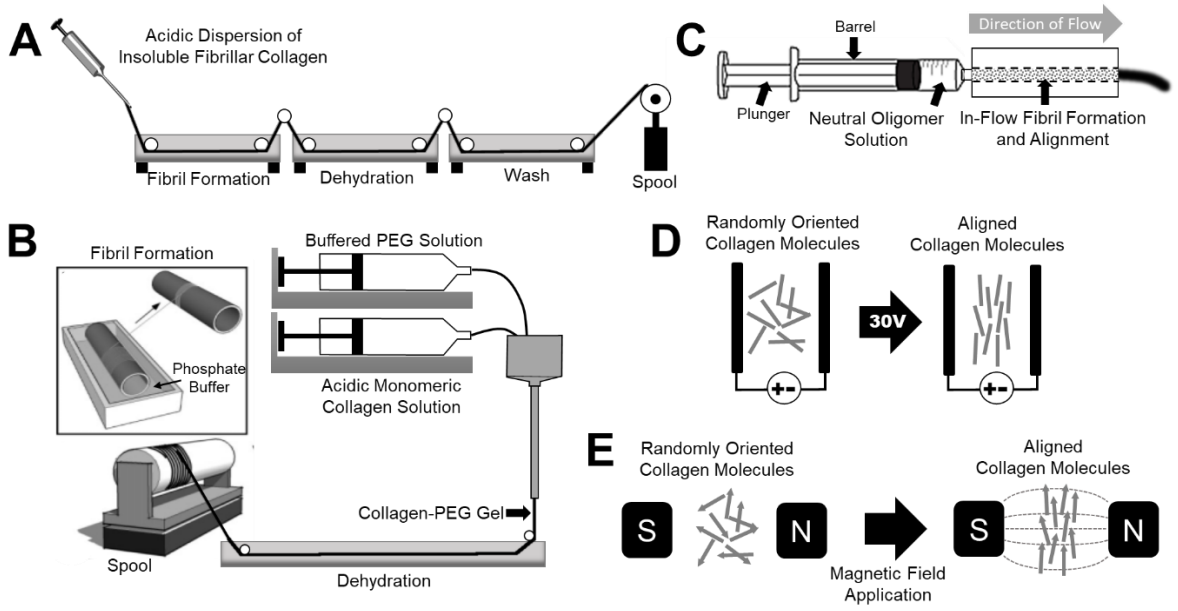

Figure 2.9. Extrusion processes for production of collagen threads and aligned collagen. A. Collagen fiber formation from acidic dispersions of insoluble fibrillar collagen (based on Kato et al., 1989). Collagen dispersions are extruded into a sodium phosphate based fiber formation buffer. Resulting threads are sequentially dehydrated in isopropyl alcohol, washed in water, and air dried prior to spooling. B. Wet spinning of collagen fibers (adapted from Caves et al., 2009). An acidic solution of collagen monomers is aggregated into a gel-like fiber by mixing with a buffered PEG solution. The extruded fiber is dehydrated in ethanol prior to collection on a spool. Resulting threads are exposed to phosphate buffer to induce formation of D-banded collagen fibrils, rinsed, and then air dried prior to spooling. C. In-flow collagen fibril formation and alignment (based on Brookes et al. 2018). Neutral solutions of oligomer collagen in the presence or absence of cells are extruded through a die, resulting in alignment of self-assembled collagen fibrils and resident cells. D. Electrochemical aggregation and alignment of collagen. Soluble collagen molecules are placed within an electrochemical cell consisting of two parallel electrode wires. Isoelectric focusing occurs with application of DC voltage resulting in molecular accumulation into compacted threads. Formation of D-banded collagen fibrils occurs when resulting collagen thread is placed in phosphate buffered saline. E. Magnetic alignment of collagen as occurs when neutralized collagen solutions are placed within high strength magnetic fields. Mechanical torque on molecules results in alignment orthogonal to the applied field.

Taking advantage of the rapid polymerization and improved mechanical integrity of type I oligomeric collagen, Brookes and co-workers described methods of extruding self-assembling oligomer solutions in the presence of muscle progenitor cells for creating engineered skeletal muscle for laryngeal reconstruction (Figure 2.9C). This process yielded mechanically stable constructs with aligned cells surrounded by highly aligned collagen fibrils[174]. Resident muscle progenitor cells readily fused, forming multi-nucleated myotubes upon culture in vitro. When

used for laryngeal muscle reconstruction in a rat hemi-laryngectomy model, these tissue-engineered muscle constructs integrated with the surrounding host tissue in absence of a significant inflammatory response. Furthermore, functional muscle regeneration and maturation occurred over a 3 month period marked by progressive increases in striations, innervation, and functional motor unit activity[174]. Other recently reported methods for achieving aligned cellularized collagen constructs include the multi-step process referred to as gel aspiration-ejection[215]. Here, isotropic, densified collagen constructs are aspirated into a syringe and then ejected through capillary tubes, 0.3 to 0.9 mm in diameter. Initial in-vitro studies showed that constructs formed by this process containing MSC showed accelerated osteoblast and neuronal differentiation when cultured in the appropriate differentiation medium formulations.

Methods other than extrusion have been used to create anisotropic collagen constructs. Specifically, collagen monomer solutions have been exposed to electrochemical processes, where isoelectric focusing is used to drive aggregation of collagen molecules (Figure 2.9D). While this process does not produce the staggered arrangement of molecules observed in native collagen fibrils, D-spacing can be achieved with exposure to phosphate buffered saline[216]. Follow-up processing of these electrochemically aligned collagen threads by sequential treatment with genipin crosslinking, peracetic acid/ethanol exposure, and heparinization in EDC/NHS yields heparinized sutures that can be used for growth factors such as platelet derived growth factor[217,218]. On the other hand, application of large magnetic fields to polymerizable collagens, which was first described in the 1980s[219,220], orients collagen molecules and associated fibril-forming counterparts perpendicular to the applied field (Figure 2.9E). This outcome is largely attributed to diamagnetism of the peptide bond[221]. Since that time, magnetic fields have been applied to generate anisotropic constructs for mechanistic studies of cell contact guidance[222] as well as generating tissue-engineered constructs cartilage[161], cornea[223,224], and peripheral nerve replacement[223,224] and regeneration. Notable findings from this work, was that orthogonal patterns of collagen fibrils, similar to those found in native cornea stroma, could be generated by polymerization-rotation-polymerization of sequential layers of collagen in the presence of a magnetic field[224]. Resident cells, whether grown in culture or infiltrating from surrounding tissue following implantation, align by contact guidance along the long axis of the fibrils. Interestingly, magnetically aligned constructs produced with atelocollagen and telocollagen showed improved handling and mechanical properties upon exogenous crosslinking[216].

However, magnetically aligned constructs produced with oligomeric collagen showed no significant change in mechanical integrity upon chemical crosslinking[161]. This observation was attributed to the fact that compared to monomers, oligomer produces more mechanically stable fibril microstructures with increased connectivity between fibrils (interfibril branching).

2.8 Conclusion and Future Directions

To date, tissue engineering and regenerative medicine approaches involving collagen-based scaffolds, cells and combinations thereof have led to a number of new, FDA-approved therapies. However, many would say that the field, in general, has still not lived up to promises and enthusiasm generated early on. The ability to replace or regenerate damaged or diseased tissues and organs remains one of the great challenges and unmet needs facing medicine and society. Continued translation and commercialization of next generation therapies must forge new pathways that interface biomolecules and cells, scalable manufacturing processes, and regulatory policy. Careful consideration of the scientific, regulatory, and business hurdles is paramount in streamlining translation and maximizing clinical impact. Integration of computational modeling for predictable, customizable design will facilitate precision medicine, applications, which works to account for the inevitable variability in health status and intrinsic healing/remodeling potential between patients. Translating these biomedical advances to medical successes will help fulfill the long-standing promise of tissue engineering and regenerative medicine to patients, clinicians, investors, and society.

2.9 References

1. Hu YH, Suo ZG. Viscoelasticity and poroelasticity in elastomeric gels. Acta Mech Solida Sin. 2012;25(5):441-58.
2. Muiznieks LD, Keeley FW. Molecular assembly and mechanical properties of the extracellular matrix: A fibrous protein perspective. Biochim Biophys Acta. 2013;1832(7):866-75.
3. Xu R, Boudreau A, Bissell MJ. Tissue architecture and function: dynamic reciprocity via extra- and intra-cellular matrices. Cancer Metastasis Rev. 2009;28(1-2):167-76.
4. Langer R, Vacanti JP. Tissue engineering. Science. 1993;260(5110):920-6.

5. Freed LE, Vunjak-Novakovic G, Biron RJ, Eagles DB, Lesnoy DC, Barlow SK, Langer R. Biodegradable polymer scaffolds for tissue engineering. Biotechnology (N Y). 1994;12(7):689-93.
6. Kim BS, Mooney DJ. Development of biocompatible synthetic extracellular matrices for tissue engineering. Trends Biotechnol. 1998;16(5):224-30.
7. Vacanti JP, Langer R. Tissue engineering: the design and fabrication of living replacement devices for surgical reconstruction and transplantation. Lancet. 1999;354 Suppl 1:SI32-4.
8. Chung L, Maestas DR, Jr., Housseau F, Elisseeff JH. Key players in the immune response to biomaterial scaffolds for regenerative medicine. Adv Drug Del Rev. 2017;114:184-92.
9. Julier Z, Park AJ, Briquez PS, Martino MM. Promoting tissue regeneration by modulating the immune system. Acta Biomater. 2017;53:13-28.
10. Ingber DE, Mow VC, Butler D, Niklason L, Huard J, Mao J, Yannas I, Kaplan D, Vunjak-Novakovic G. Tissue engineering and developmental biology: going biomimetic. Tissue Eng. 2006;12(12):3265-83.
11. Green JJ, Elisseeff JH. Mimicking biological functionality with polymers for biomedical applications. Nature. 2016;540(7633):386-94.
12. Aguado BA, Grim JC, Rosales AM, Watson-Capps JJ, Anseth KS. Engineering precision biomaterials for personalized medicine. Sci Transl Med. 2018;10(424).
13. Mao AS, Mooney DJ. Regenerative medicine: Current therapies and future directions. Proc Natl Acad Sci. 2015;112(47):14452-9.
14. BCC Research. Tissue Engineering and Regeneration: Technologies and Global Markets 2016.
15. Fratzl P. Collagen: structure and mechanics, an introduction. Collagen: Springer; 2008. p. 1-13.
16. Chattopadhyay S, Raines RT. Review collagen-based biomaterials for wound healing. Biopolymers. 2014;101(8):821-33.
17. Mackenzie D. The history of sutures. Med Hist. 1973;17(2):158-68.
18. Gibson T. Evolution of catgut ligatures: the endeavours and success of Joseph Lister and William Macewen. Br J Surg. 1990;77(7):824-5.
19. Lister J. An address on the catgut ligature. Br Med J. 1881;1(1050):219-21.
20. Ramachandran GN, Kartha G. Structure of collagen. Nature. 1954;174(4423):269-70.

21. Binet JP, Carpentier A, Langlois J, Duran C, Colvez P. [Implantation of heterogenic valves in the treatment of aortic cardiopathies]. C R Acad Sci Hebd Seances Acad Sci D. 1965;261(25):5733-4.
22. Zuhdi N, Hawley W, Voehl V, Hancock W, Carey J, Greer A. Porcine aortic valves as replacements for human heart valves. Ann Thorac Surg. 1974;17(5):479-91.
23. Manji RA, Lee W, Cooper DKC. Xenograft bioprosthetic heart valves: Past, present and future. Int J Surg. 2015;23(Pt B):280-4.
24. Ionescu MI, Pakrashi BC, Holden MP, Mary DA, Wooler GH. Results of aortic valve replacement with frame-supported fascia lata and pericardial grafts. J Thorac Cardiovasc Surg. 1972;64(3):340-53.
25. Soares JS, Feaver KR, Zhang W, Kamensky D, Aggarwal A, Sacks MS. Biomechanical behavior of bioprosthetic heart valve heterograft tissues: Characterization, simulation, and performance. Cardiovasc Eng Technol. 2016;7(4):309-51.
26. Badylak SF, Lantz GC, Coffey A, Geddes LA. Small intestinal submucosa as a large diameter vascular graft in the dog. J Surg Res. 1989;47(1):74-80.
27. Lysaght MJ, Nguy NA, Sullivan K. An economic survey of the emerging tissue engineering industry. Tissue Eng. 1998;4(3):231-8.
28. Lysaght MJ, Reyes J. The growth of tissue engineering. Tissue Eng. 2001;7(5):485-93.
29. Wainwright DJ. Use of an acellular allograft dermal matrix (Alloderm) in the management of full-thickness burns. Burns. 1995;21(4):243-8.
30. Miller EJ, Rhodes RK. Preparation and characterization of the different types of collagen. Methods Enzymol. 1982;82 Pt A:33-64.
31. Yannas IV, Burke JF. Design of an artificial skin. I. Basic design principles. J Biomed Mater Res. 1980;14(1):65-81.
32. Yannas IV, Burke JF, Gordon PL, Huang C, Rubenstein RH. Design of an artificial skin. II. Control of chemical composition. J Biomed Mater Res. 1980;14(2):107-32.
33. Dagalakis N, Flink J, Stasikelis P, Burke JF, Yannas IV. Design of an artificial skin. Part III. Control of pore structure. J Biomed Mater Res. 1980;14(4):511-28.
34. Stegman SJ, Tromovitch TA. Implantation of collagen for depressed scars. J Dermatol Surg Oncol. 1980;6(6):450-3.

35. Kablik J, Monheit GD, Yu L, Chang G, Gershkovich J. Comparative physical properties of hyaluronic acid dermal fillers. Dermatol Surg. 2009;35 Suppl 1:302-12.
36. Friedlaender GE, Perry CR, Cole JD, Cook SD, Cierny G, Muschler GF, Zych GA, Calhoun JH, LaForte AJ, Yin S. Osteogenic protein-1 (bone morphogenetic protein-7) in the treatment of tibial nonunions - A prospective, randomized clinical trial comparing rhOP-1 with fresh bone autograft. J Bone Joint Surg. 2001;83a(Pt 2):S151-S8.
37. Burkus JK, Transfeldt EE, Kitchel SH, Watkins RG, Balderston RA. Clinical and radiographic outcomes of anterior lumbar interbody fusion using recombinant human bone morphogenetic protein-2. Spine. 2002;27(21):2396-408.
38. Gross J, Highberger JH, Schmitt FO. Collagen structures considered as states of aggregation of a kinetic unit - the tropocollagen particle. Proc Natl Acad Sci. 1954;40(8):679-&.
39. Jackson DS, Fessler JH. Isolation and properties of a collagen soluble in salt solution at neutral pH. Nature. 1955;176(4471):69-70.
40. Bell E, Ivarsson B, Merrill C. Production of a tissue-like structure by contraction of collagen lattices by human fibroblasts of different proliferative potential in vitro. Proc Natl Acad Sci. 1979;76(3):1274-8.
41. Bell E, Sher S, Hull B, Merrill C, Rosen S, Chamson A, Asselineau D, Dubertret L, Coulomb B, Lapiere C, Nusgens B, Neveux Y. The reconstitution of living skin. J Invest Dermatol. 1983;81(1 Suppl):2s-10s.
42. Kreger ST, Bell BJ, Bailey J, Stites E, Kuske J, Waisner B, Voytik-Harbin SL. Polymerization and matrix physical properties as important design considerations for soluble collagen formulations. Biopolymers. 2010;93(8):690-707.
43. Antoine EE, Vlachos PP, Rylander MN. Review of collagen I hydrogels for bioengineered tissue microenvironments: characterization of mechanics, structure, and transport. Tissue Eng Part B Rev. 2014;20(6):683-96.
44. Johnson KR, Leight JL, Weaver VM. Demystifying the effects of a three-dimensional microenvironment in tissue morphogenesis. Methods Cell Biol. 2007;83:547-83.
45. An B, Kaplan DL, Brodsky B. Engineered recombinant bacterial collagen as an alternative collagen-based biomaterial for tissue engineering. Front Chem. 2014;2:40.

46. Rutschmann C, Baumann S, Cabalzar J, Luther KB, Hennet T. Recombinant expression of hydroxylated human collagen in Escherichia coli. Appl Microbiol Biotechnol. 2014;98(10):4445-55.
47. Critser PJ, Kreger ST, Voytik-Harbin SL, Yoder MC. Collagen matrix physical properties modulate endothelial colony forming cell-derived vessels in vivo. Microvasc Res. 2010;80(1):23-30.
48. Bailey JL, Critser PJ, Whittington C, Kuske JL, Yoder MC, Voytik-Harbin SL. Collagen oligomers modulate physical and biological properties of three-dimensional self-assembled matrices. Biopolymers. 2011;95(2):77-93.
49. Knott L, Bailey AJ. Collagen cross-links in mineralizing tissues: A review of their chemistry, function, and clinical relevance. Bone. 1998;22(3):181-7.
50. Eyre DR, Wu JJ. Collagen cross-links. Collagen2005. p. 207-29.
51. Shoulders MD, Raines RT. Collagen structure and stability. Annu Rev Biochem. 2009;78:929-58.
52. Kadler KE. Fell Muir Lecture: Collagen fibril formation in vitro and in vivo. Int J Exp Pathol. 2017;98(1):4-16.
53. Canty EG, Kadler KE. Procollagen trafficking, processing and fibrillogenesis. J Cell Sci. 2005;118(Pt 7):1341-53.
54. Myllyharju J, Kivirikko KI. Collagens and collagen-related diseases. Ann Med. 2001;33(1):7-21.
55. Lees JF, Tasab M, Bulleid NJ. Identification of the molecular recognition sequence which determines the type-specific assembly of procollagen. EMBO J. 1997;16(5):908-16.
56. Nagata K. Hsp47: a collagen-specific molecular chaperone. Trends Biochem Sci. 1996;21(1):22-6.
57. Wilson R, Lees JF, Bulleid NJ. Protein disulfide isomerase acts as a molecular chaperone during the assembly of procollagen. J Biol Chem. 1998;273(16):9637-43.
58. Cronlund AL, Smith BD, Kagan HM. Binding of lysyl oxidase to fibrils of type I collagen. Connect Tissue Res. 1985;14(2):109-19.
59. Eyre DR, Paz MA, Gallop PM. Cross-linking in collagen and elastin. Annu Rev Biochem. 1984;53:717-48.

60. Pasquali-Ronchetti I, Baccarani-Contri M, Young RD, Vogel A, Steinmann B, Royce PM. Ultrastructural analysis of skin and aorta from a patient with Menkes disease. Exp Mol Pathol. 1994;61(1):36-57.
61. Herchenhan A, Uhlenbrock F, Eliasson P, Weis M, Eyre D, Kadler KE, Magnusson SP, Kjaer M. Lysyl oxidase activity is required for ordered collagen fibrillogenesis by tendon cells. J Biol Chem. 2015;290(26):16440-50.
62. Maki JM, Sormunen R, Lippo S, Kaarteenaho-Wiik R, Soininen R, Myllyharju J. Lysyl oxidase is essential for normal development and function of the respiratory system and for the integrity of elastic and collagen fibers in various tissues. Am J Pathol. 2005;167(4):927-36.
63. Avery NC, Bailey AJ. Restraining cross-links responsible for the mechanical properties of collagen fibers: natural and artificial. In: Fratzl P, editor. Collagen Structure and Mechanics. New York: Springer; 2008. p. 81-110.
64. Robins SP. Biochemistry and functional significance of collagen cross-linking. Biochem Soc Trans. 2007;35(Pt 5):849-52.
65. Silver FH, Freeman JW, Seehra GP. Collagen self-assembly and the development of tendon mechanical properties. J Biomech. 2003;36(10):1529-53.
66. Wallace JM, Erickson B, Les CM, Orr BG, Banaszak Holl MM. Distribution of type I collagen morphologies in bone: relation to estrogen depletion. Bone. 2010;46(5):1349-54.
67. Fang M, Goldstein EL, Turner AS, Les CM, Orr BG, Fisher GJ, Welch KB, Rothman ED, Holl MMB. Type I collagen D-spacing in fibril bundles of dermis, tendon, and bone: bridging between nano- and micro-level tissue hierarchy. ACS Nano. 2012;6(11):9503-14.
68. Hulmes DJ, Wess TJ, Prockop DJ, Fratzl P. Radial packing, order, and disorder in collagen fibrils. Biophys J. 1995;68(5):1661-70.
69. Orgel JP, Irving TC, Miller A, Wess TJ. Microfibrillar structure of type I collagen in situ. Proc Natl Acad Sci. 2006;103(24):9001-5.
70. Kadler KE, Holmes DF, Graham H, Starborg T. Tip-mediated fusion involving unipolar collagen fibrils accounts for rapid fibril elongation, the occurrence of fibrillar branched networks in skin and the paucity of collagen fibril ends in vertebrates. Matrix Biol. 2000;19(4):359-65.

71. Whittington CF, Brandner E, Teo KY, Han B, Nauman E, Voytik-Harbin SL. Oligomers modulate interfibril branching and mass transport properties of collagen matrices. Microsc Microanal. 2013;19(5):1323-33.
72. Lanir Y, Fung YC. Two-dimensional mechanical properties of rabbit skin. II. Experimental results. J Biomech. 1974;7(2):171-82.
73. Lanir Y, Fung YC. Two-dimensional mechanical properties of rabbit skin. I. Experimental system. J Biomech. 1974;7(1):29-34.
74. Brown IA. Scanning electron microscopy of human dermal fibrous tissue. J Anat. 1972;113(Pt 2):159-68.
75. Benjamin M, Kaiser E, Milz S. Structure-function relationships in tendons: a review. J Anat. 2008;212(3):211-28.
76. Meek KM, Knupp C. Corneal structure and transparency. Prog Retin Eye Res. 2015;49:1-16.
77. Evans FG, Vincentelli R. Relation of collagen fiber orientation to some mechanical properties of human cortical bone. J Biomech. 1969;2(1):63-71.
78. Sweeney SM, Orgel JP, Fertala A, McAuliffe JD, Turner KR, Di Lullo GA, Chen S, Antipova O, Perumal S, Ala-Kokko L, Forlino A, Cabral WA, Barnes AM, Marini JC, San Antonio JD. Candidate cell and matrix interaction domains on the collagen fibril, the predominant protein of vertebrates. J Biol Chem. 2008;283(30):21187-97.
79. Kubow KE, Vukmirovic R, Zhe L, Klotzsch E, Smith ML, Gourdon D, Luna S, Vogel V. Mechanical forces regulate the interactions of fibronectin and collagen I in extracellular matrix. Nat Commun. 2015;6:8026.
80. Leitinger B, Hohenester E. Mammalian collagen receptors. Matrix Biol. 2007;26(3):146-55.
81. Bozec L, Horton M. Topography and mechanical properties of single molecules of type I collagen using atomic force microscopy. Biophys J. 2005;88(6):4223-31.
82. van der Rijt JA, van der Werf KO, Bennink ML, Dijkstra PJ, Feijen J. Micromechanical testing of individual collagen fibrils. Macromol Biosci. 2006;6(9):697-702. doi: 10.1002/mabi.200600063. PubMed PMID: 16967482.
83. Wenger MP, Bozec L, Horton MA, Mesquida P. Mechanical properties of collagen fibrils. Biophys J. 2007;93(4):1255-63.

84. Buehler MJ. Nature designs tough collagen: explaining the nanostructure of collagen fibrils. Proc Natl Acad Sci. 2006;103(33):12285-90.
85. Motte S, Kaufman LJ. Strain stiffening in collagen I networks. Biopolymers. 2013;99(1):35-46.
86. Susilo ME, Paten JA, Sander EA, Nguyen TD, Ruberti JW. Collagen network strengthening following cyclic tensile loading. Interface Focus. 2016;6(1):20150088.
87. Hosseini SM, Wilson W, Ito K, van Donkelaar CC. How preconditioning affects the measurement of poro-viscoelastic mechanical properties in biological tissues. Biomech Model Mechan. 2014;13(3):503-13.
88. Munster S, Jawerth LM, Leslie BA, Weitz JI, Fabry B, Weitz DA. Strain history dependence of the nonlinear stress response of fibrin and collagen networks. Proc Natl Acad Sci. 2013;110(30):12197-202.
89. Nam S, Hu KH, Butte MJ, Chaudhuri O. Strain-enhanced stress relaxation impacts nonlinear elasticity in collagen gels. Proc Natl Acad Sci. 2016;113(20):5492-7.
90. Nam S, Lee J, Brownfield DG, Chaudhuri O. Viscoplasticity enables mechanical remodeling of matrix by cells. Biophys J. 2016;111(10):2296-308.
91. McKee CT, Last JA, Russell P, Murphy CJ. Indentation versus tensile measurements of Young's modulus for soft biological tissues. Tissue Eng Part B Rev. 2011;17(3):155-64.
92. Yang W, Sherman VR, Gludovatz B, Schaible E, Stewart P, Ritchie RO, Meyers MA. On the tear resistance of skin. Nat Commun. 2015;6:6649.
93. Knorzer E, Folkhard W, Geercken W, Boschert C, Koch MHJ, Hilbert B, Krahl H, Mosler E, Nemetschekgansler H, Nemetschek T. New aspects of the etiology of tendon-rupture - an analysis of time-resolved dynamic-mechanical measurements using synchrotron radiation. Arch Orthop Trauma Surg. 1986;105(2):113-20.
94. Torp S. Effects of age and of mechanical deformation on the ultrastructure of tendon. Struct Fibrous Biopolymers. 1975:223-50.
95. Veres SP, Lee JM. Designed to fail: a novel mode of collagen fibril disruption and its relevance to tissue toughness. Biophys J. 2012;102(12):2876-84.
96. Veres SP, Harrison JM, Lee JM. Repeated subrupture overload causes progression of nanoscaled discrete plasticity damage in tendon collagen fibrils. J Orthop Res. 2013;31(5):731-7.

97. Guilak F, Butler DL, Goldstein SA, Baaijens FP. Biomechanics and mechanobiology in functional tissue engineering. J Biomech. 2014;47(9):1933-40.
98. Butler DL, Goldstein SA, Guilak F. Functional tissue engineering: the role of biomechanics. J Biomech Eng. 2000;122(6):570-5.
99. Mammoto T, Mammoto A, Ingber DE. Mechanobiology and developmental control. Annu Rev Cell Dev Biol. 2013;29:27-61.
100. Ingber DE, Wang N, Stamenovic D. Tensegrity, cellular biophysics, and the mechanics of living systems. Rep Prog Phys. 2014;77(4):046603.
101. Gross J, Kirk D. The heat precipitation of collagen from neutral salt solutions: some rate-regulating factors. J Biol Chem. 1958;233(2):355-60.
102. Na GC, Butz LJ, Carroll RJ. Mechanism of in vitro collagen fibril assembly. Kinetic and morphological studies. J Biol Chem. 1986;261(26):12290-9.
103. Chandrakasan G, Torchia DA, Piez KA. Preparation of intact monomeric collagen from rat tail tendon and skin and the structure of the nonhelical ends in solution. J Biol Chem. 1976;251(19):6062-7.
104. McPherson JM, Wallace DG, Sawamura SJ, Conti A, Condell RA, Wade S, Piez KA. Collagen fibrillogenesis in vitro: a characterization of fibril quality as a function of assembly conditions. Coll Relat Res. 1985;5(2):119-35.
105. Na GC, Butz LJ, Bailey DG, Carroll RJ. In vitro collagen fibril assembly in glycerol solution: evidence for a helical cooperative mechanism involving microfibrils. Biochemistry. 1986;25(5):958-66.
106. Brennan M, Davison PF. Role of aldehydes in collagen fibrillogenesis in vitro. Biopolymers. 1980;19(10):1861-73.
107. Sato K, Ebihara T, Adachi E, Kawashima S, Hattori S, Irie S. Possible involvement of aminotelopeptide in self-assembly and thermal stability of collagen I as revealed by its removal with proteases. J Biol Chem. 2000;275(33):25870-5.
108. Abraham LC, Zuena E, Perez-Ramirez B, Kaplan DL. Guide to collagen characterization for biomaterial studies. J Biomed Mater Res B Appl Biomater. 2008;87(1):264-85.
109. Holmes R, Kirk S, Tronci G, Yang X, Wood D. Influence of telopeptides on the structural and physical properties of polymeric and monomeric acid-soluble type I collagen. Mater Sci Eng C Mater Biol Appl. 2017;77:823-7.

110. Helseth D, Veis A. Collagen self-assembly in vitro. Differentiating specific telopeptide-dependent interactions using selective enzyme modification and the addition of free amino telopeptide. J Biol Chem. 1981;256(14):7118-28.
111. Blum KM, Novak T, Watkins L, Neu CP, Wallace JM, Bart ZR, Voytik-Harbin SL. Acellular and cellular high-density, collagen-fibril constructs with suprafibrillar organization. Biomater Sci. 2016;4(4):711-23.
112. Herrera-Perez M, Voytik-Harbin SL, Rickus JL. Extracellular Matrix Properties Regulate the Migratory Response of Glioblastoma Stem Cells in Three-Dimensional Culture. Tissue Eng Part A. 2015;21(19-20):2572-82.
113. Stephens CH, Orr KS, Acton AJ, Tersey SA, Mirmira RG, Considine RV, Voytik-Harbin SL. In situ type I oligomeric collagen macroencapsulation promotes islet longevity and function in vitro and in vivo. Am J Physiol Endocrinol Metab. 2018;315(4):E650-E61.
114. Hall MS, Alisafaei F, Ban E, Feng X, Hui CY, Shenoy VB, Wu M. Fibrous nonlinear elasticity enables positive mechanical feedback between cells and ECMs. Proc Natl Acad Sci. 2016;113(49):14043-8.
115. Brodsky B, Ramshaw JA. Bioengineered collagens. Fibrous Proteins: Structures and Mechanisms: Springer; 2017. p. 601-29.
116. John DC, Watson R, Kind AJ, Scott AR, Kadler KE, Bulleid NJ. Expression of an engineered form of recombinant procollagen in mouse milk. Nat Biotechnol. 1999;17(4):385-9.
117. Tomita M, Kitajima T, Yoshizato K. Formation of recombinant human procollagen I heterotrimers in a baculovirus expression system. J Biochem. 1997;121(6):1061-9.
118. Pakkanen O, Hamalainen ER, Kivirikko KI, Myllyharju J. Assembly of stable human type I and III collagen molecules from hydroxylated recombinant chains in the yeast Pichia pastoris. Effect of an engineered C-terminal oligomerization domain foldon. J Biol Chem. 2003;278(34):32478-83.
119. Ruggiero F, Exposito JY, Bournat P, Gruber V, Perret S, Comte J, Olagnier B, Garrone R, Theisen M. Triple helix assembly and processing of human collagen produced in transgenic tobacco plants. FEBS Lett. 2000;469(1):132-6.

120. Yang C, Hillas PJ, Baez JA, Nokelainen M, Balan J, Tang J, Spiro R, Polarek JW. The application of recombinant human collagen in tissue engineering. Biodrugs. 2004;18(2):103-19.
121. Ramshaw JA, Werkmeister JA, Dumsday GJ. Bioengineered collagens: emerging directions for biomedical materials. Bioengineered. 2014;5(4):227-33.
122. Stein H, Wilensky M, Tsafrir Y, Rosenthal M, Amir R, Avraham T, Ofir K, Dgany O, Yayon A, Shoseyov O. Production of bioactive, post-translationally modified, heterotrimeric, human recombinant type-I collagen in transgenic tobacco. Biomacromolecules. 2009;10(9):2640-5.
123. Kotch FW, Raines RT. Self-assembly of synthetic collagen triple helices. Proc Natl Acad Sci. 2006;103(9):3028-33.
124. Przybyla DE, Chmielewski J. Metal-triggered radial self-assembly of collagen peptide fibers. J Am Chem Soc. 2008;130(38):12610-1.
125. Rele S, Song Y, Apkarian RP, Qu Z, Conticello VP, Chaikof EL. D-periodic collagen-mimetic microfibers. J Am Chem Soc. 2007;129(47):14780-7.
126. Baez J, Olsen D, Polarek JW. Recombinant microbial systems for the production of human collagen and gelatin. Appl Microbiol Biotechnol. 2005;69(3):245-52.
127. Willard JJ, Drexler JW, Das A, Roy S, Shilo S, Shoseyov O, Powell HM. Plant-derived human collagen scaffolds for skin tissue engineering. Tissue Eng Part A. 2013;19(13-14):1507-18.
128. Strauss K, Chmielewski J. Advances in the design and higher-order assembly of collagen mimetic peptides for regenerative medicine. Curr Opin Biotechnol. 2017;46:34-41.
129. O'Leary LE, Fallas JA, Bakota EL, Kang MK, Hartgerink JD. Multi-hierarchical self-assembly of a collagen mimetic peptide from triple helix to nanofibre and hydrogel. Nat Chem. 2011;3(10):821-8.
130. Golser AV, Scheibel T. Routes towards novel collagen-like biomaterials. Fibers. 2018;6(2):21.
131. Pizzo AM, Kokini K, Vaughn LC, Waisner BZ, Voytik-Harbin SL. Extracellular matrix (ECM) microstructural composition regulates local cell-ECM biomechanics and fundamental fibroblast behavior: a multidimensional perspective. J Appl Physiol. 2005;98(5):1909-21.

132. Grinnell F. Fibroblast biology in three-dimensional collagen matrices. Trends Cell Biol. 2003;13(5):264-9.
133. Rhee S, Grinnell F. Fibroblast mechanics in 3D collagen matrices. Adv Drug Del Rev. 2007;59(13):1299-305.
134. Bell BJ, Nauman E, Voytik-Harbin SL. Multiscale strain analysis of tissue equivalents using a custom-designed biaxial testing device. Biophys J. 2012;102(6):1303-12.
135. Wood GC, Keech MK. The formation of fibrils from collagen solutions. 1. The effect of experimental conditions: kinetic and electron-microscope studies. Biochem J. 1960;75(3):588-98.
136. Roeder BA, Kokini K, Sturgis JE, Robinson JP, Voytik-Harbin SL. Tensile mechanical properties of three-dimensional type I collagen extracellular matrices with varied microstructure. J Biomech Eng. 2002;124(2):214-22.
137. Raub CB, Suresh V, Krasieva T, Lyubovitsky J, Mih JD, Putnam AJ, Tromberg BJ, George SC. Noninvasive assessment of collagen gel microstructure and mechanics using multiphoton Microscopy. Biophys J. 2007;92(6):2212-22.
138. Achilli M, Mantovani D. Tailoring mechanical properties of collagen-based scaffolds for vascular tissue engineering: the effects of pH, temperature and ionic strength on gelation. Polymers. 2010;2(4):664-80.
139. Antoine EE, Vlachos PP, Rylander MN. Tunable collagen I hydrogels for engineered physiological tissue micro-environments. PLoS One. 2015;10(3):e0122500.
140. Sapudom J, Rubner S, Martin S, Kurth T, Riedel S, Mierke CT, Pompe T. The phenotype of cancer cell invasion controlled by fibril diameter and pore size of 3D collagen networks. Biomaterials. 2015;52:367-75.
141. Berger AJ, Linsmeier KM, Kreeger PK, Masters KS. Decoupling the effects of stiffness and fiber density on cellular behaviors via an interpenetrating network of gelatin-methacrylate and collagen. Biomaterials. 2017;141:125-35.
142. da Cunha CB, Klumpers DD, Li WA, Koshy ST, Weaver JC, Chaudhuri O, Granja PL, Mooney DJ. Influence of the stiffness of three-dimensional alginate/collagen-I interpenetrating networks on fibroblast biology. Biomaterials. 2014;35(32):8927-36.

143. Liang Y, Jeong J, DeVolder RJ, Cha C, Wang F, Tong YW, Kong H. A cell-instructive hydrogel to regulate malignancy of 3D tumor spheroids with matrix rigidity. Biomaterials. 2011;32(35):9308-15.
144. Whittington CF, Yoder MC, Voytik-Harbin SL. Collagen-Polymer Guidance of Vessel Network Formation and Stabilization by Endothelial Colony Forming Cells In Vitro. Macromol Biosci. 2013;13(9).
145. Kadler KE, Hill A, Canty-Laird EG. Collagen fibrillogenesis: fibronectin, integrins, and minor collagens as organizers and nucleators. Curr Opin Cell Biol. 2008;20(5):495-501.
146. Brokaw JL, Doillon CJ, Hahn RA, Birk DE, Berg RA, Silver FH. Turbidimetric and morphological studies of type I collagen fibre self assembly in vitro and the influence of fibronectin. Int J Biol Macromol. 1985;7(3):135-40.
147. Gildner CD, Lerner AL, Hocking DC. Fibronectin matrix polymerization increases tensile strength of model tissue. Am J Physiol Heart Circ Physiol. 2004;287(1):H46-53.
148. Birk DE, Fitch JM, Babiarz JP, Doane KJ, Linsenmayer TF. Collagen fibrillogenesis in vitro: interaction of types I and V collagen regulates fibril diameter. J Cell Sci. 1990;95 (Pt 4)(4):649-57.
149. Piechocka IK, van Oosten AS, Breuls RG, Koenderink GH. Rheology of heterotypic collagen networks. Biomacromolecules. 2011;12(7):2797-805.
150. Garg AK, Berg RA, Silver FH, Garg HG. Effect of proteoglycans on type I collagen fibre formation. Biomaterials. 1989;10(6):413-9.
151. Pins GD, Christiansen DL, Patel R, Silver FH. Self-assembly of collagen fibers. Influence of fibrillar alignment and decorin on mechanical properties. Biophys J. 1997;73(4):2164-72.
152. Reese SP, Underwood CJ, Weiss JA. Effects of decorin proteoglycan on fibrillogenesis, ultrastructure, and mechanics of type I collagen gels. Matrix Biol. 2013;32(7-8):414-23.
153. Hapach LA, VanderBurgh JA, Miller JP, Reinhart-King CA. Manipulation of in vitro collagen matrix architecture for scaffolds of improved physiological relevance. Phys Biol. 2015;12(6):061002.
154. Carpentier A, Lemaigre G, Robert L, Carpentier S, Dubost C. Biological factors affecting long-term results of valvular heterografts. J Thorac Cardiovasc Surg. 1969;58(4):467-83.

155. Damink LO, Dijkstra PJ, Van Luyn M, Van Wachem P, Nieuwenhuis P, Feijen J. Glutaraldehyde as a crosslinking agent for collagen-based biomaterials. J Mater Sci Mater Med. 1995;6(8):460-72.
156. Weadock K, Olson RM, Silver FH. Evaluation of collagen crosslinking techniques. Biomater Med Devices Artif Organs. 1983;11(4):293-318.
157. Schoen FJ, Levy RJ. Calcification of tissue heart valve substitutes: progress toward understanding and prevention. Ann Thorac Surg. 2005;79(3):1072-80.
158. Schmidt CE, Baier JM. Acellular vascular tissues: natural biomaterials for tissue repair and tissue engineering. Biomaterials. 2000;21(22):2215-31.
159. Ming-Che W, Pins GD, Silver FH. Collagen fibres with improved strength for the repair of soft tissue injuries. Biomaterials. 1994;15(7):507-12.
160. Yunoki S, Matsuda T. Simultaneous processing of fibril formation and cross-linking improves mechanical properties of collagen. Biomacromolecules. 2008;9(3):879-85.
161. Novak T, Voytik-Harbin SL, Neu CP. Cell encapsulation in a magnetically aligned collagen-GAG copolymer microenvironment. Acta Biomater. 2015;11:274-82.
162. Sundararaghavan HG, Monteiro GA, Lapin NA, Chabal YJ, Miksan JR, Shreiber DI. Genipin-induced changes in collagen gels: correlation of mechanical properties to fluorescence. J Biomed Mater Res A. 2008;87(2):308-20.
163. Snedeker JG, Gautieri A. The role of collagen crosslinks in ageing and diabetes - the good, the bad, and the ugly. Muscles Ligaments Tendons J. 2014;4(3):303-8.
164. Sung HW, Chang WH, Ma CY, Lee MH. Crosslinking of biological tissues using genipin and/or carbodiimide. J Biomed Mater Res Part A. 2003;64(3):427-38.
165. Delgado LM, Bayon Y, Pandit A, Zeugolis DI. To cross-link or not to cross-link? Cross-linking associated foreign body response of collagen-based devices. Tissue Eng Part B Rev. 2015;21(3):298-313.
166. Chang Y, Tsai CC, Liang HC, Sung HW. In vivo evaluation of cellular and acellular bovine pericardia fixed with a naturally occurring crosslinking agent (genipin). Biomaterials. 2002;23(12):2447-57.
167. Shahrokhi S, Arno A, Jeschke MG. The use of dermal substitutes in burn surgery: Acute phase. Wound Repair Regen. 2014;22(1):14-22.

168. Brown RA, Wiseman M, Chuo CB, Cheema U, Nazhat SN. Ultrarapid engineering of biomimetic materials and tissues: Fabrication of nano- and microstructures by plastic compression. Adv Funct Mater. 2005;15(11):1762-70.
169. Bitar M, Salih V, Brown RA, Nazhat SN. Effect of multiple unconfined compression on cellular dense collagen scaffolds for bone tissue engineering. J Mater Sci Mater Med. 2007;18(2):237-44.
170. Cheema U, Brown RA. Rapid Fabrication of Living Tissue Models by Collagen Plastic Compression: Understanding Three-Dimensional Cell Matrix Repair In Vitro. Adv Wound Care. 2013;2(4):176-84.
171. Braziulis E, Diezi M, Biedermann T, Pontiggia L, Schmucki M, Hartmann-Fritsch F, Luginbuhl J, Schiestl C, Meuli M, Reichmann E. Modified plastic compression of collagen hydrogels provides an ideal matrix for clinically applicable skin substitutes. Tissue Eng Part C Meth. 2012;18(6):464-74.
172. Oostendorp C, Meyer S, Sobrio M, van Arendonk J, Reichmann E, Daamen WF, van Kuppevelt TH. Evaluation of cultured human dermal- and dermo-epidermal substitutes focusing on extracellular matrix components: Comparison of protein and RNA analysis. Burns. 2017;43(3):520-30.
173. Novak T, Seelbinder B, Twitchell CM, van Donkelaar CC, Voytik-Harbin SL, Neu CP. Mechanisms and microenvironment investigation of cellularized high density gradient collagen matrices via densification. Adv Funct Mater. 2016;26(16):2617-28.
174. Brookes S, Voytik-Harbin S, Zhang H, Halum S. Three-dimensional tissue-engineered skeletal muscle for laryngeal reconstruction. Laryngoscope. 2018;128(3):603-9.
175. Zhang H, Voytik-Harbin S, Brookes S, Zhang L, Wallace J, Parker N, Halum S. Use of autologous adipose-derived mesenchymal stem cells for creation of laryngeal cartilage. Laryngoscope. 2018;128(4):E123-E9.
176. Worke LJ, Barthold JE, Seelbinder B, Novak T, Main RP, Harbin SL, Neu CP. Densification of Type I Collagen Matrices as a Model for Cardiac Fibrosis. Adv Healthc Mater. 2017;6(22).
177. Matthews JA, Wnek GE, Simpson DG, Bowlin GL. Electrospinning of collagen nanofibers. Biomacromolecules. 2002;3(2):232-8.

178. Huang L, Apkarian RP, Chaikof EL. High-resolution analysis of engineered type I collagen nanofibers by electron microscopy. Scanning. 2001;23(6):372-5.
179. Huang L, Nagapudi K, Apkarian RP, Chaikof EL. Engineered collagen-PEO nanofibers and fabrics. J Biomater Sci Polym Ed. 2001;12(9):979-93.
180. Buttafoco L, Kolkman NG, Engbers-Buijtenhuijs P, Poot AA, Dijkstra PJ, Vermes I, Feijen J. Electrospinning of collagen and elastin for tissue engineering applications. Biomaterials. 2006;27(5):724-34.
181. Prabhakaran MP, Venugopal J, Ramakrishna S. Electrospun nanostructured scaffolds for bone tissue engineering. Acta Biomater. 2009;5(8):2884-93.
182. Prabhakaran MP, Venugopal JR, Ramakrishna S. Mesenchymal stem cell differentiation to neuronal cells on electrospun nanofibrous substrates for nerve tissue engineering. Biomaterials. 2009;30(28):4996-5003.
183. Boland ED, Matthews JA, Pawlowski KJ, Simpson DG, Wnek GE, Bowlin GL. Electrospinning collagen and elastin: preliminary vascular tissue engineering. Front Biosci. 2004;9:1422-32.
184. Tillman BW, Yazdani SK, Lee SJ, Geary RL, Atala A, Yoo JJ. The in vivo stability of electrospun polycaprolactone-collagen scaffolds in vascular reconstruction. Biomaterials. 2009;30(4):583-8.
185. Rho KS, Jeong L, Lee G, Seo BM, Park YJ, Hong SD, Roh S, Cho JJ, Park WH, Min BM. Electrospinning of collagen nanofibers: effects on the behavior of normal human keratinocytes and early-stage wound healing. Biomaterials. 2006;27(8):1452-61.
186. Powell HM, Boyce ST. Engineered human skin fabricated using electrospun collagen-PCL blends: morphogenesis and mechanical properties. Tissue Eng Part A. 2009;15(8):2177-87.
187. DeFrates KG, Moore R, Borgesi J, Lin G, Mulderig T, Beachley V, Hu X. Protein-based fiber materials in medicine: A review. Nanomaterials (Basel). 2018;8(7).
188. Polk S, Sori N, Thayer N, Kemper N, Maghdouri-White Y, Bulysheva AA, Francis MP. Pneumatospinning of collagen microfibers from benign solvents. Biofabrication. 2018;10(4):045004.
189. Crump SS, inventor; Stratasys, Inc, assignee. Apparatus and method for creating three-dimensional objects patent 5,121,329. 1992 October 30, 1989.

190. Knowlton S, Onal S, Yu CH, Zhao JJ, Tasoglu S. Bioprinting for cancer research. Trends Biotechnol. 2015;33(9):504-13.
191. Nguyen DG, Pentoney SL, Jr. Bioprinted three dimensional human tissues for toxicology and disease modeling. Drug Discov Today Technol. 2017;23:37-44.
192. Skeldon G, Lucendo-Villarin B, Shu W. Three-dimensional bioprinting of stem-cell derived tissues for human regenerative medicine. Philos Trans R Soc Lond B Biol Sci. 2018;373(1750).
193. Jamroz W, Szafraniec J, Kurek M, Jachowicz R. 3D printing in pharmaceutical and medical applications - Recent achievements and challenges. Pharm Res. 2018;35(9):176.
194. Ozbolat IT. Bioprinting scale-up tissue and organ constructs for transplantation. Trends Biotechnol. 2015;33(7):395-400.
195. Ji S, Guvendiren M. Recent advances in bioink design for 3D bioprinting of tissues and organs. Front Bioeng Biotechnol. 2017;5:23.
196. Murphy SV, Atala A. 3D bioprinting of tissues and organs. Nat Biotechnol. 2014;32(8):773-85.
197. Datta P, Barui A, Wu Y, Ozbolat V, Moncal KK, Ozbolat IT. Essential steps in bioprinting: From pre- to post-bioprinting. Biotechnol Adv. 2018;36(5):1481-504.
198. Yue K, Trujillo-de Santiago G, Alvarez MM, Tamayol A, Annabi N, Khademhosseini A. Synthesis, properties, and biomedical applications of gelatin methacryloyl (GelMA) hydrogels. Biomaterials. 2015;73:254-71.
199. Chen YC, Lin RZ, Qi H, Yang Y, Bae H, Melero-Martin JM, Khademhosseini A. Functional human vascular network generated in photocrosslinkable gelatin methacrylate hydrogels. Adv Funct Mater. 2012;22(10):2027-39.
200. Nichol JW, Koshy ST, Bae H, Hwang CM, Yamanlar S, Khademhosseini A. Cell-laden microengineered gelatin methacrylate hydrogels. Biomaterials. 2010;31(21):5536-44.
201. Kim BS, Kim H, Gao G, Jang J, Cho DW. Decellularized extracellular matrix: a step towards the next generation source for bioink manufacturing. Biofabrication. 2017;9(3):034104.
202. Pati F, Jang J, Ha DH, Won Kim S, Rhie JW, Shim JH, Kim DH, Cho DW. Printing three-dimensional tissue analogues with decellularized extracellular matrix bioink. Nat Commun. 2014;5:3935.

203. Jang J, Park HJ, Kim SW, Kim H, Park JY, Na SJ, Kim HJ, Park MN, Choi SH, Park SH, Kim SW, Kwon SM, Kim PJ, Cho DW. 3D printed complex tissue construct using stem cell-laden decellularized extracellular matrix bioinks for cardiac repair. Biomaterials. 2017;112:264-74.
204. Badylak SF, Gilbert TW. Immune response to biologic scaffold materials. Semin Immunol. 2008;20(2):109-16.
205. Choudhury D, Tun HW, Wang T, Naing MW. Organ-derived decellularized extracellular matrix: A game changer for bioink manufacturing? Trends Biotechnol. 2018;36(8):787-805.
206. Elsdale T, Bard J. Collagen substrata for studies on cell behavior. J Cell Biol. 1972;54(3):626-37.
207. Kato YP, Christiansen DL, Hahn RA, Shieh SJ, Goldstein JD, Silver FH. Mechanical properties of collagen fibres: a comparison of reconstituted and rat tail tendon fibres. Biomaterials. 1989;10(1):38-42.
208. Kato YP, Silver FH. Formation of continuous collagen fibres: evaluation of biocompatibility and mechanical properties. Biomaterials. 1990;11(3):169-75.
209. Wasserman AJ, Kato YP, Christiansen D, Dunn MG, Silver FH. Achilles tendon replacement by a collagen fiber prosthesis: morphological evaluation of neotendon formation. Scanning Microsc. 1989;3(4):1183-97; discussion 97-200.
210. Dunn MG, Tria AJ, Kato YP, Bechler JR, Ochner RS, Zawadsky JP, Silver FH. Anterior cruciate ligament reconstruction using a composite collagenous prosthesis. A biomechanical and histologic study in rabbits. Am J Sports Med. 1992;20(5):507-15.
211. Goldstein JD, Tria AJ, Zawadsky JP, Kato YP, Christiansen D, Silver FH. Development of a reconstituted collagen tendon prosthesis. A preliminary implantation study. J Bone Joint Surg Am. 1989;71(8):1183-91.
212. Kato YP, Dunn MG, Zawadsky JP, Tria AJ, Silver FH. Regeneration of Achilles tendon with a collagen tendon prosthesis. Results of a one-year implantation study. J Bone Joint Surg Am. 1991;73(4):561-74.
213. Lai ES, Anderson CM, Fuller GG. Designing a tubular matrix of oriented collagen fibrils for tissue engineering. Acta Biomater. 2011;7(6):2448-56.

214. Isobe Y, Kosaka T, Kuwahara G, Mikami H, Saku T, Kodama S. Oriented collagen scaffolds for tissue engineering. Materials. 2012;5(3):501-11.
215. Marelli B, Ghezzi CE, James-Bhasin M, Nazhat SN. Fabrication of injectable, cellular, anisotropic collagen tissue equivalents with modular fibrillar densities. Biomaterials. 2015;37:183-93.
216. Cheng X, Gurkan UA, Dehen CJ, Tate MP, Hillhouse HW, Simpson GJ, Akkus O. An electrochemical fabrication process for the assembly of anisotropically oriented collagen bundles. Biomaterials. 2008;29(22):3278-88.
217. Younesi M, Donmez BO, Islam A, Akkus O. Heparinized collagen sutures for sustained delivery of PDGF-BB: Delivery profile and effects on tendon-derived cells In-Vitro. Acta Biomater. 2016;41:100-9.
218. Younesi M, Knapik DM, Cumsky J, Donmez BO, He P, Islam A, Learn G, McClellan P, Bohl M, Gillespie RJ, Akkus O. Effects of PDGF-BB delivery from heparinized collagen sutures on the healing of lacerated chicken flexor tendon in vivo. Acta Biomater. 2017;63:200-9.
219. Murthy NS. Liquid crystallinity in collagen solutions and magnetic orientation of collagen fibrils. Biopolymers. 1984;23(7):1261-7.
220. Torbet J, Ronziere MC. Magnetic alignment of collagen during self-assembly. Biochem J. 1984;219(3):1057-9.
221. Worcester DL. Structural origins of diamagnetic anisotropy in proteins. Proc Natl Acad Sci. 1978;75(11):5475-7.
222. Guido S, Tranquillo RT. A methodology for the systematic and quantitative study of cell contact guidance in oriented collagen gels. Correlation of fibroblast orientation and gel birefringence. J Cell Sci. 1993;105 (Pt 2):317-31.
223. Builles N, Janin-Manificat H, Malbouyres M, Justin V, Rovere MR, Pellegrini G, Torbet J, Hulmes DJ, Burillon C, Damour O, Ruggiero F. Use of magnetically oriented orthogonal collagen scaffolds for hemi-corneal reconstruction and regeneration. Biomaterials. 2010;31(32):8313-22.
224. Torbet J, Malbouyres M, Builles N, Justin V, Roulet M, Damour O, Oldberg A, Ruggiero F, Hulmes DJ. Orthogonal scaffold of magnetically aligned collagen lamellae for corneal stroma reconstruction. Biomaterials. 2007;28(29):4268-76.

3. DESIGN AND BIOFABRICATION OF DERMAL REGENERATION SCAFFOLDS: ROLE OF OLIGOMERIC COLLAGEN FIBRIL DENSITY AND ARCHITECTURE

This chapter is reproduced with permission from:

Sohutskay, David O., Kevin P. Buno, Sunil S. Tholpady, Samantha J. Nier, and Sherry L. Voytik-Harbin. "Design and biofabrication of dermal regeneration scaffolds: role of oligomeric collagen fibril density and architecture." *Regenerative Medicine* 15.2 (2020): 1295-1312.

3.1 Abstract

Aim: To evaluate dermal regeneration scaffolds custom-fabricated from fibril-forming oligomeric collagen where the total content and spatial gradient of collagen-fibrils was specified. **Methods:** Microstructural and mechanical features were verified by electron microscopy and tensile testing. The ability of dermal scaffolds to induce regeneration of rat full-thickness skin wounds was determined and compared to no fill control, autograft skin, and a commercial collagen dressing. **Results:** Increasing fibril content of oligomer scaffolds inhibited wound contraction and decreased myofibroblast marker expression. Cellular and vascular infiltration of scaffolds over the 14-day period varied with the graded density and orientation of fibrils. **Conclusion:** Fibril content, spatial gradient, and orientation are important collagen scaffold design considerations for promoting vascularization and dermal regeneration while reducing wound contraction.

3.2 Introduction

Difficult-to-heal and chronic wounds of the skin are among the most common and costly medical problems experienced. A variety of mechanisms can lead to this, such as trauma, burns, oncologic resection, or systemic disease[1], with the scope and magnitude of therapy varying significantly with individual age, etiology, and severity. For non-healing and large wounds, autologous split-thickness skin grafts (STSG) can be a reasonable option despite limitations in their availability and capacity to fully recapitulate dermal function which leads to frequent scarring and contracture[2]. These tissue grafts also suffer from low take rates, especially in cases of chronic wounds due to systemic disease[3]. As an alternative, several dermal substitutes have been developed and are commercially available. Of these, the most prevalent is decellularized scaffolds

derived from xenogeneic or allogeneic tissues (e.g., placenta, dermis) and bioengineered resorbable collagen sponges fashioned from fibrillar collagen microparticulate in the presence and absence of glycosaminoglycans (GAGs). These dermal replacements are also generally slow to cellularize and vascularize, requiring host-cell deposition of collagen as the scaffold actively degrades (resorbs) via an inflammatory mediated process[4]. Additionally, cellularization is often accompanied by myofibroblasts, known contributors to wound contraction and contracture[2, 5, 6]. Collectively, it is for the above stated reasons, that a need exists for new therapeutic approaches designed to accelerate wound closure and improve dermal regeneration to reduce morbidity and mortality associated with difficult-to-heal wounds.

Normal healing of acute skin wounds, where both the epidermal and dermal layers are breached, is a well-orchestrated "repair" process. This process involves four overlapping phases including hemostasis, inflammation, granulation, and remodeling/maturation, with the length of these phases varying based on wound etiology and severity[7]. Large surface area and chronic (remain unhealed for >12 weeks) wounds, on the other hand, fail to proceed through these phases in an orderly fashion. Although these wounds vary significantly, common features include prolonged or dysregulated inflammation and excessive destruction (proteolytic degradation) or contraction of the newly deposited collagen matrix[8]. The lack of sufficient and persistent dermal collagen within the wound space not only prevents the wound from moving forward in the healing process but also leads to the influx of more inflammatory cells thus amplifying the inflammation cycle[9]. This situation is further exacerbated in elderly patients or certain pathological conditions (e.g., diabetes), where wound healing is characterized by delayed and reduced collagen deposition, delayed vascularization, and increased senescence of fibroblasts and relevant stem/progenitor cell populations[7].

The dermal layer of skin is primarily comprised of a fibrillar type I collagen scaffold, which is responsible for imparting both structural and mechanical integrity. For this reason, substantial emphasis has been directed toward development of dermal substitutes that recapitulate various compositional and physical features of the native dermal extracellular matrix (ECM), such as the fibrillar collagen microstructure and the complex macromolecular composition including growth factors [10]. Additionally, there has been increasing interest in defining the multi-scale physical forces between cells and the surrounding collagen scaffold and their role in modulating fundamental cell behavior as well as tissue generation[11, 12]. This mechanobiology perspective

highlights the fact that cells probe, attach, and tug on (remodel) the fibrillar scaffold via specific cell surface receptors known as integrins. The mechanical forces experienced at these linkages in turn result in activation of downstream mechanochemical signaling pathways ultimately regulating cell phenotype and function. In the case of wounds, this hierarchical mechanochemical signaling imparted by the dermis is disrupted and the physical context of the surrounding tissue scaffold and constituent cells dramatically altered[11]. The loss of mechanical stability requires host cells to produce, deposit, and remodel their own new ECM, delaying healing and leading to complications such as fluid loss, infection, and scarring. Here we converge principles and practices of mechanobiology and collagen polymer-based material customization with the goal of prioritizing design criteria for the scalable fabrication of mechano-instructive fibrillar collagen scaffolds for dermal regeneration.

Our bioinspired design strategy involves type I oligomeric collagen, a highly-purified, fibril-forming collagen that, unlike monomeric formulations (e.g., atelocollagen and telocollagen), retains natural intermolecular crosslinks[13]. Conventional monomeric collagens that are acid-solubilized and purified from tissues represent single triple-helical molecules (telocollagen: full length tropocollagen molecule; atelocollagen: truncated tropocollagen molecule) consisting of three polypeptide chains (typically two $\alpha 1$ and a single $\alpha 2$ chains). Oligomeric collagen, on the other hand, represents acid-soluble aggregates of collagen molecules (e.g., trimers of tropocollagen molecules) that are covalently bonded by a crosslink chemistry produced by the lysyl oxidase family of enzymes during in-vivo collagen assembly[13, 14]. Differences between atelocollagen, telocollagen, and oligomeric collagen have been documented, including their molecular composition, average molecular weight, and, most importantly, in-situ fibril-forming capacity upon neutralization (i.e., their inherent capacity to undergo self-assembly to form fibrillar matrices)[13-15]. Compared to monomeric collagen, oligomers display more rapid fibril formation (~60 seconds at body temperature), yielding matrices (scaffolds) with increased fibril-fibril connectivity. The increased connectivity between fibrils, together with the presence of natural intermolecular crosslinks, contributes to improved stability (shape retention; resistance to proteolytic degradation) and mechanical properties of formed fibrillar scaffolds[13, 15, 16]. Further, in-vitro studies show that differences between oligomer and monomer scaffolds can be sensed by cells, with the increased resistance to cellular traction forces provided by oligomer scaffolds modulating fundamental cell behavior, including proliferation, migration, differentiation,

and tissue morphogenesis [13, 14, 17, 18]. Since collagen oligomers overcome a number of apparent limitations inherent to monomeric formulations, our group continues to evaluate their utility as a platform natural polymer for a variety of tissue engineering and regenerative medicine applications (see [19] for a recent review).

When formed at relatively low fibril content (≤ 5 mg/mL), oligomer scaffolds can be further processed via confined compression to controllably reduce the interstitial fluid content and increase the overall content of collagen fibrils (weight percent of fibrillar collagen). This scalable biofabrication technique, which represents a modified version of collagen gel compression methods described by Brown and co-workers[20], has been applied for i) customization of scaffolds varying in geometry and overall fibril content as well as ii) creation of scaffolds with continuous gradients of varying fibril density (porosity) and/or fibril orientation [16, 21]. In this way, anisotropic properties displayed by the fibrillar collagen component of tissues can be better approximated and the contributions of cell-collagen mechanochemical signaling during tissue remodeling and regeneration elucidated.

In the present study, we hypothesized that the total content and spatial gradient of collagen fibrils, as controlled by confined compression, are important determinants of oligomer scaffold mechanics and the *in-vivo* tissue response following application to rat full-thickness excisional wounds. More specifically, based on previous work, we anticipated that increasing the total fibrillar collagen content would increase the mechanical modulus and strength of scaffolds and reduce wound contraction, while providing a barrier to cellular infiltration. As such, we hypothesized that fabrication of scaffolds with a spatial gradient in collagen fibrils, progressing upward from low to high collagen-fibril content (i.e., high to low porosity) would facilitate cellularization and vascularization while maintaining the necessary macro-scale mechanical properties. First, cryogenic scanning electron microscopy (cryo-SEM) and tensile mechanical testing were used to define the microstructure and bulk tensile properties of bioengineered oligomer scaffolds compared to normal rat dermis and HeliCote. HeliCote was selected for comparison since it represents a bioengineered collagen wound dressing fabricated from fibrillar collagen microparticulate and is non-crosslinked[22]. Next, oligomer scaffolds, along with the commercial dressing, autograft skin, and no fill controls, were evaluated in an established rat full-thickness excisional skin model, where gross appearance and wound contraction were measured

over a 14-day period. Harvested tissues were processed and analyzed histologically for general tissue response, as well as specific markers of myofibroblast activation and tissue vascularization.

3.3 Materials and Methods

3.3.1 Controlled Confined Compression Device for Oligomer Dermal Scaffold Fabrication

Oligomer dermal scaffolds were fabricated with a custom-designed confined compression device (Figure 3.1). The device consisted of a compression head that was designed in SolidWorks (SolidWorks, Waltham, MA) and 3D-printed using a Stratasys 3D Printer (Stratasys, Eden Prairie, MN) for use with a standard 24-well culture plate. The compression head was adapted with small cylinders (1.5 cm diameter) of porous polyethylene foam (0.25" thick, 50 μm pores; Scientific Commodities Inc., Lake Havasu City, AZ). Indentations drilled into the center of each foam cylinder allowed press-fitting onto the compression head. The compression head was sterilized with gas plasma for 30 minutes, after which foam ends were rinsed with sterile phosphate buffered saline (PBS) to remove any residuals.

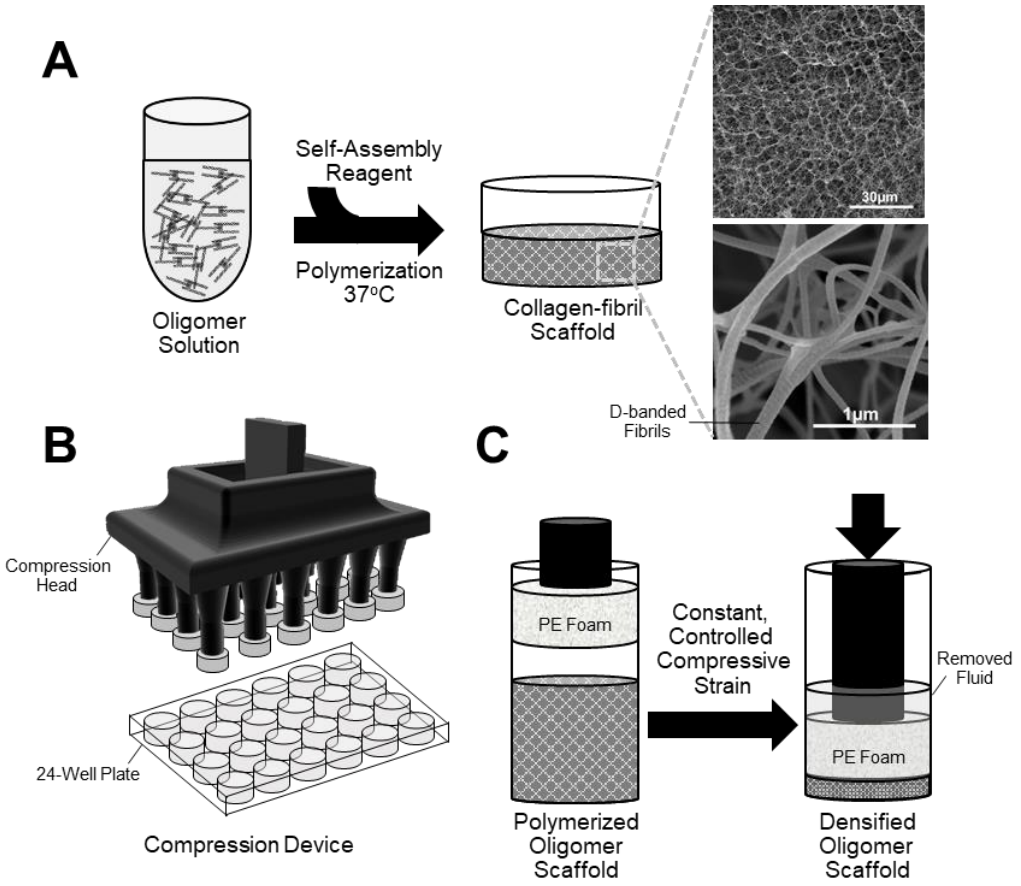

Figure 3.1. Process diagrams for preparation of oligomer dermal scaffolds. (A) Acid-soluble oligomer solution (4 mg/mL) was neutralized and polymerized at 37oC, yielding a low-density oligomer matrix. (B) Schematic of confined compression device, featuring a compression head with porous polyethylene (PE) foam platens. (C) Application of different levels of strain in a confined compression format to low-density matrices yields densified scaffolds that vary in total content and spatial gradient of collagen fibrils.

3.3.2 Oligomer Dermal Scaffolds and Commercial Collagen Dressing

Oligomer dermal scaffolds representing various total content and spatial gradients of collagen fibrils were fabricated from type I oligomeric collagen derived from the dermis of market weight pigs as described previously[13]. Before use, lyophilized collagen was dissolved in 0.01N hydrochloric acid and concentration determined by a Sirius red assay. To induce polymerization (self-assembly) of collagen-fibril scaffolds, acidic solutions of oligomer were neutralized to physiologic pH and ionic strength with a proprietary neutralization reagent and warmed to 37°C. All oligomeric collagen formulations were standardized based molecular composition and polymerization capacity in accordance with ASTM International standard F3089-14[23]. Here,

polymerization capacity is defined by the shear storage modulus (G', Pa) of a polymerized scaffold as a function of oligomer concentration of the polymerization reaction[13]. The resultant polymerization capacity curves for an oligomeric collagen formulation must be consistent with our historic database[13] to be deemed acceptable.

To fabricate oligomer dermal scaffolds, neutralized oligomer solutions (4.0 mg/mL) were pipetted into 24-well plates at specific volumes (230 µL, 1150 µL, and 2300 µL) and polymerized at 37°C. Following polymerization, wells containing 230 µL oligomer were not further processed, yielding 4 mg/cm^3 scaffolds (Oligomer-4) with a diameter of 15.6 mm and thickness of 1.2 mm. This thickness was chosen to approximate the thickness of rat dermis[24]. Wells containing 1150 µL and 2300 µL oligomer were subjected to controlled confined compression[16, 21] to a thickness of 1.2 mm, yielding 20 mg/cm^3 (Oligomer-20) and 40 mg/cm^3 (Oligomer-40) scaffolds, respectively. Confined compression at a strain rate of 0.1/s was conducted with the compression head adapted to a universal mechanical testing machine (TestResources, Shakopee, MN). All oligomer dermal scaffolds were stored in sterile PBS prior to surgical implantation.

HeliCote, a commercial collagen wound dressing, was obtained from Integra Miltex (York, PA). HeliCote is manufactured via a proprietary methodology that involves lyophilization of a slurry of comminuted bovine tendon, yielding a freeze-dried collagen sponge.

3.3.3 Ultra- and Micro-structure Analysis

Ultra- and micro-structure analysis of oligomer dermal scaffolds, commercial collagen dressing, and normal rat dermis was performed via cryo-SEM using an FEI NOVA nanoSEM 200 (FEI, Hillsboro, OR) varying between an Everhart-Thronley (<10,000x magnification) or immersion lens (>10,000x magnification) detector[16]. Samples were flash-frozen by submersion into critical point liquid nitrogen, transferred to a CT1000 cold-stage attachment (Oxford Instruments North America, Inc., Concord, MA), and sublimated under vacuum. Samples were subsequently sputter coated with platinum and imaged. Images (15,000x magnification) were analyzed using FIJI/ImageJ and the directionality tool used to create histograms of fibril orientation. To analyze porosity, the DiameterJ plugin was used to binarize the images using a statistical region-merging algorithm[25, 26]. The Analyze Particles tool was used to measure pore diameters.

3.3.4 Rat Full-thickness Excisional Skin Model

All animal studies were conducted according to protocols approved by the Purdue University Institutional Animal Care and Use Committee. Male Sprague-Dawley rats, weighing 200 to 250 g (7 to 9 weeks of age; Charles River Laboratories, Wilmington, MA), were anesthetized using isoflurane gas. A sterile punch (15 mm diameter) was used to create a total of two full-thickness skin wounds, including the panniculus carnosus muscle, positioned on either side of the sagittal plane of the rat dorsum. Wounds were randomly assigned to experimental treatment and control groups, with experimental treatment groups consisting of Oligomer-4, Oligomer-20, Oligomer-40, and commercial collagen dressing (n = 4-10). Oligomer-20 and Oligomer-40 samples, which exhibited sidedness owing to the graded microstructure, were positioned with their more porous (less dense), isotropic region on the bottom of the wound bed. For a subset of animals, the excised full-thickness skin was applied to the opposite wound, serving as an autograft (positive control). Wounds left as unfilled (no fill) served as negative controls. Materials with sufficient handling and suturability, specifically Oligomer-20, Oligomer-40, and autograft, were sutured into place with non-absorbable 5-0 silk sutures (Perma-Hand Silk, Ethicon, Somerville, NJ). All wounds were covered with an occlusive petrolatum gauze to prevent moisture loss (XeroformTM, Covidien, Dublin, Ireland), a non-adherent pad (McKesson, San Francisco, CA), and an adhesive film dressing (Tegaderm, 3M, St. Paul, MN). For additional support, the rats were wrapped with self-adherent cohesive bandages (VetRap, 3M, St. Paul, MN) and secured with a non-stretch porous tape (ZONAS, Johnson & Johnson, Inc., Arlington, TX). Investigators were not blinded to treatment groups due to the apparent visual and handling differences between implant materials.

Dressing changes were performed at 7 days or as needed. Photographs of wound areas were taken with a ruler in the field of view at 0, 7, and 14 days. At 7- and 14-day study endpoints, animals were euthanized and wound areas and associated implants were excised *in toto* and processed for histopathological analysis. Absolute wound areas were quantified using a MATLAB (The Mathworks, Natick, MA) script and normalized to original wound areas. Autografts that did not successfully take after 7 days, as determined by visual color changes indicating extensive tissue necrosis, were not included in the analysis.

3.3.5 Histopathological Analysis

Excised tissue was fixed in 4% paraformaldehyde for at least 24 hours and then transferred to PBS. Bisected samples were embedded in paraffin and sectioned (4 μm thickness). Sections were stained with hematoxylin and eosin (H&E) and Masson's Trichrome for general histopathological analysis. Additional paraffin sections were stained with primary antibodies for alpha-smooth muscle actin (α-SMA; ab5694, Abcam, Cambridge, UK; 1:500 dilution) and CD31 (AF3628SP, R&D Systems, Minneapolis, MN; 1:50 dilution). After incubation with a secondary antibody (α-SMA: GoRb ImmPRESS HRP, Vector Laboratories, Burlingame, CA) according to manufacturer instructions, slides were developed with 3,3'-diaminobenzidine (DAB) (ImmPACT DAB, Vector Laboratories) for 5 minutes, washed, and counterstained with hematoxylin. Light microscopy was performed on an upright microscope (Eclipse E200, Nikon, Melville, NY) adapted with a Leica DFC480 camera (Leica, Buffalo Groove, IL).

3.3.6 Uniaxial Tensile Testing

Uniaxial tensile testing was performed in ambient air on dog-bone shaped samples with a gauge length, width, and thickness of 4 mm, 2 mm, and 1.2 mm, respectively ($n \geq 4$). The average duration of mechanical testing from set up to completion was less than 10 seconds and sample dehydration was not observed. All samples were tested in uniaxial tension to failure at a strain rate of 38.4% per second using a servo electric material testing system (TestResources) adapted with a 25 N load cell at a sampling rate of 100 Hz. This testing protocol has been applied previously for mechanical properties testing of oligomer scaffolds [16] and rat skin [27]. Young's modulus (E_T) was calculated from the linear region of the stress strain curve. Ultimate tensile stress (UTS) represented peak stress experienced by the sample, and failure strain (ε_f) was the strain at which samples experienced total failure. Samples that failed outside the gauge region were excluded from data analysis.

3.3.7 Statistical Analysis

Statistical analyses were performed using statistical analysis software (SAS, Cary, NC). Unless otherwise stated, comparisons were made using one-way analysis of variance (ANOVA) with a Tukey post hoc test. A critical global p-value of 0.05 was used.

3.4 Results

3.4.1 Controlled Confined Compression of Low-Density Oligomer Matrices Supports Custom Fabrication of Dermal Scaffolds.

Confined compression of low-density oligomer matrices at specified strain rates has been used previously to fabricate collagen scaffolds varying in total content and spatial gradients of collagen fibrils [16, 21]. Here, this method was used to create densified dermal scaffolds, namely Oligomer-20 (5x compression of a 4 mg/cm^3 matrix to 20 mg/cm^3) and Oligomer-40 (10x compression of a 4 mg/cm^3 matrix to 40 mg/cm^3), each of which had the same final dimensions of 15.6 mm diameter and 1.2 mm thickness. Scaffold ultra- and micro-structures were visualized by cryo-SEM and compared to uncompressed scaffolds (Oligomer-4; 4 mg/cm^3 matrix), normal rat skin, and HeliCote (commercial collagen dressing), with an emphasis on fibril density, fibril orientation, and estimated scaffold pore size (Figure 3.2A-C).

As expected, the dermal layer of normal rat skin featured a layered construction, which was evident both qualitatively and quantitatively (Figure 3.2A-B) and consistent with previously published cryo-SEM studies of mammalian skin[28, 29]. Fibrils and/or fibril bundles aligned in a basket-weave pattern parallel and oblique to the skin surface at all levels. The upper papillary dermis region appeared as loose, porous connective tissue bordered by dense sheets of fibrillar collagen. The underlying reticular dermis featured densely packed individual fibrils, with apparent fibril bundles aligned parallel to the surface. Estimated pore diameters for the reticular dermis ranged from 0.2 to 3 μm, with more uniform and well-defined pores (on the order of 5 μm) evident within the papillary dermis.

Evaluation of Oligomer-20 and Oligomer-40 revealed a greater overall collagen-fibril content compared to uncompressed Oligomer-4, with Oligomer-40 exhibiting the greatest (Figure 3.2). Spatial gradients differing in fibril content and orientation were apparent within Oligomer-20 and Oligomer-40 (Figure 3.2A-B). High-density regions near the surface appeared as aggregates or bundles of fibrils aligned parallel to the surface, with fibril density and extent of alignment decreasing with distance from the surface. Fibril alignment, which was induced during scaffold fabrication, was observed reproducibly within the upper two-thirds of Oligomer-40 scaffolds, while Oligomer-20 displayed aligned fibrils only in the upper one-third region (Figure 3.2A-B). Toward the bottom, individual fibrils were randomly oriented, giving rise to an isotropic,

porous network which was similar to that observed for uncompressed Oligomer-4. Within the porous regions, estimated pore diameters were on the order of 3 μm, while more dense, aligned regions had more varied pore sizes (0.8-3 μm) similar to that of the reticular dermis. The commercial dressing, on the other hand, exhibited a dramatically different construction, with its loose, porous network formed by small meshes of fibrillar collagen microparticulate (Figure 3.2C). The pore size for this material was on the order of 100 μm, which is consistent with published values[6] and more than an order-of-magnitude greater than that observed for rat skin and oligomer scaffolds.

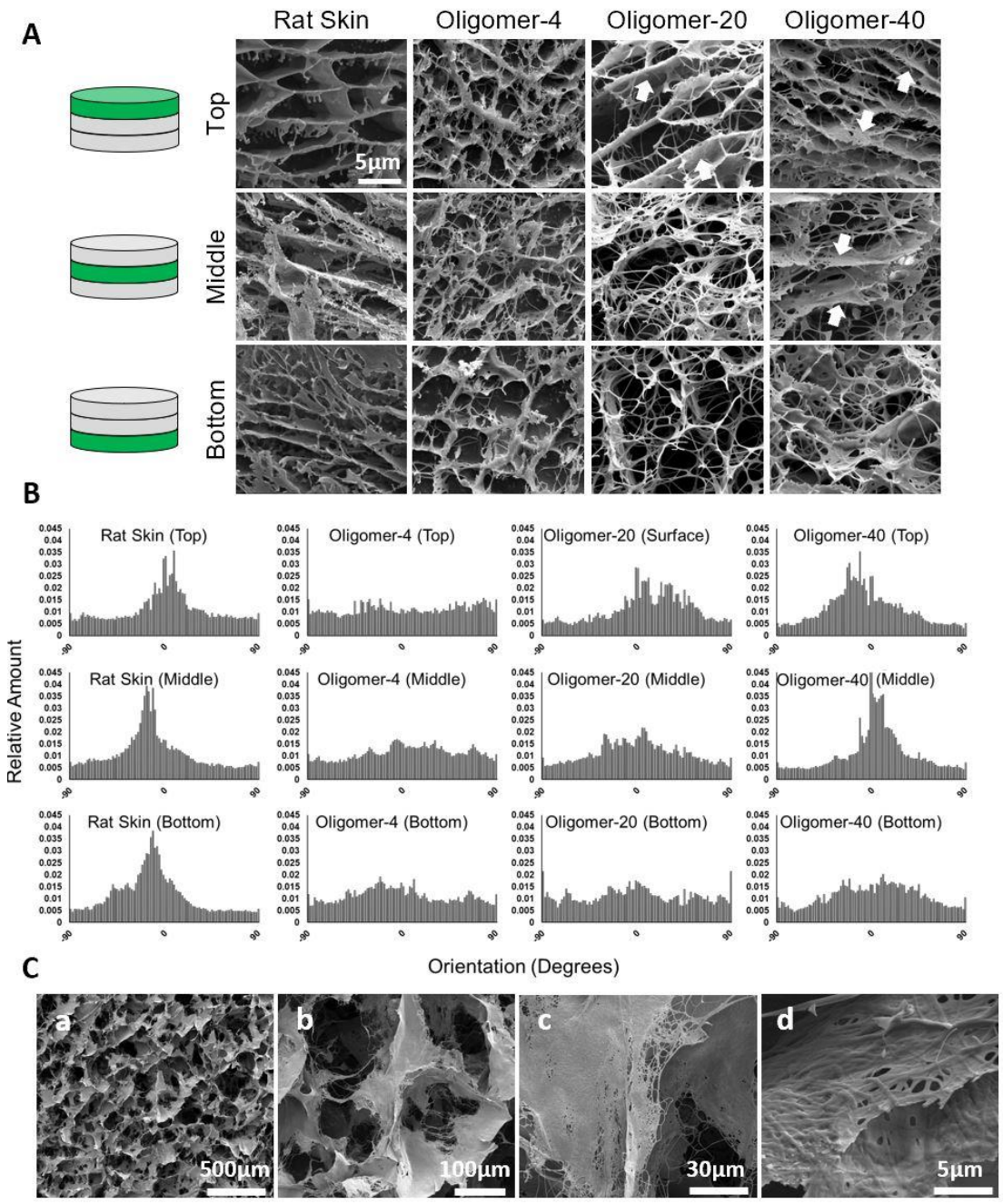

Figure 3.2. (A) Cryo-SEM images showing layered ultra and micro-structure of normal rat skin and oligomer dermal scaffolds. Arrows highlight fibril bundling and alignment within Oligomer-20 and Oligomer-40 scaffolds. Scalebar: 5 µm. (B) Fibril directionality histograms for normal rat skin and oligomer dermal scaffolds. Alignment is indicated in the histogram profile, where a peak near 0 degrees corresponds to alignment parallel to the surface of the tissue. (C) Cryo-SEM images showing ultra- and micro-structure of commercial collagen dressing. At low magnification the relatively large porous microstructure formed by tissue microparticulate is evident (a,b). High magnification images reveal dense fibrillar collagen within particulated tissue (c,d). Scalebars: a: 500 µm; b: 100 µm; c: 30 µm; d: 5 µm.

3.4.2 Tensile Properties of Oligomer Dermal Scaffolds Increase with Collagen Content.

In addition to microstructure features, mechanical properties of fabricated collagen scaffolds are important design considerations, dictating not only macro-scale mechanical properties (e.g., handling, suturability) but also cell-collagen mechanochemical signaling. Representative stress-strain plots for oligomer scaffolds and the commercial collagen dressing are shown in Figure 3.3A. As expected, oligomer scaffold tensile properties increased with their overall collagen fibril content. All oligomer groups were statistically different, with E_T and UTS values ranging from 230 $\pm$ 32.4 kPa and 79.7 $\pm$ 11.81 kPa for Oligomer-4 to 985 $\pm$ 265 kPa and 336 $\pm$ 60.2 kPa for Oligomer-40 (Figures 3.3B-C). Mechanical properties for the commercial collagen dressing were most similar to Oligomer-20 with E_T of 753 $\pm$ 137 kPa and UTS of 210 $\pm$ 30.3 kPa (Figure 3.3B-C), despite differences in their method of fabrication and microstructure. Interestingly, no statistical difference was observed in failure strain, which measured roughly 25% for all materials (Figure 3.3D).

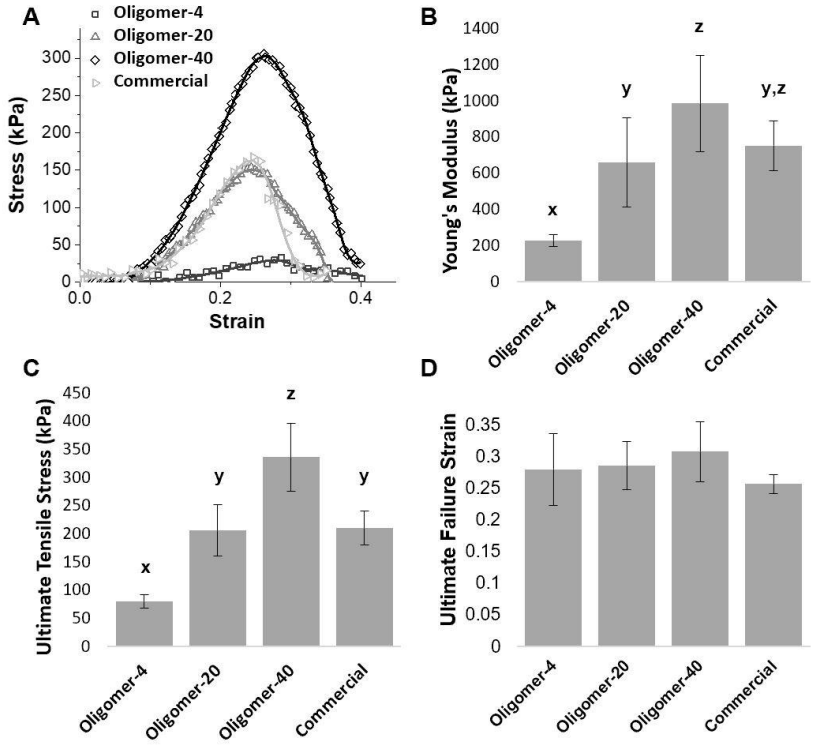

Figure 3.3. Tensile mechanical properties for oligomer dermal scaffolds and commercial collagen dressing. Dog-bone shaped samples with gauge length, width, and thickness of 4 mm, 2 mm, and 1.2 mm, respectively, were subjected to uniaxial tensile loading. (A) Representative stress-strain curves, (B) Young's modulus, (C) ultimate stress, and (D) failure strain, are shown (mean ± SD; $n \geq 4$). Letters indicate statistically different groups; $p < 0.05$.

3.4.3 Oligomer-20 and Oligomer-40 Scaffolds Persist within the Wound Bed and Resist Wound Contraction.

Efficacy of regenerative dermal replacements is dependent, in part, on their ability to resist wound contraction and provide a persistent biological scaffold that induces rapid cellularization, vascularization, and epithelialization. To test the hypothesis that the total content and spatial gradient of collagen fibrils within oligomer scaffolds are important determinants of wound healing outcomes, scaffolds were applied to full-thickness excisional skin wounds prepared on the rat dorsum. Compressed scaffolds, which demonstrated a spatial gradient of fibrils, were placed with the porous (less dense), isotropic region near the wound base to facilitate cellular integration. Representative wound images taken on days 0, 7, and 14 for the various treatment groups are shown in Figure 3.4A, with normalized wound area measurements in Figure 3.4B. As expected, autografts were most effective at limiting wound contraction. The majority of autografts showed a cyanotic discoloration by day 7 (Figure 3.4A), with a small number of grafts (20%) failing to take, as evidenced by extensive necrosis and black coloration. Initial contraction of the autograft and wound site contributed to roughly a 25% decrease in wound area within the first 7 days with no further changes observed on day 14. By contrast, unfilled wounds showed progressive and substantial contraction over the 14-day study period. At 14 days, only about 10% of the wound area remained, appearing as elongated scars with sagittal plane alignment. Similar results were observed for wounds treated with Oligomer-4 and the commercial dressing.

Interestingly, Oligomer-20 and Oligomer-40 served as dermal replacements that modulated wound contraction based on total collagen content (Figure 3.4A-B). Upon gross examination after 7 days, Oligomer-20 and Oligomer-40 constructs persisted within the wound bed and showed no discoloration (Figure 3.4A). By 14 days, these constructs showed signs of epithelialization and integration with the surrounding normal skin (Figure 3.4A). While Oligomer-20 and Oligomer-40 yielded statistically similar wound areas that measured roughly 50-60% at day 7, Oligomer-40 wound sizes stabilized, showing no additional significant reduction in size at day 14 (Figure 3.4B). By contrast, wounds treated with Oligomer-20 showed a more progressive decrease in wound size over the 14-day period; however, the observed contraction rate was decreased compared to Oligomer-4, commercial dressing, and no fill groups. Notably, both Oligomer-20 and Oligomer-40 scaffolds showed no evidence of rapid resorption or proteolytic degradation at either the 7- or 14-day time points.

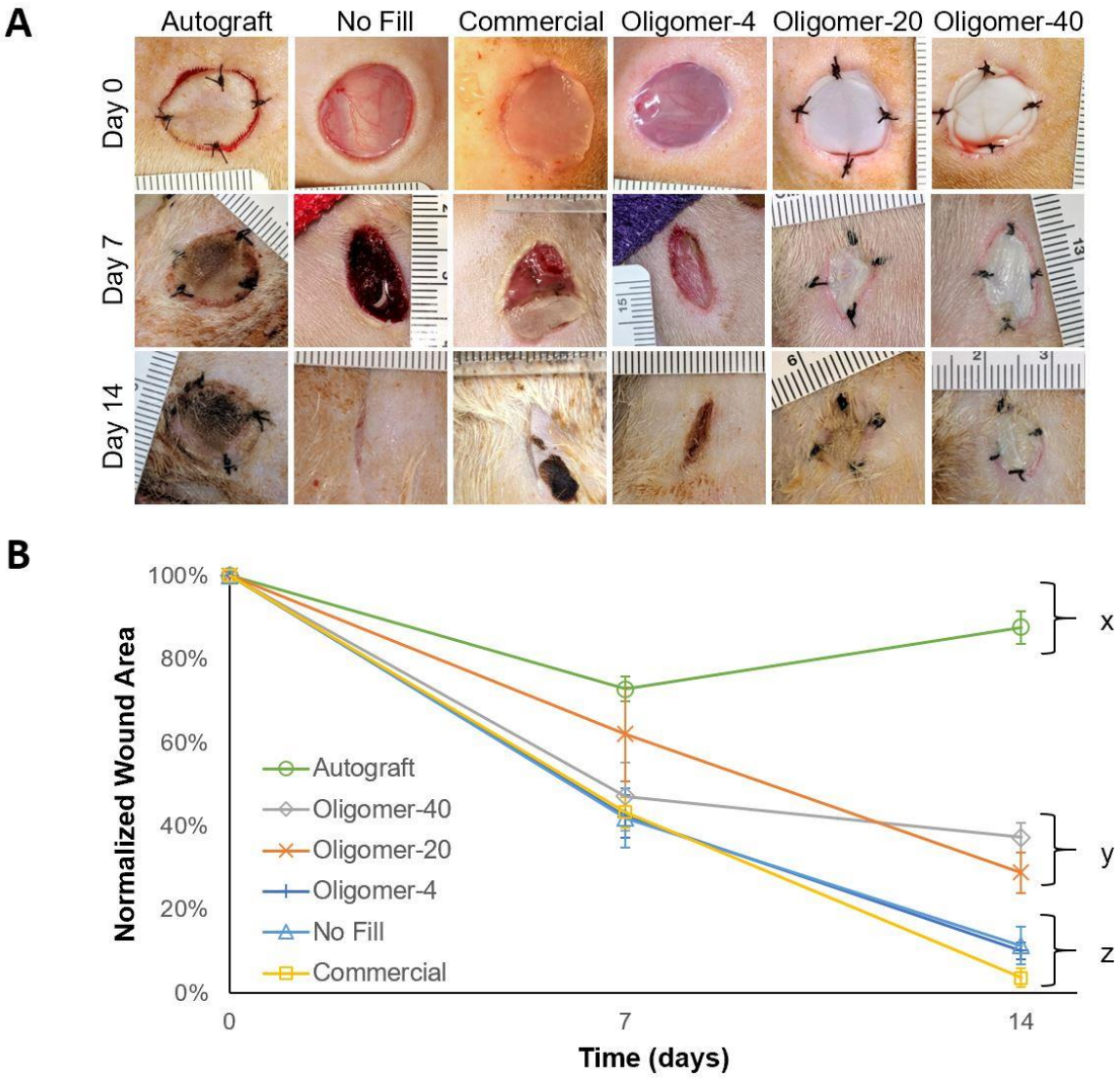

Figure 3.4. (A) Representative gross images of full-thickness skin wounds at 0, 7, and 14 days following various treatments. (B) Graph showing time-dependent changes in normalized wound area for each group (mean ± SD; n = 4-8 for control and experimental groups). Letters indicate statistically different groups; $p < 0.05$.

3.4.4 Spatial Gradient of Collagen Fibrils Modulates Timing and Extent of Cellularization and Vascularization

In addition to modulating wound contraction, dermal replacements should induce rapid cellularization and vascularization to encourage tissue regeneration rather than classic wound healing with scar formation. Histopathological analysis was performed on excised tissue sections stained with H&E (data not shown) as well as Masson's trichrome (Figure 3.5), which facilitates

collagen visualization. Additionally, immunostaining for myofibroblasts (Figure 3.6A) and endothelial cells (Figure 3.6B) was used to investigate patterns of cellularization and vascularization for each treatment group.

Autograft-treated wounds showed limited revascularization and cellular infiltration over the 14-day period (Figure 3.5). Even in grafts which took successfully, numerous necrotic cells, including atrophying muscle cells of the panniculus carnosus muscle were evident. This tissue devitalization contributed to the development of regional inflammation, which was evident throughout the graft material, especially at 14 days. A decrease in the health and thickness of the epidermis was also noted at both 7 and 14 days. Unfilled wounds, on the other hand, displayed the classic phases of wound healing over the 14-day period which was facilitated by substantial contraction of wound edges (Figure 3.5). A low-density provisional wound matrix was evident at day 7, populated by numerous inflammatory cells, including macrophages and neutrophils. By day 14, the narrowed wound area was largely populated by myofibroblasts (Figure 3.6A), with increased amounts of fibrillar collagen that stained dark blue, and a multilayered epithelium along the surface. By contrast, wounds treated with the commercial dressing showed limited cellular migration and vascularization at day 7 (Figure 3.5). By 14 days, the porous dark blue staining material showed gradual resorption, as evidenced by active proteolytic degradation and phagocytosis by macrophages and giant cells, especially within the lower regions of the material (Figure 3.5). As the commercial dressing degraded and the wound contracted, it was replaced with fibrous collagen deposited by host cells, and neovascularization and epithelialization were evident (Figure 3.5,3.6B). While no myofibroblasts were observed within central regions of the commercial dressing, they were evident within areas of newly deposited collagen (Figure 3.6A).

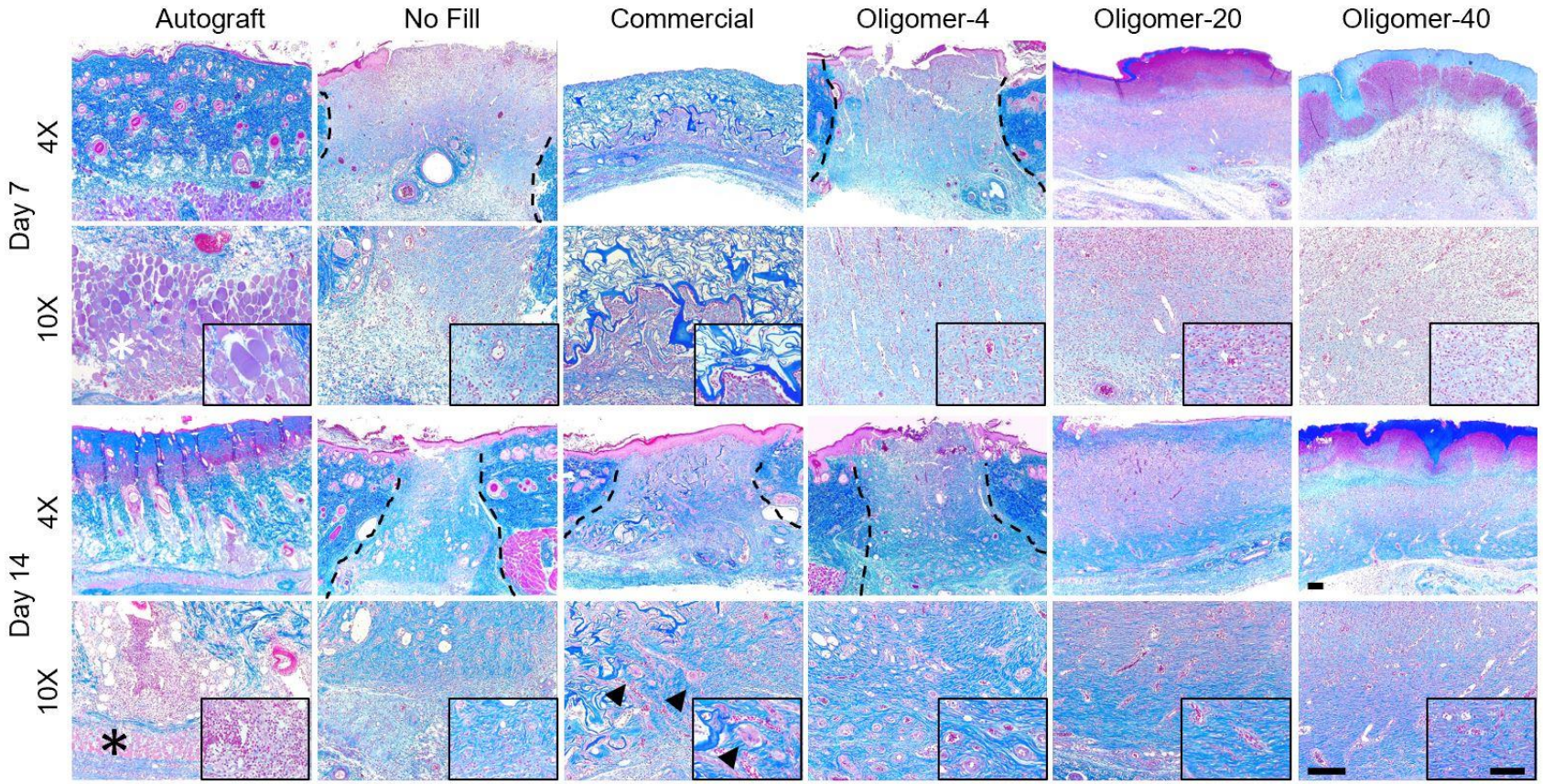

Figure 3.5. Histological cross-sections (4x and 10x with 40x inset) of excised skin wounds 7 days (above) and 14 days (below) stained with Masson's trichrome following treatment with autograft, no fill, commercial dressing, Oligomer-4, Oligomer-20, and Oligomer-40. Images represent center region of wound with inset focused on cellular response. Asterisks denote atrophying panniculus carnosus muscle, arrowheads denote giant cells, and dashed lines indicate wound borders if visible. Scalebars: 4x: 200 μm; 10x: 200 μm; 40x: 100 μm.

All oligomer scaffolds fostered rapid cellularization and vascularization that proceeded upward and inward from the wound edges at a rate that was dependent upon fibril density and orientation (Figure 3.5). Although numerous mononuclear and polymorphonuclear cells infiltrated oligomer-treated wounds, limited activated macrophages and scaffold proteolysis were observed, which was especially apparent for Oligomer-20 and Oligomer-40. For these materials, light blue staining, which is characteristic of oligomeric collagen material, persisted and was evident within the wound bed at both 7 and 14. Interestingly, the overall percentage of myofibroblasts observed within oligomer-treated wounds was decreased compared to the no fill controls (Figure 3.6A). Furthermore, the myofibroblast number decreased with increasing scaffold collagen content. Epithelialization, with identifiable stratified epidermis and stratum corneum (Figure 3.7), was also apparent in all oligomer-treated wounds and progressed from the wound edges toward the wound center. As expected, the extent of epithelial coverage at 14 days was increased for contracted wounds, which had a smaller area to cover.

Functional vascularization throughout Oligomer-4 was observed at 7 days, as evidenced by red blood cells within vessel lumens and CD31+ endothelial cells (Figures 3.5,3.6B). Rapid vascularization also occurred in Oligomer-20 and Oligomer-40; however, the level of penetration toward the surface was modulated by the graded microstructure (Figure 3.5,3.6B). More specifically, the lower two-thirds of Oligomer-20 and Oligomer-40 scaffolds were vascularized at day 7. By 14 days, this extent of vascularization progressed to near 90% for Oligomer-20 and 70% for Oligomer-40.

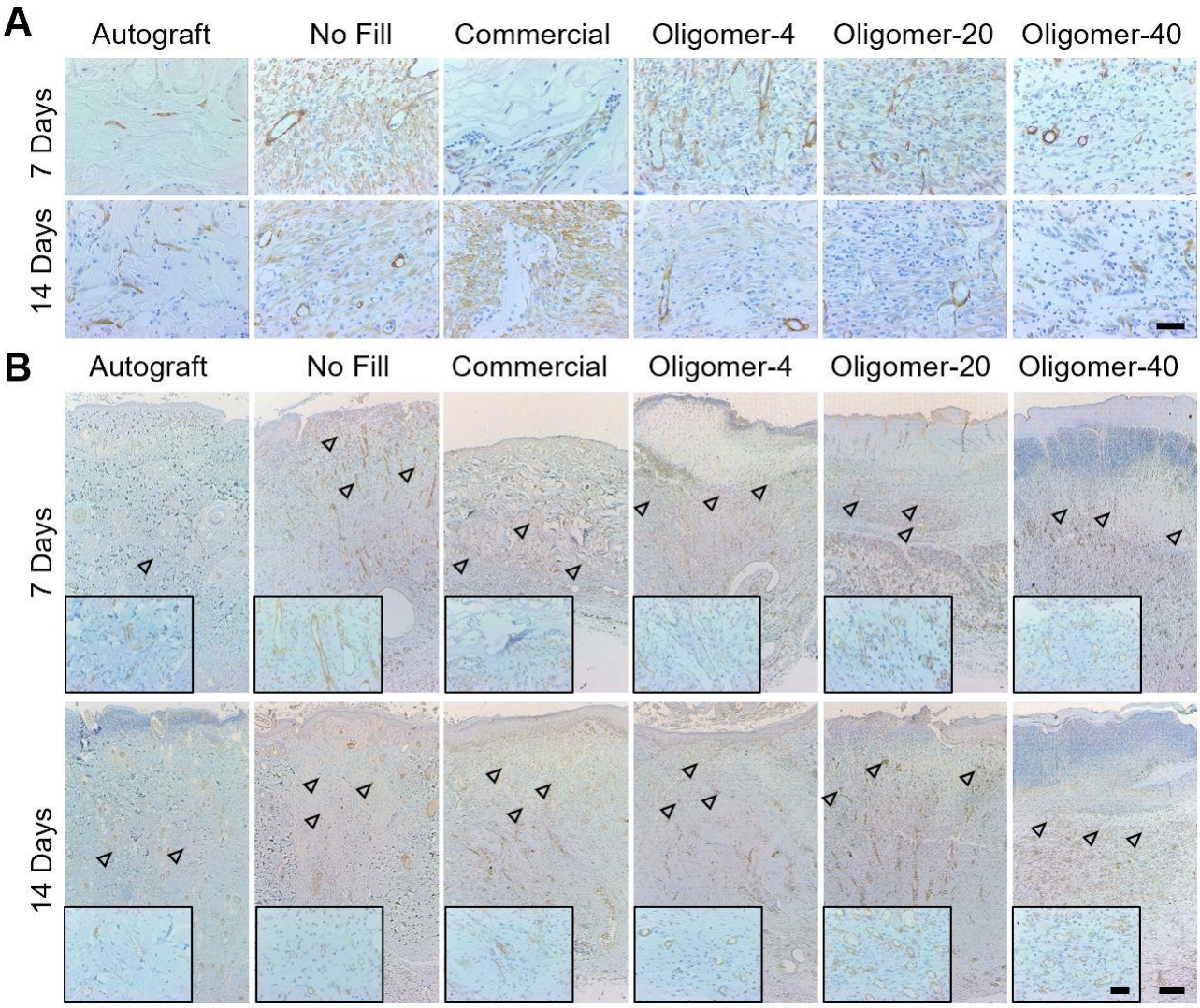

Figure 3.6. (A) Histological cross-sections of excised wound tissues stained for blood vessel and myofibroblast marker α-SMA (brown; 7 and 14 days) and (B) endothelial cell marker CD31 (brown; 7 and 14 days) following treatment with autograft, no fill, commercial dressing, Oligomer-4, Oligomer-20, and Oligomer-40. Arrowheads denote presumed level of vascularization based on presence of CD31 positive stained lumens with identifiable red blood cells. Scalebars: A: 50 μm; B: 200 μm, B, inset: 50 μm.

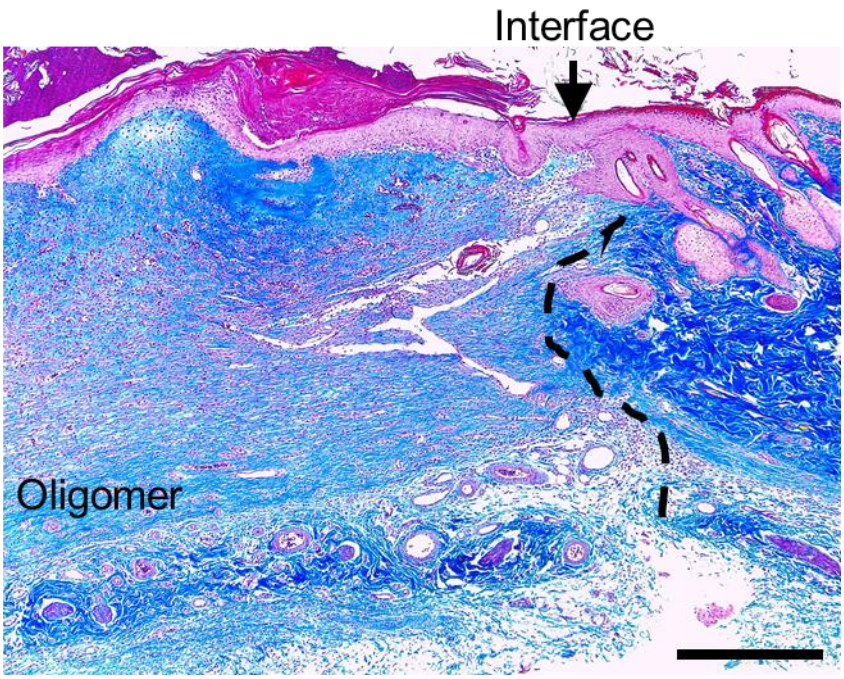

Figure 3.7. Histological cross-section stained with Masson's trichrome showing integration of Oligomer-20 scaffold with adjacent normal skin at 14 days. Arrowhead and dashed line indicate interface between scaffold and native tissue with epithelium migrating across wound. Scalebar: 500 μm

3.5 Discussion

Large volume and chronic non-healing wounds continue to place a tremendous socioeconomic burden on affected individuals, clinicians, wound care specialists, and payers around the world[1]. While patient autografts and present-day dermal and dermal-epidermal substitutes remain the therapeutic strategies of choice, autografts are not always available in sufficient quantity and both autografts and skin substitutes are often associated with contracture, scarring, repeat procedures, and growth limitations[30]. Dermal regeneration strategies aim to provide new therapeutic options for such wounds by restoring, as rapidly and accurately as possible, original dermal structure and function which is essential for achieving desired clinical outcomes. In this study, oligomer collagen polymers were interfaced with the scalable biomanufacturing technique confined compression for multi-scale design and fabrication of fibrillar collagen scaffolds as a permanent and integrating dermal replacement. Our findings show that total collagen content, together with spatial gradients in fibril density and orientation, are important design considerations, with these features contributing not only to scaffold-level

mechanical properties but also to cellular-level mechanochemical signaling important for dermal regeneration.

Skin biomechanics and associated cell-collagen mechanobiology is fundamental to skin morphogenesis, homeostasis, and repair, and has been implicated in a number of skin pathologies[11, 12]. For example, conditions leading to abnormal collagen-fibril assembly and crosslinking, as observed with deficient levels of ascorbic acid (scurvy) and certain forms of Ehlers Danlos syndrome, are often associated with weak and fragile skin as well as defective wound healing[31, 32]. On the other hand, extrinsically-induced increases in skin tension are associated with hypertrophic scarring[33], a process that has been linked to altered cell-collagen and inflammatory signaling[34]. Further corroborating evidence comes from in-vitro studies, where fibroblasts cultured within three-dimensional collagen matrices of varied microstructure and stiffness sense and respond to such cues by modulating their proliferation, migration, collagen deposition, and contractile properties [35-38]. Likewise, endothelial cells and their progenitors respond to these cues by modulating the extent, length, and morphology of vascular networks formed in vitro and in vivo [14, 17, 18, 39]. Collectively, these results suggest that the collagen-fibril microstructure is a critical determinant of how mechanical load information is transmitted across multiple size scales, from tissue to cellular level and vice versa, suggesting its potential as an important design consideration for dermal regeneration therapies[11, 12, 40].

While collagen is recognized as a vital component to skin mechanobiology and wound healing, surprisingly few strategies have targeted the microstructure of fibrillar collagen scaffolds, largely because of challenges associated with the accurate and reproducible control of such features. Early reports of creating collagen constructs with dermal-like histology and consistency involved seeding fibroblasts within polymerized monomeric collagen matrices, and in turn, allowing the cells to contract and densify the surrounding fibrils over a 2-week period[41]. Seeding keratinocytes that formed a multilayered epidermis on the surface of this dermal equivalent gave rise to the first tissue-engineered living skin, which gained FDA approval in 1998. In 2005, Brown reported a “cell-independent” approach for densifying monomeric collagen matrices that could be applied in the presence and absence of cells[20]. Here, plastic compression in an unconfined format, along with capillary fluid flow into absorbent layers, was used to increase the collagen density by reducing the fluid content [20]. In vitro and in vivo studies by Hu[42], Ananta[43], and Braziulis[44] have applied this compression method to produce dermal or dermo-epidermal

substitutes. While these approaches have contributed to the development and translation of cellularized skin equivalents, limited focus has been placed on how specific collagen microstructure features contribute to skin mechanics, mechanobiology, and regeneration.

Other bioengineering approaches have targeted dermal and skin regeneration through the design and fabrication of acellular scaffolds from fibrillar collagen microparticulate, a strategy originally described by Yannas and Burke[45-47]. While this insoluble form of collagen can be swollen in dilute acid solutions, it does not exhibit the de novo fibril-forming capacity of monomeric and oligomeric collagens. Scaffold fabrication, in this case, involves lyophilization of viscous suspensions of bovine tendon microparticulate in the absence or presence of glycosaminoglycans (chondroitin 6-sulfate) to create a freeze-dried sponge-like material. Microparticulate density, lyophilization parameters, along with various levels of exogenous glutaraldehyde and dehydrothermal crosslinking are used to control pore size, cellular adhesion and infiltration, and degradation (resorption) rate (for a recent review see [48]). This approach has yielded a portfolio of commercial collagen wound dressings, including the bilayered Integra Dermal Regeneration Template (collagen-GAG sponge covered with a thin silicone layer), which is indicated for skin replacement. Since the objective of the present study was to define the role of specific collagen scaffold microstructure features in dermal regeneration, HeliCote, a collagen sponge dressing fabricated without glycosaminoglycans and exogenous crosslinking was selected for comparison.

An essential and differentiating element of our approach was the use of oligomeric collagen, an acid-soluble and fibril-forming collagen formulation that retains mature intermolecular crosslinks (e.g., histidinohydroxylysino-nor-leucine (HHL)) naturally found in dermis and other connective tissues [49, 50]. These crosslink chemistries are important determinants of in-vivo collagen structure and function, serving to decrease collagen turnover rate (increase proteolytic resistance), increase fibril stability, and increase tissue mechanical integrity [49, 50]. Our group has also documented that these crosslinks are critical to the in-vitro fibril-forming properties of purified oligomeric collagen, giving rise to fibrillar collagen scaffolds that better approximate those within the body's tissues[51]. Type I oligomeric collagen exhibits not only fibrillar but also suprafibrillar assembly, yielding highly interconnected collagen-fibril scaffolds with substantially improved proteolytic resistance and mechanical integrity compared to conventional monomeric collagens (atelocollagen and telocollagen)[13, 15]. Collectively, this

connectivity exhibited at both the molecular and fibrillar size scales defines the multi-scale structure and mechanical properties of polymerized oligomer scaffolds [15, 16].

As unmodified natural collagen polymers, oligomers are well suited for tissue engineering and regenerative medicine applications, since the collagen primary sequence and associated crosslink chemistries are highly conserved between species[50, 52]. For this study, oligomeric collagen was derived from porcine dermis, since this tissue source is readily available and can be obtained from specific pathogen free herds, facilitating translation into the clinic. Although concerns have been raised in the past regarding immunogenicity of xenogeneic collagen, contributions of material format, processing, and impurities (e.g., cellular by-products and denatured collagen) have yet to be fully delineated[53]. To date, no evidence of pathological immunogenicity has been observed with oligomer materials when implanted in different species and tissue microenvironments, which is likely due to their high-level purity as well as the absence of exogenous additives and crosslinking[14, 18, 54-58]. In this way, the multi-faceted biosignaling capacity inherent to collagen fibrils is preserved, including i) integrin-mediated cell adhesion[59], ii) ECM molecule and soluble factor (e.g., growth factors) binding and sequestration[59], and iii) immune modulation[60, 61].

For this work, plastic compression was applied to low-density oligomer matrices in a confined rather than an unconfined format to controllable modulate the collagen-fibril microstructure. Interestingly, this approach is not suitable for monomeric collagen matrices due to the inability of their fibril microstructure to sustain or support associated compressive and fluid shear forces[16]. It is noteworthy that confined compression provides control over both the amount and direction of fluid removal, facilitating customization of spatial gradients in fibril density and orientation. Specifically, total collagen content of the compressed scaffold is controlled through modulation of the starting volume and concentration of the original scaffold together with the applied compressive strain[16, 21]. Additionally, strain rate can be varied to control steepness of the fibril density gradient, and placement of porous polyethylene foam and associated porous-solid boundary condition can be used to define high-order spatial fibril organization (e.g., alignment, directional gradient) (see [19] for a more detailed review).

All oligomer scaffolds fabricated for this study featured a randomly-oriented, porous fibrillar network near the bottom. Oligomer-20 and Oligomer-40 were fashioned with a vertical gradient in fibril density, with varied extents of fibril alignment and bundling near their surface to

recapitulate some of the anisotropies found in normal dermis. In terms of estimated pore sizes, oligomer scaffolds were most similar to that of normal rat dermis and more than an order of magnitude less than HeliCote. Although, the pore size for bioengineered collagen sponge dressings has been rigorously documented as a critical design feature for controlling cellularization and vascularization [48], there is no reason to a priori believe the optimal porosity for collagen sponges and oligomer scaffolds would be the same. While both HeliCote and oligomer scaffolds are primarily composed of fibrillar collagen and non-crosslinked, their fundamental design and method of fabrication is different, ultimately yielding scaffolds with different overall microstructures, mechanical properties, and mechanisms of action. Further to this point, while the bulk tensile properties for HeliCote were statistically similar to Oligomer-20, the in-vivo tissue responses of these two materials were dramatically different. In summary, the Young's modulus for oligomer scaffolds ranged from 0.2 MPa for Oligomer-4 to nearly 1MPa for Oligomer-40, which falls within reported ranges for human cornea (0.1-11.1MPa), aorta (0.6-3.5MPa), and dermis (0.6-15MPa)[62, 63]. The bulk mechanical properties of Oligomer-20 and Oligomer-40, but not Oligomer-4, facilitated handling and suturing in place.

When evaluated within an established full-thickness excisional skin model, the dense microstructure of autograft skin was most effective at minimizing contraction but showed delayed cellularization and vascularization. In the present study, roughly 20% of autografts were unable to re-establish the necessary nutrient flow prior to necrosis and failed to take. This observed graft failure rate is consistent with previously reported values for rodent models[64]. Additionally, as expected, no fill controls healed primarily by contraction over the 14-day period. The tissue response observed with the commercial dressing was also consistent with its design[65], with controlled infiltration of cells and progressive active scaffold degradation occurring via inflammatory mediators, most notably macrophages and giant cells, over the two-week period. This observed high rate of degradation (resorption) and wound contraction are consistent with other published studies in rodents[66] and can be attributed to the absence of glycosaminoglycans and exogenous crosslinking, which are known to slow these processes[48].

The provision of densified oligomer dermal scaffolds that persisted within the wound bed and integrated with surrounding normal tissue, was effective at limiting both wound contraction and the myofibroblast phenotype. Oligomer-20 and Oligomer-40 scaffolds appeared to recapitulate, in part, the stress-shielding provided by normal dermal collagen, where fibroblasts

adopt their spindle-shaped morphology and down regulate α-SMA [5]. In this case, the relatively rigid fibrillar microstructure provided by these scaffolds was sufficient to resist significant cellular contraction, while supporting the necessary cellular traction forces to facilitate migration. Recent work has shown that fibroblast phenotype and behavior, including apoptosis signaling, matrix metalloproteinase activity, and differentiation into myofibroblasts, are strongly linked to the rigidity or laxity of the ECM, even independent of transforming growth factor (TGF-β) signaling[67, 68]. By persisting and modulating fibroblast function, these oligomer scaffolds appear to circumvent contraction and reduce the burden on host cells to deposit collagen and rebuild the dermis, which collectively speeds up the healing process and improves outcomes. To the best of our knowledge this is the first report of self-assembled collagen materials that persist and integrate, effectively decreasing cutaneous wound contraction and the myofibroblast phenotype in absence of exogenous crosslinking or reinforcing materials.

There has been significant interest in designing dermal and skin replacements with improved vascularization, with the majority of approaches involving soluble angiogenic factors, such as fibroblast growth factor 2 (FGF2) and vascular endothelial growth factor (VEGF), either alone or in combination with other matrix molecules[69, 70]. Here we show that Oligomer-20 and Oligomer-40 were not only effective inhibitors of contraction but also promoters of vascularization, which is critical to dermal regeneration as well as the support of epithelialization or a secondarily-applied epidermal layer. Vessel networks were well-formed at 2 weeks, staining for both CD31 and α-SMA. However, an interesting finding was that the fibril bundling and alignment within scaffolds appeared to hinder or delay vessel progression toward the surface. Such findings are consistent with observations for decellularized tissue scaffolds, which are reported to require 2-4 weeks to vascularize sufficiently to support overlying STSG, and the fact that human auto- or allografts thicker than 0.4 mm show delayed angiogenesis and failure to take [71, 72].

3.6 Conclusion

This work serves as an important first step in development of mechano-instructive dermal scaffolds that promote rapid cellularization and vascularization while simultaneously reducing wound contraction and scarring. We show custom fabrication of dermal replacements with high bulk mechanical integrity that facilitate handling and suturing, factors that are important for

adoption by wound care specialists and surgeons. Our work also documents that oligomer scaffolds persist, restoring important mechanobiology cues by serving as a surrogate dermis. Finally, our findings show that precision tuning collagen-fibril microstructure can be used to modulate mechanotransduction pathways involved in tissue regeneration. This study has some limitations. While no animal model perfectly replicates wound healing in humans, important information can be inferred from established animal models, such as the rodent full-excisional skin model used here. Follow-up experimental and computational modeling studies are now underway to further define how specific microstructure features of oligomer scaffolds affect, more broadly, multi-scale mechanical properties as well as mechanotransduction mechanisms underlying cellularization, vascularization, and epithelialization. Finally, studies involving large animal wound models as well as models of compromised healing are necessary to further validate efficacy and scalability of our approach.

3.7 Translational Perspective

Tissue-engineered dermal replacements have now become a well-established part of clinical care for difficult-to-treat wounds. This study represents an advancement in the bio-inspired design of dermal replacements that can reduce morbidity and mortality of patients with severe and difficult-to-heal wounds by regenerating lost tissue while preventing scar formation. Our design strategy involves creation of persistent fibrillar collagen scaffolds whose microstructure is defined and designed to promote skin regeneration by re-establishing mechanical continuity across the tissue and cellular size scales, restoring essential skin mechanobiology. Oligomeric collagen was manufactured and standardized from porcine dermis according to relevant ASTM International standards for polymerizable (fibril-forming) collagens. Oligomer scaffold microstructures were customized using confined plastic compression, a scalable and controllable biomanufacturing process. This initial preclinical study documented that total content and spatial gradients in collagen-fibril density and orientation are important considerations when designing scaffolds to promote rapid cellularization and vascularization while simultaneously preventing wound contraction. Further mechanistic-based design iterations along with preclinical evaluation in large animal wound models is needed to further validate the translational potential of our strategy.

3.8 Summary Points

- Difficult-to-heal wounds are a significant burden on patients, providers, and the healthcare system as a whole.
- Current wound management strategies include conservative treatment, skin grafting, and tissue engineered replacements; however, scarring and loss-of-function continue to be common outcomes for patients with severe wounds.
- Our dermal regeneration strategy targets fabrication of fibrillar collagen scaffolds, whose microstructure is defined and designed to restore necessary mechanochemical signaling by supporting the reciprocal transmission of mechanical forces across tissue and cellular size scales.
- Oligomeric collagen, a fibril-forming collagen that retains intermolecular crosslinks and exhibits improved persistence and mechanical stability, together with confined plastic compression was used to create scaffolds with varied total content and spatial gradients of collagen fibrils.
- We evaluated three groups, Oligomer-4, Oligomer-20, and Oligomer-40 against a commercial absorbable collagen sponge, no fill control, and autograft skin within a rat full-thickness excisional skin model.
- The dense collagen fibril microstructure of autograft skin was most effective at decreasing wound contraction but hindered vascularization leading to tissue necrosis and 20% graft loss.
- No fill wounds displayed the classic healing response with rapid contraction.
- A commercial non-crosslinked collagen sponge fabricated by lyophilization of fibrillar collagen microparticulate, rapidly resorbed over the 14-day period via inflammatory mediated degradation and did not inhibit wound contraction.
- The rate and extent of contraction decreased as the total collagen content of oligomer scaffolds increased.
- A vertical gradient in fibril density and orientation that proceeded from a porous, isotropic organization to a high density of bundled fibrils oriented parallel to the surface facilitated rapid cellularization, vascularization, and epithelialization.

- Oligomer scaffolds did not rapidly degrade but rather persisted within the wound bed where they modulated cellular traction and contraction forces based on their microstructure features.
- Additional investigations are necessary to further the mechanistic-based design and fabrication of oligomer scaffolds to promote skin regeneration for treatment of difficult-to-heal wounds.

3.9 References

1. Sen CK, Gordillo GM, Roy S et al. Human skin wounds: a major and snowballing threat to public health and the economy. Wound Repair Regen. 17(6), 763-771 (2009).
2. Harrison CA, Macneil S. The mechanism of skin graft contraction: an update on current research and potential future therapies. Burns 34(2), 153-163 (2008).
3. Donegan RJ, Schmidt BM, Blume PA. An overview of factors maximizing successful split-thickness skin grafting in diabetic wounds. Diabetic Foot & Ankle 5(1), 24769 (2014).
4. Macneil S. Biomaterials for tissue engineering of skin. Mater Today 11(5), 26-35 (2008).
5. Tomasek JJ, Gabbiani G, Hinz B, Chaponnier C, Brown RA. Myofibroblasts and mechano-regulation of connective tissue remodelling. Nat Rev Mol Cell Biol. 3(5), 349-363 (2002).
6. Yannas IV, Tzeranis DS, So PTC. Regeneration of injured skin and peripheral nerves requires control of wound contraction, not scar formation. Wound Repair Regen. 25(2), 177-191 (2017).
7. Eming SA, Martin P, Tomic-Canic M. Wound repair and regeneration: mechanisms, signaling, and translation. Sci Transl Med. 6(265), 265sr266 (2014).
8. Young PK, Grinnell F. Metalloproteinase activation cascade after burn injury: a longitudinal analysis of the human wound environment. J Invest Dermatol. 103(5), 660-664 (1994).
9. Wiegand C, Schönfelder U, Abel M, Ruth P, Kaatz M, Hipler U-C. Protease and pro-inflammatory cytokine concentrations are elevated in chronic compared to acute wounds and can be modulated by collagen type I in vitro. Arch Dermatol. 302(6), 419-428 (2010).

10. Rennert RC, Rodrigues M, Wong VW et al. Biological therapies for the treatment of cutaneous wounds: phase III and launched therapies. Expert Opin Biol Ther. 13(11), 1523-1541 (2013).
11. Wong VW, Akaishi S, Longaker MT, Gurtner GC. Pushing back: wound mechanotransduction in repair and regeneration. J Invest Dermatol. 131(11), 2186-2196 (2011).
12. Agha R, Ogawa R, Pietramaggiori G, Orgill DP. A review of the role of mechanical forces in cutaneous wound healing. J Surg Res. 171(2), 700-708 (2011).
13. Kreger ST, Bell BJ, Bailey J et al. Polymerization and matrix physical properties as important design considerations for soluble collagen formulations. Biopolymers 93(8), 690-707 (2010).
14. Bailey JL, Critser PJ, Whittington C, Kuske JL, Yoder MC, Voytik-Harbin SL. Collagen oligomers modulate physical and biological properties of three-dimensional self-assembled matrices. Biopolymers 95(2), 77-93 (2011).
15. Whittington CF, Brandner E, Teo KY, Han B, Nauman E, Voytik-Harbin SL. Oligomers modulate interfibril branching and mass transport properties of collagen matrices. Microsc Microanal. 19(5), 1323-1333 (2013).
16. Blum KM, Novak T, Watkins L et al. Acellular and cellular high-density, collagen-fibril constructs with suprafibrillar organization. Biomater Sci. 4(4), 711-723 (2016).
17. Whittington CF, Yoder MC, Voytik-Harbin SL. Collagen-polymer guidance of vessel network formation and stabilization by endothelial colony forming cells in vitro. Macromol Biosci. 13(9), 1135-1149 (2013).
18. Critser PJ, Kreger ST, Voytik-Harbin SL, Yoder MC. Collagen matrix physical properties modulate endothelial colony forming cell-derived vessels in vivo. Microvasc Res. 80(1), 23-30 (2010).
19. Sohutskay DO, Puls TJ, Voytik-Harbin SL. Collagen Self-assembly: Biophysics and Biosignaling for Advanced Tissue Generation. In: Multi-scale Extracellular Matrix Mechanics and Mechanobiology, Zhang KY (Ed.). Springer International Publishing, 203-245 (2020).

20. Brown RA, Wiseman M, Chuo CB, Cheema U, Nazhat SN. Ultrarapid engineering of biomimetic materials and tissues: Fabrication of nano- and microstructures by plastic compression. Adv Funct Mater. 15(11), 1762-1770 (2005).
21. Novak T, Seelbinder B, Twitchell CM, Van Donkelaar CC, Voytik-Harbin SL, Neu CP. Mechanisms and microenvironment investigation of cellularized high density gradient collagen matrices via densification. Adv Funct Mater. 26(16), 2617-2628 (2016).
22. Wang J, Wang L, Zhou Z et al. Biodegradable polymer membranes applied in guided bone/tissue regeneration: A review. Polymers 8(4), 115 (2016).
23. ASTM F3089-14, Standard Guide for Characterization and Standardization of Polymerizable Collagen-Based Products and Associated Collagen-Cell Interactions. (2014).
24. Takeuchi H, Ishida M, Furuya A, Todo H, Urano H, Sugibayashi K. Influence of Skin Thickness on the in Vitro Permeabilities of Drugs through Sprague-Dawley Rat or Yucatan Micropig Skin. Biol Pharm Bull. 35(2), 192-202 (2012).
25. Hotaling NA, Bharti K, Kriel H, Simon Jr CG. DiameterJ: A validated open source nanofiber diameter measurement tool. Biomaterials. 61 327-338 (2015).
26. Anguiano M, Castilla C, Maška M et al. Characterization of three-dimensional cancer cell migration in mixed collagen-Matrigel scaffolds using microfluidics and image analysis. PLoS One 12(2), e0171417 (2017).
27. Dombi GW, Haut RC, Sullivan WG. Correlation of high-speed tensile strength with collagen content in control and lathyritic rat skin. J Surg Res. 54(1), 21-28 (1993).
28. Tan G, Xu P, Lawson LB et al. Hydration effects on skin microstructure as probed by high-resolution cryo-scanning electron microscopy and mechanistic implications to enhanced transcutaneous delivery of biomacromolecules. J Pharm Sci. 99(2), 730-740 (2010).
29. Meyer W, Kacza J, Zschemisch N-H, Godynicki S, Seeger J. Observations on the actual structural conditions in the stratum superficiale dermidis of porcine ear skin, with special reference to its use as model for human skin. Annals of Anatomy-Anatomischer Anzeiger 189(2), 143-156 (2007).
30. Bottcher-Haberzeth S, Biedermann T, Reichmann E. Tissue engineering of skin. Burns 36(4), 450-460 (2010).

31. Myllyharju J, Kivirikko KI. Collagens and collagen-related diseases. Ann Med. 33(1), 7-21 (2001).
32. Prockop DJ, Kivirikko KI. Collagens: molecular biology, diseases, and potentials for therapy. Annu Rev Biochem. 64(1), 403-434 (1995).
33. Aarabi S, Bhatt KA, Shi Y et al. Mechanical load initiates hypertrophic scar formation through decreased cellular apoptosis. FASEB J 21(12), 3250-3261 (2007).
34. Wong VW, Rustad KC, Akaishi S et al. Focal adhesion kinase links mechanical force to skin fibrosis via inflammatory signaling. Nat Med. 18(1), 148-152 (2011).
35. Hadjipanayi E, Mudera V, Brown RA. Close dependence of fibroblast proliferation on collagen scaffold matrix stiffness. J Tissue Eng Regen Med. 3(2), 77-84 (2009).
36. Hadjipanayi E, Mudera V, Brown RA. Guiding cell migration in 3D: a collagen matrix with graded directional stiffness. Cell Motil Cytoskeleton 66(3), 121-128 (2009).
37. Pizzo AM, Kokini K, Vaughn LC, Waisner BZ, Voytik-Harbin SL. Extracellular matrix (ECM) microstructural composition regulates local cell-ECM biomechanics and fundamental fibroblast behavior: a multidimensional perspective. J Appl Physiol. 98(5), 1909-1921 (2005).
38. Grinnell F, Petroll WM. Cell motility and mechanics in three-dimensional collagen matrices. Annu Rev Cell Dev Biol. 26 335-361 (2010).
39. Buno KP, Chen X, Weibel JA et al. In Vitro Multitissue Interface Model Supports Rapid Vasculogenesis and Mechanistic Study of Vascularization across Tissue Compartments. ACS Appl Mater Interfaces 8(34), 21848-21860 (2016).
40. Roeder BA, Kokini K, Voytik-Harbin SL. Fibril microstructure affects strain transmission within collagen extracellular matrices. J Biomech Eng. 131(3), 031004 (2009).
41. Bell E, Sher S, Hull B et al. The reconstitution of living skin. J Invest Dermatol. 81(1 Suppl), 2s-10s (1983).
42. Hu K, Shi H, Zhu J et al. Compressed collagen gel as the scaffold for skin engineering. Biomed Microdevices 12(4), 627-635 (2010).
43. Ananta M, Brown RA, Mudera V. A rapid fabricated living dermal equivalent for skin tissue engineering: an in vivo evaluation in an acute wound model. Tissue Eng Part A 18(3-4), 353-361 (2012).

44. Braziulis E, Diezi M, Biedermann T et al. Modified plastic compression of collagen hydrogels provides an ideal matrix for clinically applicable skin substitutes. Tissue Eng Part C Meth. 18(6), 464-474 (2012).
45. Yannas IV, Burke JF. Design of an artificial skin. I. Basic design principles. J Biomed Mater Res. 14(1), 65-81 (1980).
46. Yannas IV, Burke JF, Gordon PL, Huang C, Rubenstein RH. Design of an artificial skin. II. Control of chemical composition. J Biomed Mater Res. 14(2), 107-132 (1980).
47. Dagalakis N, Flink J, Stasikelis P, Burke JF, Yannas IV. Design of an artificial skin. Part III. Control of pore structure. J Biomed Mater Res. 14(4), 511-528 (1980).
48. Yannas IV, Tzeranis D, So PT. Surface biology of collagen scaffold explains blocking of wound contraction and regeneration of skin and peripheral nerves. Biomed Mater. 11(1), 014106 (2015).
49. Eyre DR, Paz MA, Gallop PM. Cross-linking in collagen and elastin. Annu Rev Biochem. 53 717-748 (1984).
50. Eyre DR, Wu J-J. Collagen Cross-Links. In: Collagen: Primer in Structure, Processing and Assembly, Brinckmann J,Notbohm H,Müller PK (Ed.). Springer Berlin Heidelberg, Berlin, Heidelberg 207-229 (2005).
51. Verzijl N, Degroot J, Thorpe SR et al. Effect of collagen turnover on the accumulation of advanced glycation end products. J Biol Chem. 275(50), 39027-39031 (2000).
52. Stover DA, Verrelli BC. Comparative Vertebrate Evolutionary Analyses of Type I Collagen: Potential of COL1a1 Gene Structure and Intron Variation for Common Bone-Related Diseases. Mol Biol Evol. 28(1), 533-542 (2010).
53. Lynn A, Yannas I, Bonfield W. Antigenicity and immunogenicity of collagen. J Biomed Mater Res, B. Appl Biomater. 71(2), 343-354 (2004).
54. Stephens CH, Orr KS, Acton AJ et al. In situ type I oligomeric collagen macroencapsulation promotes islet longevity and function in vitro and in vivo. Am J Physiol Endocrinol Metab. 315(4), E650-E661 (2018).
55. Brookes S, Voytik-Harbin S, Zhang H, Zhang L, Halum S. Motor endplate-expressing cartilage-muscle implants for reconstruction of a denervated hemilarynx. Laryngoscope 129(6), 1293-1300 (2018).

56. Brookes S, Voytik-Harbin S, Zhang H, Halum S. Three-dimensional tissue-engineered skeletal muscle for laryngeal reconstruction. Laryngoscope 128(3), 603-609 (2018).
57. Zhang H, Voytik-Harbin S, Brookes S et al. Use of autologous adipose-derived mesenchymal stem cells for creation of laryngeal cartilage. Laryngoscope 128(4), E123-E129 (2018).
58. Critser PJ, Voytik-Harbin SL, Yoder MC. Isolating and defining cells to engineer human blood vessels. Cell Prolif. 44 Suppl 1 15-21 (2011).
59. An B, Lin Y-S, Brodsky B. Collagen interactions: Drug design and delivery. Adv Drug Del Rev. 97 69-84 (2016).
60. Kuczek DE, Larsen AMH, Thorseth ML et al. Collagen density regulates the activity of tumor-infiltrating T cells. J Immunother Cancer. 7(1), 68 (2019).
61. Lebbink RJ, De Ruiter T, Adelmeijer J et al. Collagens are functional, high affinity ligands for the inhibitory immune receptor LAIR-1. J Exp Med. 203(6), 1419-1425 (2006).
62. Mckee CT, Last JA, Russell P, Murphy CJ. Indentation versus tensile measurements of Young's modulus for soft biological tissues. Tissue Eng Part B Rev. 17(3), 155-164 (2011).
63. Silver FH, Seehra GP, Freeman JW, Devore D. Viscoelastic properties of young and old human dermis: a proposed molecular mechanism for elastic energy storage in collagen and elastin. J Appl Polym Sci. 86(8), 1978-1985 (2002).
64. Pakyari M, Farokhi A, Khosravi-Maharlooei M, Kilani RT, Ghahary A, Brown E. A new method for skin grafting in murine model. Wound Repair Regen. 24(4), 695-704 (2016).
65. Mahesh L, Kurtzman GM, Shukla S. Regeneration in Periodontics: Collagen-A Review of Its Properties and Applications in Dentistry. Compend Contin Educ Dent. 36(5), 358-363 (2015).
66. Shafritz TA, Rosenberg LC, Yannas IV. Specific effects of glycosaminoglycans in an analog of extracellular matrix that delays wound contraction and induces regeneration. Wound Repair Regen. 2(4), 270-276 (1994).
67. Hinz B. The myofibroblast: paradigm for a mechanically active cell. J Biomech. 43(1), 146-155 (2010).
68. Tracy LE, Minasian RA, Caterson EJ. Extracellular matrix and dermal fibroblast function in the healing wound. Adv. Wound Care 5(3), 119-136 (2016).

69. Nillesen S, Lammers G, Wismans R et al. Design and in vivo evaluation of a molecularly defined acellular skin construct: reduction of early contraction and increase in early blood vessel formation. Acta Biomater. 7(3), 1063-1071 (2011).
70. Shilo S, Roth S, Amzel T et al. Cutaneous wound healing after treatment with plant-derived human recombinant collagen flowable gel. Tissue Eng Part A. 19(13-14), 1519-1526 (2013).
71. Sahota PS, Burn JL, Heaton M et al. Development of a reconstructed human skin model for angiogenesis. Wound Repair Regen. 11(4), 275-284 (2003).
72. Macneil S. Progress and opportunities for tissue-engineered skin. Nature 445(7130), 874-880 (2007).

4. MECHANOBIOLOGICAL WOUND MODEL FOR IMPROVED DESIGN AND TESTING OF COLLAGEN DERMAL REPLACEMENT SCAFFOLDS

This chapter has been submitted for review for publication as an additional manuscript.

4.1 Abstract

Wounds of the skin are among the most common and costly medical problems experienced. Despite the myriad of treatment options, such wounds continue to lead to displeasing cosmetic outcomes and also carry a high burden of loss-of-function, scarring, contraction, or nonhealing. As a result, the need exists for new therapeutic options that rapidly and reliably restore skin cosmesis and function. Here we present a new mechanobiological computational model to further the design and evaluation of next-generation regenerative dermal scaffolds fabricated from polymerizable collagen. A Bayesian framework, along with microstructure-mechanical property data from engineered dermal scaffolds and autograft skin, was used to calibrate constitutive models for collagen density, fiber alignment and dispersion, and stiffness. A chemo-bio-mechanical finite element model including collagen, cells, and representative cytokine signaling was adapted to simulate no-fill, dermal scaffold, and autograft skin outcomes observed in a preclinical animal model of full-thickness skin wounds, with a focus on permanent contraction, collagen realignment, and cellularization. The statistical model fit the constitutive equations well. Finite element model simulations demonstrated wound cellularization and contraction behavior that was similar to that observed experimentally. A sensitivity analysis suggested collagen fiber stiffness and density are important scaffold design features for predictably controlling wound contraction. Finally, predictive simulations indicated that scaffolds with increased fiber dispersion (isotropy) exhibited reduced and more uniform wound contraction while supporting cell infiltration. By capturing the link between multi-scale scaffold biomechanics and cell-scaffold mechanochemical interactions, simulated healing outcomes aligned well with preclinical animal model data.

4.1.1 Statement of Significance

Skin wounds continue to be a significant burden to patients, physicians, and the healthcare system. Advancing the mechanistic understanding of the wound healing process, including multi-scale mechanobiological interactions amongst cells, the collagen scaffolding, and signaling molecules, will aide in the design of new skin restoration therapies. This work represents the first step towards integrating mechanobiology-based computational tools with in-vitro and in-vivo preclinical testing data for improving the design and evaluation of custom-fabricated collagen scaffolds for dermal replacement. Such an approach has potential to expedite development of new and more effective skin restoration therapies as well as improve patient-centered wound treatment.

4.1.2 Highlights

- This work provides a new computational model of 3D wound healing, with utility in mechanistic evaluation of design parameters to improve engineered collagen scaffolds for dermal regeneration.
- The new computational model integrates multi-scale structure and mechanics of fibrillar collagen scaffolds, cell-scaffold interactions, and mechanobiological signaling for purposes of improving predictability of *in vivo* healing outcomes.
- Both *in vivo* skin wound experiments and the *in silico* model show that collagen scaffold fibril density and orientation modulate healing processes including cellularization and wound contraction.
- This work represents the first step toward using both *in vivo* and *in silico* model information to guide the design of patient-specific tissue restorative therapies.

4.2 Introduction

Wounds of the skin, especially those that are large and affect multiple tissue layers, remain a major burden to those that they affect as well as our healthcare system[1]. Because these tissue defects supersede the body's natural healing capacity, normal skin anatomy and functional integrity is not restored in an orderly and timely fashion, leading to devastating consequences such as long healing times, pain, infection, scarring, and loss of mobility and function owing to contraction[2]. While numerous options exist for managing such wounds, including bioactive

scaffolds, negative pressure wound therapy (wound vacs), or surgical reconstruction with autologous tissue grafts, none reliably restore skin appearance and function. In fact, a primary shortcoming of present-day wound care products is the reliance on the body's cells to deposit and remodel the necessary tissue collagen scaffolding, a capacity which is obviously limited. Further, conventional implantable materials exhibit inflammatory-mediated foreign body responses and/or degradation, which further compromises healing outcomes. Surgical reconstruction, on the other hand, requires extra surgical procedures, has limited tissue supply, causes donor site morbidity, and may not be available to all patients. In addition, post-surgical complications, including infection, necrosis, scarring, and contraction, are frequent and contribute to patient debilitation, increased healthcare cost, and overall patient and physician dissatisfaction. Therefore, it is not surprising that one of the grand challenges in medicine has been the development of new tissue regeneration strategies, with the goal of restoring, as closely as possible, original tissue structure, function, and aesthetics.

Fundamentally, cutaneous wound healing is characterized by four overlapping phases: hemostasis, inflammation, proliferation, and remodeling, with the duration of these phases varying based on wound etiology, severity, and presence of co-morbidities. This process is multi-scale in nature, involving molecules, cells, and viscoelastic scaffolds that are known to modulate reaction-diffusion responses as well as wound biomechanical properties[3]. In absence of a tissue graft or implantable biomaterial, the body first forms a blood clot, where platelets are entrapped within an initial fibrin scaffold. While this initial fibrin scaffold is lacking in mechanical integrity, it helps stop bleeding and promotes inflammation. Platelet degranulation signals the influx of inflammatory mediators, which are responsible for eliminating pathogens and tissue debris and attracting key contributors of the proliferative phase, namely fibroblasts and endothelial cells. Primary events during the proliferative phase include vascularization, and the synthesis and deposition of a fibrillar collagen scaffold. While the newly developed collagen scaffold improves the mechanical integrity of the wound, it is largely disorganized and the subject of contraction and scar formation over time[4].

Given that the collagen scaffold of the dermis is a vital component to skin mechanobiology and wound healing, our skin restoration strategy has focused on defining how specific collagen microstructure features contribute to the multi-scale properties and healing response of dermal replacement scaffolds. This effort involves the use of type I oligomeric collagen, which represents

a fibril-forming (polymerizable) formulation purified from porcine dermis[5, 6]. This biopolymer, together with scalable fabrication methods such as controlled confined compression[7], supports multi-scale design of dermal replacement scaffolds, where the total content, spatial gradient, and orientation of collagen fibrils can be controlled and specified[8] [9]. Preclinical evaluation of three Oligomer dermal replacement scaffolds, namely Oligomer-4, Oligomer-20, and Oligomer-40, using a rat full-thickness skin model revealed that healing outcomes, including extent of wound contraction, vascularization, and cellularization, were dependent upon an interplay of multi-scale mechanobiological design criteria[9]. For example, the young's modulus of the scaffold was critical for minimizing wound contraction and aligned, high density architectures slowed cellularization and vascularization. Furthermore, unlike conventional skin autografts and commercial biodegradable collagen dressings, Oligomer scaffolds did not evoke an inflammatory-mediated foreign body response. This and other recent tissue restoration studies suggest that maintenance of stromal collagen and its associated mechanobiological continuum are associated with improved regenerative healing outcomes, including large-volume surgical voids of the breast and full-thickness laryngeal defects[10, 11].

In addition to the development of new biomaterials for improved tissue restoration, there has been increasing interest in recent years in continuum models of tissue growth and remodeling, skin biophysics, wound healing, and biomaterial mechanics[12, 13]. To accurately describe the mechanics of collagenous tissues such as skin, computational models that take into consideration the collagen microstructure have been developed[14, 15]. Given the complexity of the biological systems, the interplay of chemical and mechanical signaling of cells during healing, and the broad design space for regenerative healing strategies, integrated use of computational models can assist in (1) providing novel therapeutic approaches through improved mechanistic insight into wound healing mechanobiology, (2) reducing expensive prototyping and animal studies, and (3) more rapid iterations to support patient-specific wound healing scenarios.

While a number wound healing models include coupled multiphysics components comprised of reaction-diffusion systems and mechanical deformations[16], many lack detailed descriptions of nonlinear skin mechanics, growth, and permanent remodeling. Furthermore, mechanoregulation of cell phenotypes is a critically important feature that has only been integrated into wound healing models in recent years[17]. Mechanical cues must guide the cells to first actively remodel the surrounding matrix, but also stop once a homeostatic state has been reached.

Yet, the vast majority of computational models of wound healing do not incorporate the effects of matrix properties on cell migration, proliferation, and contractile force, and do not include permanent remodeling of scaffold architecture. To bridge this gap, we previously developed a model which incorporates cell-scaffold mechanobiology and a finite growth framework for plastic remodeling[18-21]. In addition, while some authors have collected experimental mechanics data to calibrate the constitutive laws of skin mechanics[15] meador2020regional}, the complete integration of architectural and mechanical information with experimental wound healing data is largely missing. Finally, computational models of wound healing have yet to be applied to inform the design of dermal replacement scaffolds.

In this study, we extended our prior computational model [18, 20] of wound healing, integrating experimental data relevant to Oligomer dermal scaffold design. This new model is able to simulate no-fill control, rat skin autograft, and scaffold-treated wounds (Figure 4.1). We improved the mechanobiological coupling between cell behavior and collagen structure to match our recent longitudinal *in vivo* experimental results. We calibrated model structural and mechanical parameters to *in vitro* scaffold and rat skin data using a Bayesian model, then conducted representative simulations and a local sensitivity analysis focused on wound contraction and healing, comparing this to *in vivo*} findings. Finally, we look to the future and see how the model can be used to predict performance of additional scaffold designs. This work bridges experimental and computational tools, highlighting the increasing role of mathematical models in tissue engineering design and their potential to contribute to improved and more personalized wound therapies.

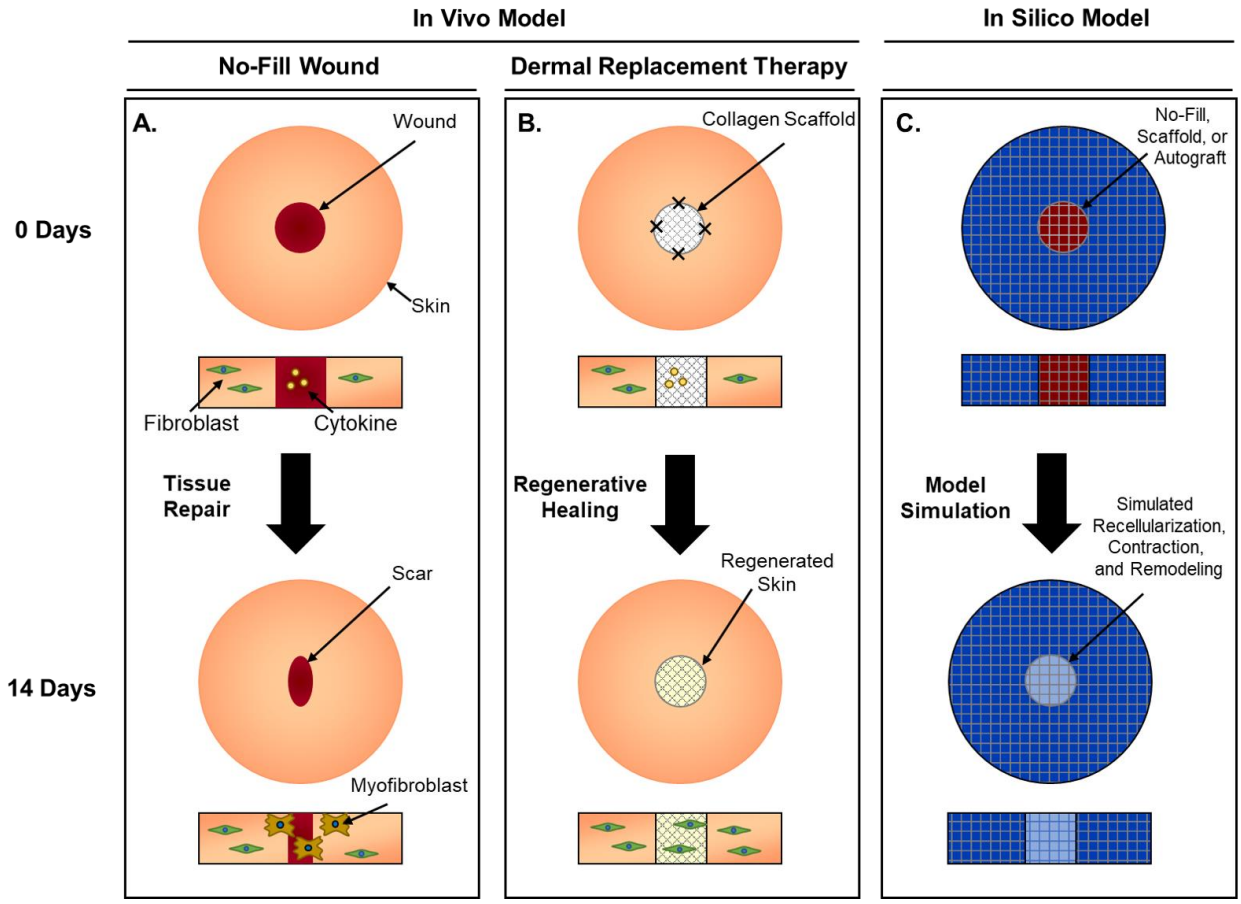

Figure 4.1. Schematic showing integration of experimental *in vivo* and *in silico* models of wound healing, supporting design and development of dermal replacement therapeutic approach. A. No-Fill treated experimental wounds exhibit significant contraction as cells migrate in and interact with the provisional matrix under the influence of chemical and mechanical signals. B. Collagen scaffolds placed within the wounds provides mechanical resistance to contraction and mechanobiological signals which leads to regenerative healing. C. Computational model approximates the geometry and conditions of the experimental wounds. Cell, cytokine, and collagen fields are simulated to predict wound healing and contraction outcomes of different conditions.

4.3 Materials and Methods

4.3.1 Custom-Fabricated Dermal Scaffolds

Collagen dermal scaffolds representing various total content and spatial gradients of collagen fibrils were fabricated from type I oligomeric collagen derived from the dermis of market weight pigs as described previously[7]. In brief, neutralized oligomer solutions (4.0 mg/mL) were pipetted into 24-well plates at specific volumes (230 μL, 1150 μL, and 2300 μL) and polymerized

at 37°C. Following polymerization, wells containing 230 μL oligomer were not further processed, yielding 4 mg/cm^3 scaffolds (Oligomer-4) with a diameter of 15.6 mm and thickness of 1.2 mm to match thickness of rat dermis[22]. Wells containing 1150 μL and 2300 μL oligomer were subjected to controlled confined compression[7] (0.1/s strain rate) to the same final thickness of 1.2 mm, yielding 20 mg/cm^3 (Oligomer-20) and 40 mg/cm^3 (Oligomer-40) scaffolds, respectively. All collagen dermal scaffolds were stored in sterile PBS prior to testing or surgical implantation.

4.3.2 Animal Model

Experimental data derived from a previously published rat full-thickness skin wound study [9] was used for computational model calibration and validation. In brief, male Sprague-Dawley rats, weighing 200 to 250 g (7 to 9 weeks of age; Charles River Laboratories, Wilmington, MA), were anesthetized using isoflurane gas. A sterile punch (15 mm diameter) was used to create two full-thickness skin wounds, including the panniculus carnosus muscle, positioned on either side of the sagittal plane of the rat dorsum. Wounds were randomly assigned to experimental treatment and control groups, with treatment groups consisting of Oligomer-4, Oligomer-20 and Oligomer-40 (n = 4-10). For a subset of animals, the excised full-thickness rat skin was applied to the opposite wound, serving as an autograft (positive control). Untreated (no-fill) wounds served as negative controls. Photographs of wound areas were taken with a ruler in the field of view at 0, 7, and 14 days. At 7- and 14-day study endpoints, animals were euthanized and wound areas and associated implants were excised *in toto* and processed for histopathological analysis.

4.3.3 Data Collection

Experimental data used to calibrate and validate the computational model consisted of i) collagen density, collagen fibril microstructure, mechanical properties of normal rat skin and Oligomer scaffolds and ii) time-dependent wound contraction measured using the rat skin wound model. Further details of the dataset (black nodes in Figure 4.2) are given next.

Density data φ^m

Density of Oligomer scaffolds was calculated based on the total collagen content used for fabrication and final volume of the scaffolds after compression (*n = 5-10* per group). The collagen density for rat skin was assumed to be on the order of 100mg/cm^3 [23].

Microstructure data p^m

Microstructure analysis of Oligomer dermal scaffolds and normal rat skin was performed via cryo-SEM using an FEI NOVA nanoSEM 200 (FEI, Hillsboro, OR) with an Everhart-Thronley detector [7]. Samples were flash-frozen by submersion into critical point liquid nitrogen, transferred to a CT1000 cold-stage attachment (Oxford Instruments North America, Inc., Concord, MA), and sublimated under vacuum. Samples were subsequently sputter coated with platinum and imaged. Images (3,000x magnification) were analyzed using FIJI/ImageJ and the directionality tool used to create the measured histograms of fibril orientation denoted p^m (n = 8-12 per group). The data was smoothed using a moving average filter with a span range of 5° [24].

Mechanics data σ^m, λ^m

Experimental stress σ^m and deformation λ^m data was obtained by performing uniaxial tensile testing in ambient air on dog-bone shaped specimens with a gauge length, width, and thickness of 4 mm, 2 mm, and 1.2 mm, respectively (n = 4-12 per group). The duration of mechanical testing from set up to completion was less than 10 seconds and sample dehydration was not observed. Uniaxial tests were performed to failure at a strain rate of 38.4% per second using a servo electric material testing system (TestResources, Shakopee, MN) with a 25 N load cell at a sampling rate of 100 Hz. Samples that failed outside the gauge region were excluded from data analysis.

Wound healing outcomes data ξ^m

Various wound healing outcomes ξ^m included wound recellularization, changes in collagen architecture, and wound contraction. Wound areas ($\mathcal{J}$) were traced and measured on the experimental dataset using a MATLAB (The Mathworks, Natick, MA) script and normalized to the original wound areas.

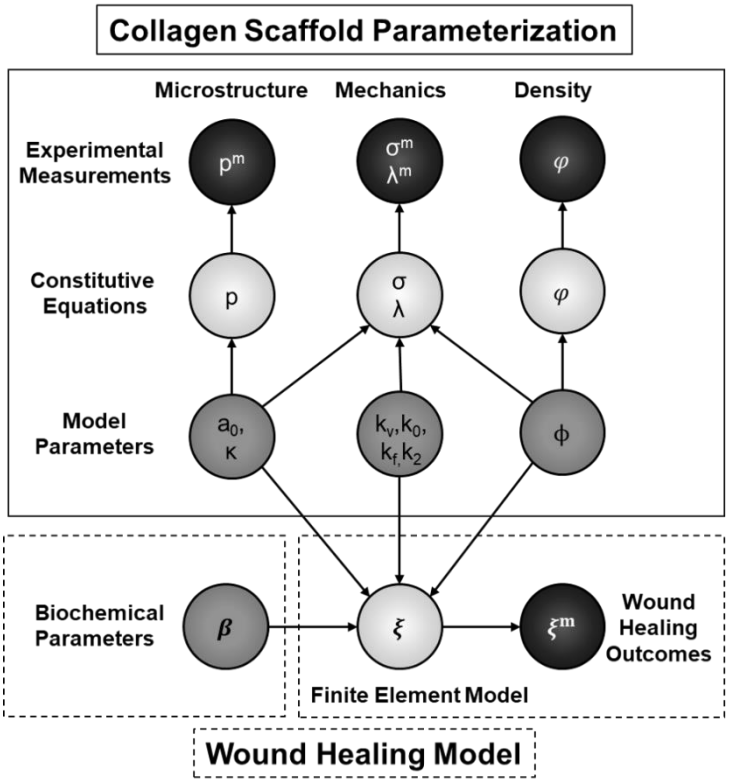

Figure 4.2. Causal model diagram of structural parameter inference for the corresponding constitutive models (top) and wound healing finite element model (bottom). Black, light gray, and dark gray circles represent observed experimental measurements, constitutive equations, and model parameters, respectively.

4.3.4 Bayesian Parameter Calibration

Given the observed data for collagen fiber density φ^m, fiber angle probability distribution p^m, and stress/strain (σ^m, λ^m), the goal of the Bayesian calibration step is to determine the model parameters (dark grey nodes in Figure 4.2) that best explain the data. The model parameters are connected to the data through constitutive equations (light grey nodes in Figure 4.2). Briefly, statistical models of the general form

$$\mathcal{D} = f_i(\theta) + \epsilon \tag{1}$$

were considered, where $\mathcal{D}$ is the data, $f_i(\theta)$ are the constitutive models which depend on parameters θ, and ϵ is the experimental error. The likelihood function is the probability of observing the data given a choice of parameters. The likelihood was assumed Gaussian

$$\mathcal{L}(\mathcal{D}|\theta) = \frac{1}{\sqrt{2\pi Var[\epsilon]}} exp\left(-\frac{1}{2}\sum \frac{f_i(\theta) - \mathcal{D}}{Var[\epsilon]}\right).$$

To fit all data, a multilevel Bayesian Monte Carlo Markov Chain (MCMC) model was developed. The goal of this calibration problem was to learn the value of parameters θ, which were not observed but were needed in the computational model. The schematic of the inference problem is shown in Figure 4.2, showing the connection between data, parameters and models in more detail. In the Bayesian framework, the goal is to obtain posterior probabilities $p(\theta|\mathcal{D})$ of the parameters θ of the model conditioned on the observed data using Bayes' rule.

$$p(\theta|\mathcal{D}) = \frac{p(\mathcal{D}|\theta)p(\theta)}{p(\mathcal{D})} \tag{2}$$

where $p(\mathcal{D}|\theta)$ is the likelihood introduced previously, $p(\theta)$ is the prior probability of the parameters, i.e. our knowledge about the parameter range or values before observing any data, and $p(\mathcal{D})$ is called the evidence

$$p(\mathcal{D}) = \int p(\mathcal{D}|\theta)p(\theta)d\theta \tag{3}$$

However, instead of obtaining the posterior directly, the best strategy is to sample from the posterior without ever achieving an analytical description. To do so, a Markov chain process that samples from this posterior was created[25]. The model was coded in PyStan. Standard normal priors were used for all measured variables, and a weak exponential prior was used for standard deviations. The gradient was calculated automatically to allow the use of
The Hamiltonian Monte Carlo (HMC) No-U Turn (NUTS) sampler was used. Four chains were randomly initialized and run in parallel for 1000 tuned steps and 1000 samples. Specific constitutive equations and parameters are introduced next.

Density parameter ϕ

The normalized collagen density ϕ is related to the collagen density measurements via $\phi = \varphi/\varphi^{RS}$, i.e. normalized density with respect to rat skin. The parameter ϕ is also included in the constitutive model of the mechanical constitutive behavior below.

Microstructure parameters $\boldsymbol{a_0}, \boldsymbol{\kappa}$

The constitutive model used for the microstructure was a circular Von Mises distribution for the fiber orientation. The circular von Mises distribution can be characterized with two parameters, b, and $\boldsymbol{a}_0$, which represent the fiber dispersion and principle direction of the distribution, respectively. Alternatively, the parameter b can be replaced by an equivalent dispersion parameter κ, which is the parameter used in the constitutive model of skin and scaffold mechanics. Additionally, the fiber direction $\boldsymbol{a}_0$ can be described with the angle μ_a such that $\boldsymbol{a}_0 = [cos(\mu_a), sin(\mu_a), 0]$. The equation for the distribution in two dimensions is

$$p(a_0, b) = \exp(b\frac{cos(2-\mu_a)}{I_0(b)}$$

$$\kappa = \frac{1}{\pi}\int_{-\frac{\pi}{2}}^{\frac{\pi}{2}} p(a_0, b)\, sin^2(a_0) da_0 = \frac{1}{2}\left(1 - \frac{I_1(b)}{I_0(b)}\right) \quad (4)$$

where $I(b)$ is a modified Bessel function.

Mechanics parameters $\boldsymbol{k_v}, \boldsymbol{k_0}, \boldsymbol{k_f}, \boldsymbol{k_2}$

The constitutive law for the stress as a function of deformation uses a fiber-based generalized structural tensor approach. We assumed that the collagen scaffold and collagen in the native tissue have similar mechanical properties, as suggested by our previous studies [7]. The fitting procedure follows [15] with a modified strain energy density with parameters k_v, k_0, k_f, k_2,

$$\Psi = \phi\left(\frac{k_v}{2}(J^e - 1)^2 - 2k_0 ln(J^e) + k_0(I_1^e - 3) + \frac{k_f}{2k_2}\exp(k_2(\kappa\, I_1^e + (1-3\kappa)I_4^e - 1)^2)\right), (5)$$

where J^e, I_1^e, I_4^e are deformation-related quantities which can be derived from the stretch λ imposed in the uniaxial tests and the fiber orientation parameters $\boldsymbol{a}_0, \kappa$. The model also depends on collagen density ϕ. Parameters were inferred for dermal scaffolds (Oligomer-4, Oligomer-20, and Oligomer-40) and also for rat skin. Evaluating the mechanical constitutive law for the uniaxial test required the solution of a nonlinear system of equations, the hybrid (modified Powell) root-finding algorithm was used to solve for the stress and off-axis extension values at each strain.

Biochemical parameters $\boldsymbol{\beta}$

The last set of parameters are associated with the finite element model of wound healing. The finite element model incorporates the microstructure, density, and mechanical parameters defined already. It additionally requires a set of biochemical parameters denoted $\boldsymbol{\beta}$. One of the many outputs $\boldsymbol{\xi}$ of the finite element model is the area change $\mathcal{J}$, which can be compared to the measured wound area $\mathcal{J}^m$. The biochemical parameters are specified next as part of the finite element model description.

4.3.5 Finite Volume Growth and Remodeling Theory

The continuum finite element model that we had previously developed was modified for use in this work[20]. We applied a finite growth model with a structural tensor approach. Relevant portions of the model are described in brief below. For a full description of the original model see [18, 20].

Kinematics

The reference geometry of the tissue, $\boldsymbol{B}_0$ is given in material coordinates $\boldsymbol{X} \in \boldsymbol{R}^3$. The geometry, meshing, and boundary conditions are shown in Figure 4.3. The wound was approximated as a full-thickness 15 mm diameter cylinder within a 75 mm diameter cylindrical block of tissue.

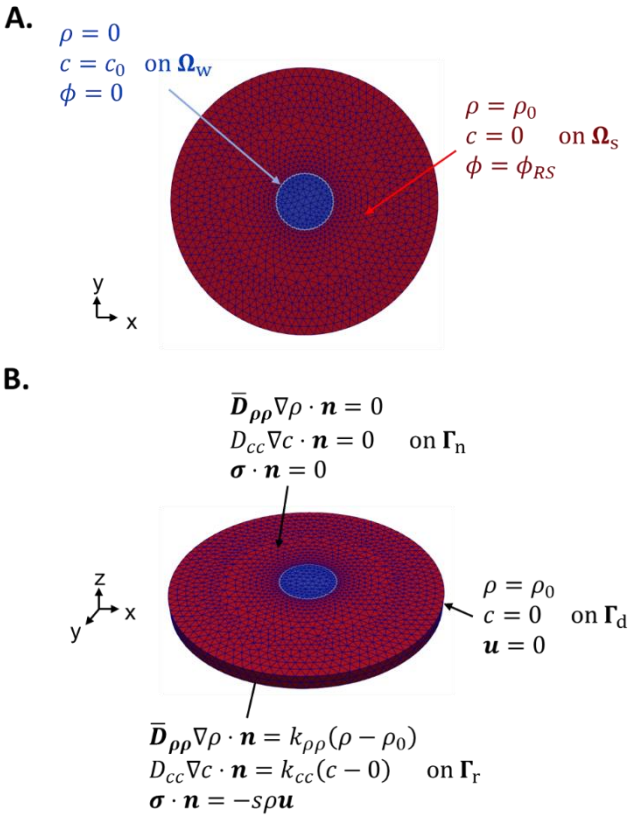

Figure 4.3. Geometry, meshing, and boundary conditions shown in projected (A.) and isometric (B.) views. The mesh consists of greater than 10000 linear tetrahedra or 2000 hexahedra. The wound domain at the center, Ω_w, is characterized by an initial lack of cells, $\rho(\Omega_w, 0) = 0$, and high cytokine concentration, $c(\Omega_w, 0) = c_0$. The surrounding skin, Ω_s, has physiological values. Displacements are constrained on the outer boundary Γ_d. For the biochemical species, the top boundary, Γ_n, has no flux conditions and the bottom boundary, Γ_r, has mixed constraints. For the simulations in this study, we set $k = 0.01\,D$ such that the majority of cells migrate through the tissue edge rather than from the underlying fascia, and set $s = 0$ so there is no spring force, consistent with the loose skin of rodents [26].

The mapping from reference to current configuration is $\boldsymbol{x} = \chi(\boldsymbol{X})$. The biological, chemical, and material fields are given by $\rho(\boldsymbol{x}, t)$, $c(\boldsymbol{x}, t)$, and $\phi(\boldsymbol{x}, t)$, respectively, which may represent a cell (fibroblast) population, activating cytokine, and collagen matrix. The matrix has an associated collagen density ϕ and orientation $(\kappa, \boldsymbol{a}_0)$. The deformation gradient $\boldsymbol{F} = \nabla\chi = \partial\chi/\partial\boldsymbol{X}$ describes the local geometric change. The right Cauchy Green deformation tensor is denoted $\boldsymbol{C} = \boldsymbol{F}^T\boldsymbol{F}$. The multiplicative decomposition $\boldsymbol{F} = \boldsymbol{F}^e \cdot \boldsymbol{F}^p$ is used to model the plastic deformation associated with growth. The superscripts e and p are used to refer to elastic and plastic deformation. Likewise, The elastic part of the Cauchy green deformation tensor is $\boldsymbol{C}^e = \boldsymbol{F}^{eT}\boldsymbol{F}^e$

and its invariants are $I_1^e = tr(\boldsymbol{C}^e), I_4^e = \boldsymbol{a}_0 \cdot \boldsymbol{C}^e \cdot \boldsymbol{a}_0$. The Jacobian can be decomposed as $J = J^e J^p$. We assume the plastic deformation (contraction) applies primarily in the plane of the skin, so we can introduce an orthonormal basis $[\boldsymbol{a}_0, \boldsymbol{s}_0, \boldsymbol{n}_0]$ and construct

$$\boldsymbol{F}^p = \lambda_a^p \boldsymbol{a}_0 \otimes \boldsymbol{a}_0 + \lambda_s^p \boldsymbol{s}_0 \otimes \boldsymbol{s}_0 + \lambda_n^p \boldsymbol{n}_0 \otimes \boldsymbol{n}_0 \tag{6}$$

where for the current simulations $\lambda_n^p \approx 1$.

The microstructure of the collagen is described with a generalized structural tensor approach. The principal fiber direction $\boldsymbol{a}_0$ and dispersion parameter κ are used to define the 3D structural tensor $\boldsymbol{A}_0 = \kappa \boldsymbol{I} + (1 - 3\,\kappa)\boldsymbol{a}_0 \otimes \boldsymbol{a}_0$. Upon deformation, the structural tensor transforms as $\boldsymbol{A} = \boldsymbol{F}\boldsymbol{A}_0\boldsymbol{F}^T = \kappa \boldsymbol{b} + (1 - 3\,\kappa)\,\boldsymbol{a} \otimes \boldsymbol{a}$. After normalization, $\widehat{\boldsymbol{A}} = \boldsymbol{A}/tr(\boldsymbol{A})$. Likewise, the updated principal direction is $\boldsymbol{a} = \boldsymbol{F}\boldsymbol{a}_0$, and $\widehat{\boldsymbol{a}} = \boldsymbol{a}/||\boldsymbol{a}||$. Note that the parameters describing the microstructure of rat skin and wound matrix are the same as those used to model the Oligomer scaffolds.

Balance laws

The growth and movement of the biological and chemical species is described using transport equations. In this work, a single chemical cytokine and a single fibroblastic cell population are considered. The extracellular matrix mechanics are defined using the balance of mass, linear, and angular momentum. The balance of mass is given by $\dot{\phi} + \phi \nabla \cdot \boldsymbol{v} = \boldsymbol{g}$, where ϕ is mass, $\boldsymbol{v}$ is velocity, and $\boldsymbol{g}$ is the mass addition through biological growth. The balance of angular momentum enforces the symmetric stress tensor $\boldsymbol{\sigma} = \boldsymbol{\sigma}^T$. The balance of linear momentum is $\phi \boldsymbol{a} = \nabla \cdot \boldsymbol{\sigma} + \phi \boldsymbol{b}$, but neglecting the inertial term and body force, this reduces to

$$\nabla \cdot \boldsymbol{\sigma} = \boldsymbol{0} \tag{7}$$

The scalar equations for chemical activity are given below in the Eulerian (current) configuration but can be pulled back to the Lagrangian (reference) configuration by $c_0 = Jc, \rho_0 = J\rho$, and the flux pulled back as $\boldsymbol{Q} = J\boldsymbol{F}^{-1}\boldsymbol{q}$. The equations for cell proliferation and motility as well as cytokine transport are

$$\dot{\rho} = -\nabla \cdot \bar{\boldsymbol{D}}_{\rho\rho} \nabla\rho - \nabla \cdot \bar{\boldsymbol{D}}_{\rho c} \rho \nabla c + s_\rho \tag{8}$$

$$\dot{c} = -\nabla \cdot D_{cc} \nabla\, c \;+\; s_c \tag{9}$$

Constitutive equations

Starting with the mass balance for the cell field, special attention is given to the modified diffusion coefficient used here, which takes into account the dependence on matrix density and alignment

$$\bar{\boldsymbol{D}}_{\rho\rho} \;=\; 3\left(\frac{A_0}{tr(A)}\right)^{\varrho}\left(D_0 - \phi(D_0 - D_\infty)\right) \tag{10}$$

In the absence of other information we set $\varrho \;=\; 1$, but this could be modified to increase the dependence of cell migration on fiber alignment. The source terms for the cells and cytokine are defined as

$$s_\rho = \left(p_\rho + \frac{p_{\rho c} c}{K_{\rho,c} + c} + \; p_{\rho,J^e}\widehat{H}\right)\left(1 - \frac{\rho}{K_{\rho\rho}}\right)\rho \;-\; d_\rho \rho \tag{11}$$

$$s_c = \left(p_{c,\rho} c + p_{c,J^e}\widehat{H}\right)\frac{\rho}{K_{c,c} + c} \;-\; d_c c \tag{12}$$

where $\widehat{H}(J^e - \vartheta^e) = 1/(1 + \exp(-\gamma_{J^e}(J^e - \vartheta^e)))$ is a logistic mechanoactivation function. The nonlinear hyperelastic mechanical behavior of the matrix in both the scaffold and surrounding tissue was introduced already in eq. 5. In addition to the strain energy which described the passive mechanical response of the tissue, an active stress by cell contractility is considered. Following Olsen et al., we include a factor for matrix-mediated inhibition of myofibroblast contractility [23].

$$\boldsymbol{\sigma}^{act} = \frac{\rho\phi}{K_\tau^2 + \phi^2}\left(\tau_f + \frac{\tau_{m,c} c}{K_{\tau,c} + c}\right)\widehat{\boldsymbol{A}} \tag{13}$$

This stress, as the other constitutive models up to this point, is presented in the current configuration but can be pulled back to the reference configuration [18, 20]. We based the parameters for τ_f, $\tau_{m,c}$, and K_τ off of [23, 27]. However, since rat wounds undergo severe contraction not typically seen in human wounds, we tuned the τ_f and $\tau_{m,c}$ to increase contraction, while tuning of K_τ was used to control the effect of different collagen densities.

Finally, local extracellular matrix remodeling is described by a system of ordinary differential equations

$$\dot{\phi} = \left(p_\phi + \frac{p_{\phi,c} c}{K_{\phi,c} + c} + p_{\phi,J^e} \widehat{H} \right) \frac{\rho}{K_{\phi,\rho} + \phi} - \left(d_\phi + c\rho d_{\phi,c} \right) \phi \tag{14}$$

$$\dot{\boldsymbol{a}}_0 = \frac{2\pi \dot{\phi}^+}{\tau_\omega} \lambda_0 (\boldsymbol{I} - \boldsymbol{a}_0 \otimes \boldsymbol{a}_0) \boldsymbol{e}_0 \tag{15}$$

$$\dot{\kappa} = \frac{\dot{\phi}^+}{\tau_\kappa} \left(\frac{1}{2} \left(\frac{\lambda_0}{\lambda_1} \right)^{\gamma^\kappa} - \kappa \right) \tag{16}$$

$$\dot{\boldsymbol{\lambda}}^p = \frac{\dot{\phi}^+}{\tau_\lambda} (\boldsymbol{\lambda}^e - 1) \tag{17}$$

where $\dot{\phi}^+$ is the collagen synthesis rate (first term of equation 16), λ_i is an eigenvalue and $\boldsymbol{e}_i$ the associated eigenvector.

Finite element implementation

The model was implemented in a total Lagrangian nonlinear finite element analysis. A full description of this method can be found in [18, 20]. In brief, the spatial variables are discretized using a Galerkin approach, followed by a time discretization by finite differences. The time derivative is approximated with a backward-Euler scheme $\dot{c} = [c - c_n]/\Delta t$ and $\dot{\rho} = [\rho - \rho_n]/\Delta t$. The resulting system of nonlinear algebraic equations is solved using a Newton-Raphson scheme. The Newton-Raphson scheme is accomplished by a consistent linearization as previously described. For the local problem, we used a forward-Euler method. Note that in this case, as the

local solver requires a smaller time step than the global finite element solver, the monolithic procedure requires the chain rule derivatives of the local variables (Θ) with respect to the global variables (Ξ), $\partial\Theta^{n+1}/\partial\Xi = \sum \Delta\, t_{local}\, \partial\Theta^{n}/\partial\Xi$, which are summed up over all local time steps.

4.3.6 Uncertainty Propagation Through the Finite Element Model

For a local sensitivity analysis of the finite element model to input values, we used a derivative-based perturbation scheme [28, 29]. Approximating the solution locally with a linear truncated Taylor series allows the variance of the contraction output $\mathcal{J}$ due to uncertainty in the material inputs θ to be estimated using a sensitivity vector $\partial\mathcal{J}/\,\partial\theta$ and covariance matrix Cov[θ] of the constitutive parameters,

$$Var[\mathcal{J}] = \frac{\partial \mathcal{J}}{\partial \theta}^{T} Cov[\theta] \frac{\partial \mathcal{J}}{\partial \theta} \tag{18}$$

and define a sensitivity index $S = \sqrt{Var[\theta]}\partial\mathcal{J}/\partial\theta$ to measure the sensitivity of the model to each input parameter [29].

4.4 Results

For a comprehensive description of our experimental animal model results, see[9]. The following sections describe the dermal scaffold microstructural and mechanical data analysis and subsequent simulations of the healing response for the dermal scaffold and control groups evaluated using our animal model.

4.4.1 Bayesian Calibration of Structural and Mechanical Parameters

Differences in collagen microstructure and stress-strain behavior of dermal scaffolds and normal rat dermis were readily apparent from both qualitative and quantitative assessments (Figure 4.4). Constitutive models fit the measured data well, with MCMC diagnostics showing an effective sample size (ESS) greater than 500 for all samples and $\hat{R}$ near 1.0. The 2.5%, 50%, and 97.5% posterior density values for all parameters are listed in Table 1. When considering the width of posterior distributions, the orientation parameters μ_a and κ parameters were identified with a high

degree of certainty. More variation came from the mechanical parameters and density measurements. Additional statistical model results and fittings can be found in Appendix B.

Oligomer-4 featured the lowest fibril density (about 13% of rat skin), with an architecture that was roughly isotropic ($\kappa = 0.31$). Oligomer-20 and Oligomer-40 scaffolds exhibited increased densities, roughly 32% and 43% of rat skin, respectively, and collagen dispersion and alignment values that progressively approached those found in rat skin (Table 1). Note that a dispersion of $\kappa = 1/3 \approx 0.33$ represents perfect isotropy, i.e. there is no preferred fiber orientation and all the fibers are randomly oriented, while $\kappa = 0$ represents perfect anisotropy, i.e. all fibers are aligned in the same orientation characterized by the angle μ_a. Rat skin was anisotropic, with fibers preferentially oriented in-plane. We used the mean orientation of rat skin fibers to define $\mu_a = 0$ and along with a measured dispersion of $\kappa = 0.23$.

The tensile stress-strain curves for dermal scaffolds and rat skin (Figure 4.4C) showed the expected nonlinearity, with different low and high strain regime responses. As expected, dermal scaffold stress scaled with increasing density, and both dermal scaffold and rat skin properties were consistent with published values[7, 9].

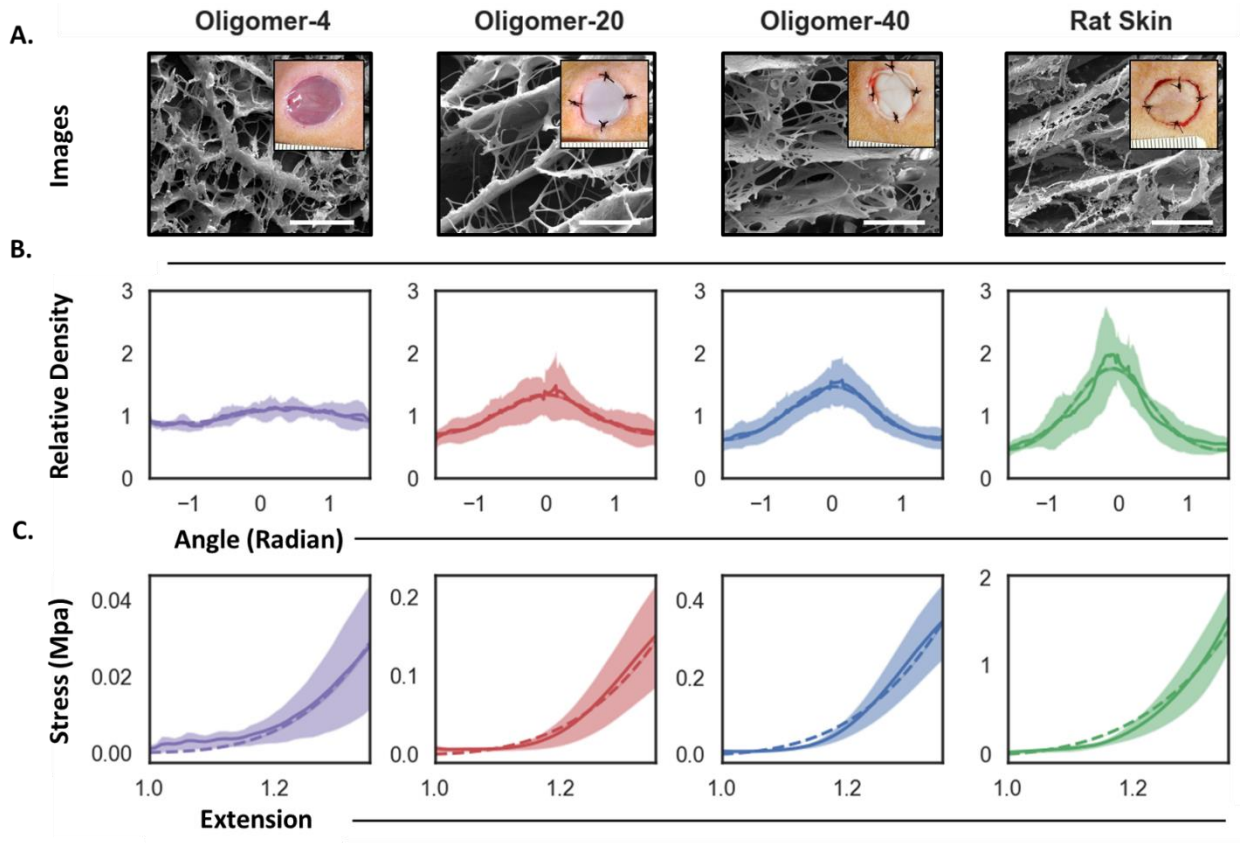

Figure 4.4. Comparison of collagen microstructure and uniaxial stress-strain plots for collagen scaffolds and rat skin. A. Cryo-SEM images of collagen microstructure. Inset shows gross images of scaffolds and rat skin autograft placed within experimental *in vivo* wounds. Scale bar: 5 μm. B.-C. Model calibration results from Bayesian analysis. B. Collagen fiber orientation and dispersion measurements (solid lines) and associated posterior prediction from the calibrated periodic von Mises distribution (dashed lines denote the mean and shaded region indicate confidence interval). C. Stress-strain measurements (solid lines) and Bayesian posterior prediction using the exponential strain energy based on the structural tensor of fiber orientation (dashed lines and shaded region).

Table 2. Posterior values for structural constitutive parameters for collagen scaffolds and Rat Skin groups inferred with the Bayesian framework.

Parameter	**Group**	**Value (2.5%-50%-97.5%)**			**Physical Meaning**
k_v	-	0.51	0.73	1.28	Compressibility
k_0	-	9.8e-5	2.9e-3	0.01	Linear stiffness
k_f	-	4.16	5.41	6.47	Linear fiber stiffness
k_2	-	0.3	1.92	4.0	Nonlinear stiffness
ϕ	Oligomer-4	0.08	0.09	0.11	Collagen density
	Oligomer-20	0.22	0.24	0.26	
	Oligomer-40	0.39	0.42	0.46	
	Rat Skin	1.00	1.00	1.00	
κ	Oligomer-4	0.310	0.312	0.314	Collagen dispersion
	Oligomer-20	0.280	0.281	0.283	
	Oligomer-40	0.262	0.263	0.265	
	Rat Skin	0.224	0.226	0.230	
μ_a	Oligomer-4	0.37	0.42	0.46	Collagen alignment
	Oligomer-20	-0.01	6e-3	0.02	
	Oligomer-40	9.9e-3	0.02	0.03	
	Rat Skin	-0.01	-0.09	-0.07	

4.4.2 3D Simulations of Untreated and Dermal Scaffold Treated Wounds

We first conducted finite element simulations of untreated (no-fill) full-thickness wounds (Figure 4.5, upper). Gross experimental images of untreated wounds are also shown for comparison. For these simulations, cells rapidly entered the wound space and proliferated under the influence of the mechanotransductive and chemical signals. By day 14 in the simulation, the wound and surrounding tissue had a high cell population density of 1900 cells/mm^3, compared to the physiological value of approximately 1000 cells/mm^3. Cytokine concentration decayed rapidly due to degradation by cells and diffusion out of the wound. As cells migrated in, they deposited and realigned collagen. Collagen density in the wound increased from $\phi = 0.01$ at day 0 to roughly 0.4 at day 14. Collagen fibers in regions surrounding the wound became oriented toward the wound gap, and fibers within the wound slowly reoriented to the direction of maximum tension. Significant permanent contraction J^p was visible in the wound and surrounding tissue, which was drawn towards the injury. Note that $J^p = 1$ denotes no change, i.e. the tissue volume stayed the same. At day 0, $J^p = 1$ for the entire geometry. For the no-fill case, values of J^p in the wound reached 0.2 by day 14, indicative of severe permanent contraction of 80% with respect to the initial area. In the cross-section, we saw dimpling of the skin inward to the centerline, with similar behavior observed histologically in contracted rodent wounds (Figure 4.5A)[30].

The model was then used to predict changes in cellularization and collagen remodeling for scaffold-treated wounds, with Oligomer-40 simulation results provided in Figure 4.5B. Gross experimental images from *in vivo* wounds treated with Oligomer-40 are also shown. Model results were in good agreement with experiments that demonstrate collagen density is an important regulator of cellularization, collagen remodeling, and wound contraction. Cells migrated more slowly into scaffold filled wounds, concentrating in an outer ring. Oligomer-40 treatment reduced contraction and reduced fiber re-alignment compared to untreated wound simulations. Again, these results closely matched those observed *in vivo*. For Oligomer-40, the permanent volume change reached values of around $J^p = 0.35$ in the wound periphery but only $J^p = 0.55$ in the wound center by day 14, in contrast to the severe contraction of $J^p = 0.15$ in the center of untreated wounds.

Modulation of the healing process by the various treatments was further evident upon evaluation of time dependent changes in the density of cells, cytokine, and collagen as well as collagen dispersion within the wound center (Figure 4.6). The rate of wound cellularization measured by ρ/ρ_{phys}, decreased as collagen density increased (Figure 4.6A). This was particularly

evident for the rat skin autograft, likely due to the high collagen density as well as decreased contraction in this case. For rat skin autograft, the central region had a normalized cell density still near 0 at day 7, and only reached 0.9 by day 14. For no-fill treated wounds, cell density remained low for 3 days, after which time it increased steadily, reaching two times physiological values by day 14. Such findings are consistent with literature reports for these highly contractile wounds [31, 32]. Similar cellularization trends were observed for scaffold treated wounds, with curves showing a modest rightward shift with increasing collagen content. The cytokine kinetics, c/c_0, were similar for all treatment groups, with a slight divergence observed near the end of the simulation (Figure 4.6B).

When evaluating collagen density over time, $\phi = \varphi/\varphi^{RS}$ (Figure 4.6C), no-fill treated wounds exhibited the most rapid increase, reaching a value of 0.4 by day 14. For scaffold treated wounds, relative collagen density maintained its initial value during the first 4 days of the simulation and then increased for all cases. For scaffold treated wounds, collagen density at 14 days ranged from about 0.4 for Oligomer-4 to 0.6 for Oligomer-40. Interestingly, the rat skin autograft underwent a brief period of resorption reaching density values of roughly 0.8 toward the end of the simulation, something that was not apparent in scaffold-treated wounds. While collagen density profiles for no-fill and scaffold-treated wounds displayed progressive increases over time, changes in dispersion, κ, were notably different for these groups (Figure 4.6D). Scaffolds which begin as dense and aligned (e.g., Oligomer-40) underwent less rapid remodeling during the early stages of wound healing compared to lower density scaffolds or untreated wounds. For Oligomer-40 scaffolds, the initial dispersion was slightly anisotropic ($\kappa \approx 0.26$) and remained relatively constant over the 14 day time period. The rat skin autograft had a similar response. In contrast, the no-fill case, which had a low density and high dispersion (isotropy) at the beginning of the simulation, rapidly surpassed the other scaffolds in becoming aligned due to severe contraction. By 14 days, untreated wounds exhibited a dispersion value of $\kappa \approx 0.17$, indicative of high collagen alignment characteristic of scarring[4, 33, 34].

Both *in vivo* animal experiments and computational simulations indicated that wound contraction was non-linearly related to initial collagen density within the wound (Figure 4.7). In experimental studies, wounds treated with rat skin autograft underwent the least amount of permanent contraction, maintaining 80-90% of the initial wound size. The no fill and Oligomer-4 cases showed similar contraction profiles, yielding wound areas that were roughly 5-20% of the

initial wound area. Both Oligomer-20 and Oligomer-40 scaffolds decreased contraction, with wound areas that were 20-40% of the initial wound area. While Oligomer-20 treated wounds showed a nearly linear decrease in wound area over the 14-day period, Oligomer-40 contraction slowed considerably after 7 days. Computational results aligned with our experimental observations as shown in Figure 4.7, with modest differences noted in contraction curve shape for each treatment group.

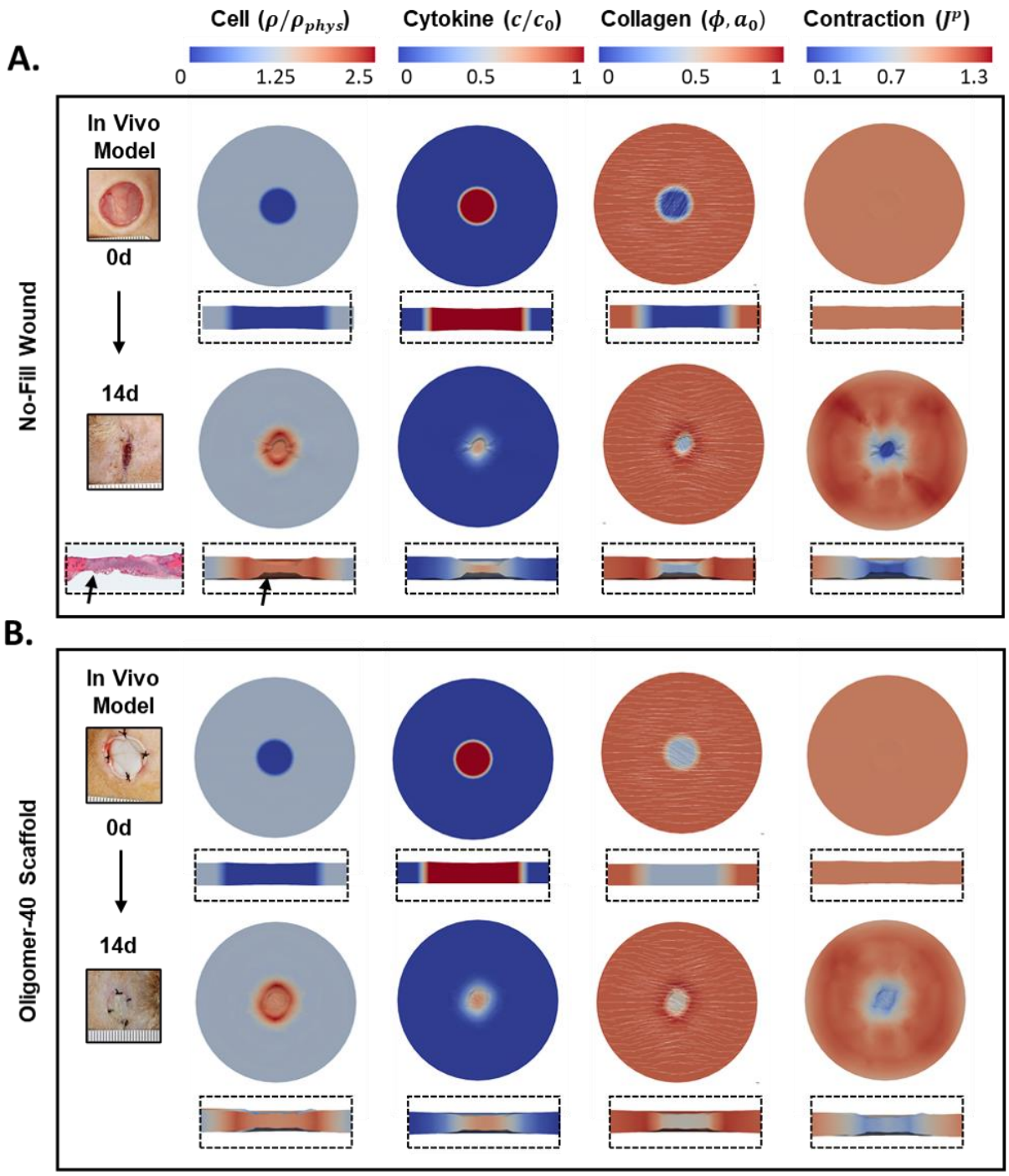

Figure 4.5. Representative simulation of A. no-fill and B. collagen scaffold (Oligomer-40) treated wounds showing cell, cytokine, and collagen density with orientation, and plastic deformation at 0 and 14d time points. Overhead and cross-section perspectives are shown. Representative gross images of experimental *in vivo* wounds are also shown for comparison, illustrating the similar contraction responses obtained with the experimental and computational models.

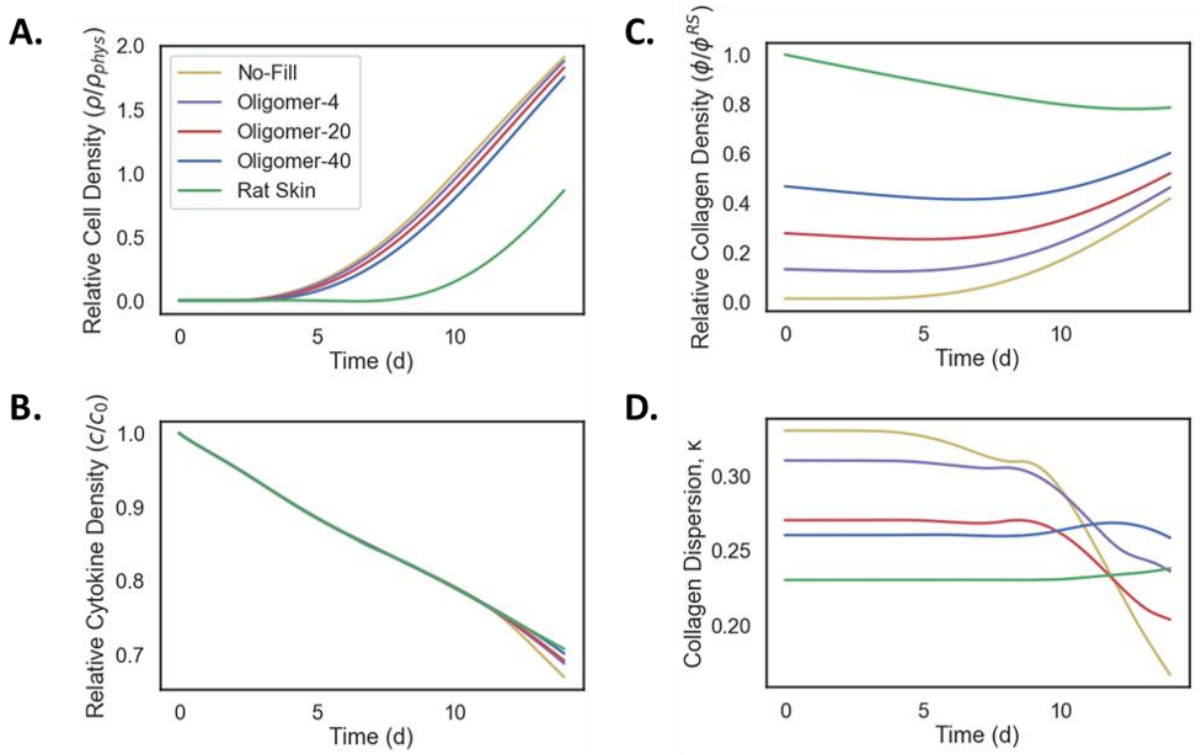

Figure 4.6. Evolution of model outcomes, including A. cell density, B. cytokine concentration, C. collagen density, and D. collagen dispersion, for collagen scaffold and control groups as measured at the wound center. Cell density shows an increase in all groups which is delayed by increasing collagen density. Cytokine density shows a characteristic decay for all groups. Collagen density also varies between samples, with a slight decrease for the skin graft. Collagen dispersion decreases more rapidly in lower density grafts (decreasing κ corresponds to greater alignment).

4.4.3 Uncertainty Analysis

We performed uncertainty propagation and sensitivity analyses using a perturbation method to better define model features that have the greatest influence on wound healing outcomes, in particular permanent contraction $\mathcal{J}$.

The sensitivity indices for each model parameter are shown in Figure 4.8. The model is most sensitive to changes in k_f and ϕ, which represent collagen fiber stiffness and collagen density, respectively. These results indicate that collagen fiber density and stiffness of scaffolds are important design criteria for controlling wound healing outcomes $\mathcal{J}$. In contrast, features such as initial fiber dispersion κ or nonlinearity of the stress-strain response had less impact on wound contraction magnitude but may contribute to other mechanobiological functions and healing outcomes.

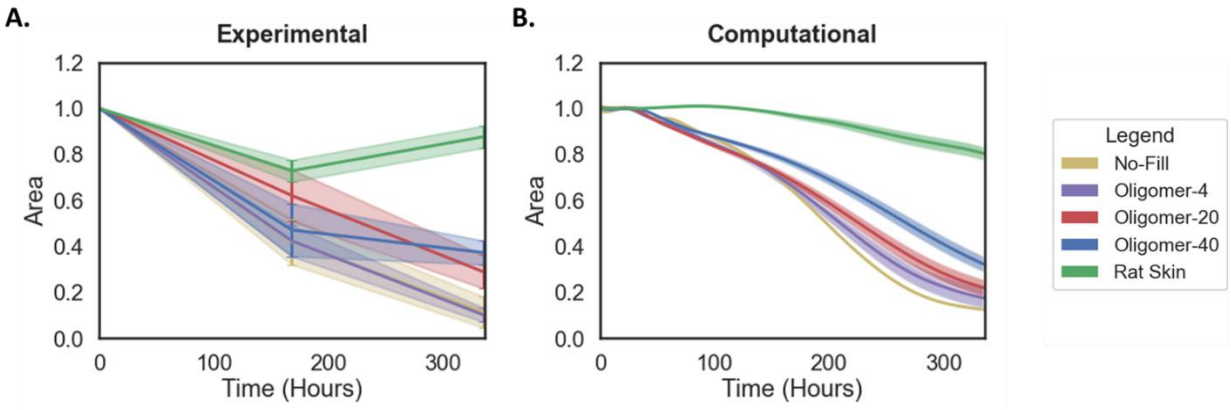

Figure 4.7. Time-dependent changes in wound area for no-fill, collagen scaffold, and rat skin groups as determined in experimental *in vivo* model (A.) and computational model (B.). Note, the no-fill group has no associated uncertainty since mechanical parameters cannot be measured and assigned. Both models indicate that wound contraction is nonlinearly related to initial collagen density within the wound.

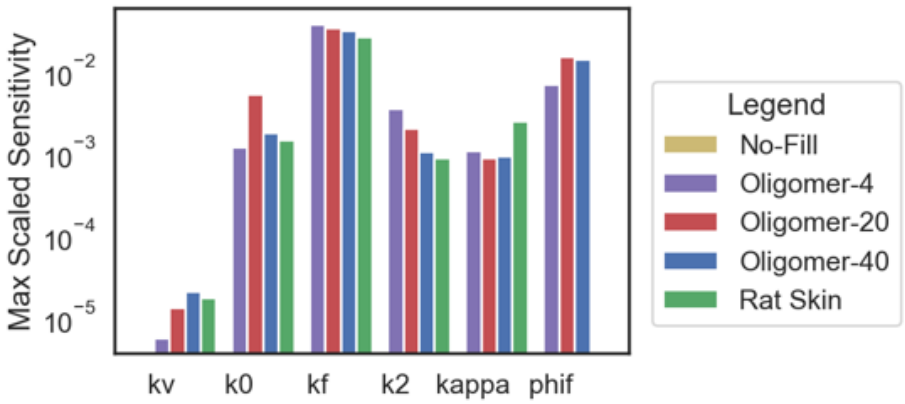

Figure 4.8. Sensitivity analysis of the computational model to parameter perturbations. The structural parameters with greatest influence, k_f and ϕ, describe collagen stiffness and collagen density, respectively.

4.4.4 Predictive Simulations for Dermal Scaffolds of Varied Fiber Alignment

To further demonstrate the utility of our model for informing dermal scaffold design iterations, we investigated a scenario that was not part of the initial experimental dataset. An interesting outcome from initial scaffold simulations was the time-dependent changes in collagen dispersion exhibited by the various groups. While Oligomer-40 showed little change in fiber dispersion, the Oligomer-4 scaffold went from fairly isotropic $\kappa = 0.31$ to aligned $\kappa = 0.17$ over the 14-day period. Because alignment is both a mechanical regulator of cell behavior as well as an

indicator of scarring, we decided to quantify the effect of independently controlling the initial scaffold alignment and density on simulated wound healing. Oligomer-40 scaffolds with either aligned ($\kappa = 0.2$) or dispersed ($\kappa = 0.3$) fibers and either fibers that were parallel to the surrounding tissue ($\mu_a = 0$) or oblique ($\mu_a = \pi/2$) were tested and cellularization (Figure 4.9A) and contraction (Figure 4.9B) results compared. While wound contraction was obviously impacted by collagen alignment, no changes in cellularization were observed. Scaffolds with more isotropic fiber microstructures ($\kappa = 0.3$) contracted less rapidly and showed more uniform contraction when compared to those with low fiber dispersion ($\kappa = 0.2$). Interestingly, fiber orientation within the scaffold affected the shape of the wound at the 14 day time point. For example, for the case where fiber direction within the scaffold and the surrounding tissue was the same, $\mu_a = 0$, the wound contracted more in the horizontal direction and the wound area became a vertically aligned ellipse. In addition, the plastic deformation field was relatively symmetric with respect to both the vertical and horizontal axes. However, when there was a mismatch between the angle of fibers in the scaffold and the surrounding skin ($\mu_a = \pi/2$), there was asymmetric wound contraction.

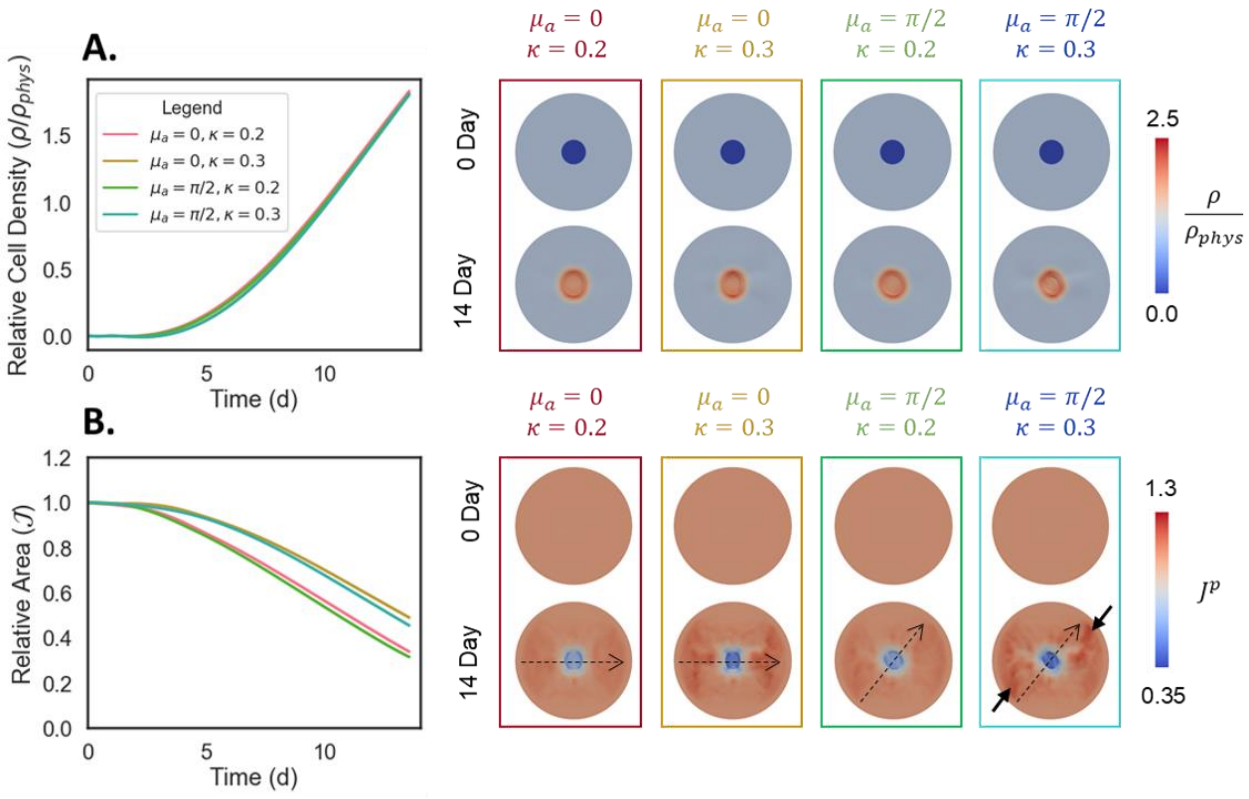

Figure 4.9. Effect of dermal scaffold (Oligomer-40) fiber orientation relative to normal surrounding skin (μ_a) and fiber dispersion (κ) on A. cellularization and B. contraction of wounds. Scaffolds with relatively isotropic fiber distributions ($\kappa = 0.3$) yield slower and more uniform circular contraction, while aligned scaffolds ($\kappa = 0.2$) contract faster. Scaffold fiber orientation dictates the angle of contraction during wound healing. When scaffold fibers are oriented parallel to the surrounding skin ($\mu_a = 0$) vertically-oriented scars result, while angled scaffolds ($\mu_a = \pi/2$) produce asymmetric contraction fields. Dashed arrows show direction of fibers in the graft. Solid arrows emphasize the asymmetric deformation field.

4.5 Discussion

Wound healing is a significant cause of morbidity and mortality worldwide. To address this grand challenge, biomaterials capable of guiding functional skin restoration *in lieu* of pathological scarring are the subject matter of continued research and development [35, 36]. Unfortunately, fundamental gaps in our understanding of wound mechanobiology and lack of predictive tools pose roadblocks to the efficient engineering design of tissue restorative solutions. Without accurate computational models of wound healing biomechanics and mechanochemical signaling, researchers must rely on conventional trial-and-error approaches, which are tremendously burdensome and inefficient in terms of animal number requirements, resources, and overall time

and cost. In this work, we developed a new mechanobiological computational model of wound healing that comprehensively describes the large 3D deformation, permanent contraction, and collagen fiber alignment observed in pathological healing. The same modeling framework is also able to capture the outcomes of wounds treated with engineered collagen dermal scaffolds. The core of our computational model is the coupling of a physical description of extracellular matrix/collagen scaffold microstructure and nonlinear mechanics with a cell and cytokine mechanobiological signaling model.

4.5.1 A Comprehensive Framework for 3D Coupling of Skin Mechanics and Mechanobiology

Accurate modeling of permanent contraction and collagen re-alignment is essential in the context of wound healing and biomaterial scaffold design for tissue restoration. Rodent skin wounds that are left untreated show significant deformation over time, leading to scar tissue characterized by a closely packed and aligned collagen network[34]. Treatment with Oligomer scaffolds, on the other hand, leads to improved outcomes, in large part, by restoring dermal structural and mechanical continuity, while, at the same time, providing the necessary fibrillar microstructure to support cellularization and resist cellular contractile forces [9]. Permanent changes in tissue volume and properties over time can be described within continuum mechanics. The finite volume growth framework explains permanent changes in tissue volume and mass [37], while use of structural tensors can capture fiber reorientation [38]. These tools have been used previously to successfully describe cardiac muscle adaptation to changes in load [39], skin growth in tissue expansion [21], and brain folding [40], to name a few examples.

The work presented here adopts a similar framework. We used a multiplicative decomposition of the deformation gradient to describe the contraction observed in untreated and dermal scaffold treated rat skin wounds. Tissue microstructure was modeled with a structural tensor that evolved over time based on changes in fiber alignment and dispersion as seen experimentally. In contrast, most existing computational models of wound healing use purely elastic models. For such models, wound contraction remains only as long as the cell population stays constant, which has limited pathophysiologic relevance. To date, permanent contraction and collagen remodeling have only been explored in a select few wound models, such as our own previous work [20], a morphoelastic model for burn healing [41], and a morphoelastic model for

dermal wound closure[42], though the latter did not include biochemical coupling. Other wound healing models that address collagen remodeling rely on restrictive simplifying assumptions. For example, the Maxwell fluid model was used to model wounds in the seminal work by Olsen et al. [23], with similar approaches reported by others [43-45]. Collectively, such models have led to an advanced understanding of cell mechanobiology. In fact, several components of our coupled model are based on insights gained from such efforts. Alternative approaches have focused on collagen geometry while ignoring permanent tissue deformations, as is observed in models prioritizing individual cell behavior [33]. However, by modeling the nonlinear mechanics of soft tissue, including growth and remodeling, we filled an existing need for the design of biomaterial scaffolds that aim to reduce pathological contraction and fiber alignment. The multiplicative split of the deformation gradient is not the only theory that can describe growth and remodeling. The constrained mixture model by Humphrey and Rajagopal [46] is another framework that has been successfully applied to explain mechanobiological phenomena of arterial remodeling [47].

A major outcome of wound healing is tissue contraction and remodeling, the underlying mechanism of which is the mechanobiological response of cells, primarily myofibroblasts, acting on nearby matrix components [48]. This is why many wound healing models have focused on this cellular process [49, 50]. Knowledge from this earlier work on cell mechanobiology was incorporated into our nonlinear mechanics framework, with key innovations in our coupling scheme including: i) active stress by cells, ii) collagen deposition and remodeling linked directly to changes in mechanical properties, and iii) feedback from collagen density and structure on cell migration and active stress. In addition to modeling wound healing [17, 23], the use of active stress terms to represent cell contractility has been applied in previous work to describe tissue remodeling following heart valve replacement [51] and fibrin gel remodeling [52]. In our model, the cell population and cytokine densities were coupled to the active stress through eq. 13. Collagen mass fraction change due to cell deposition is a central part of existing wound healing models, e.g. [33]; however, in the present work, the collagen density was also a key determinant of the overall mechanical behavior through eq. 5. Mechanobiology models of cell migration and contractility based on collagen density were proposed in [23, 53], and used here in eqs. 10 and 13. Additionally, strain was coupled to contractility, collagen deposition, and cytokine production in eqs. 11, 12, 13, 14. This type of stretch-driven cell behavior is based on previous work on fibroblast mechanobiology modeling [54, 55]. Overall, our computational model integrates a large body of

evidence and progress in mechanobiology modeling, coupled with a nonlinear mechanics framework that describes growth and remodeling. As a result, the proposed model represents a unified approach to understand the coupled phenomena characteristic of wound healing.

4.5.2 Comprehensive Dataset and Bayesian Calibration

In addition to the comprehensive modeling framework, a key contribution of our work is the integration of *in vitro* and *in vivo* data from Oligomer scaffold characterization and preclinical animal testing. Due to the inherent complexity of wound healing mechanobiology, computational models of this process entail coupled equations with many parameters, which poses significant challenges for model calibration and validation. We addressed this challenge by generating a dataset of wound healing that reflected the structure and parameters of the modeling framework. The experimental data consisted of uniaxial extension data and ultrastructure images of normal rat dermis and engineered dermal scaffolds, as well as contraction and recellularization measurements in full-thickness rodent wounds. These data informed the corresponding structural and mechanobiological parameters used in the computational model as outlined in Figure 4.2. Another recent example of how biomechanical models can guide device design is the work in A combined in vitro imaging and multi-scale modeling system for studying the role of cell matrix interactions in cutaneous wound healing [51], where a computational model of tissue growth and remodeling was combined with *in vitro* mechanical and *in vivo* performance data from living tissue-engineered heart valve replacements. The tight integration between simulations and experiments showcased here also speaks to the ongoing regulatory push to use computer models as a standard part of medical device design and evaluation [56].

Default calibration of computer models in biomechanics involves minimization of error between model and experiment outcomes [15], which fails to recognize the importance of uncertainty in the mechanical and biological responses of tissues. Such approaches also often rely on sequential or independent calibration of variables. We addressed this gap by using a Bayesian framework. This approach has been used for calibration of other constitutive equations for fibrous materials [57]. Through Bayesian calibration, rat skin and dermal scaffold microstructural parameters were identified with high certainty. Slightly more variance was observed with stiffness parameters for these materials. This may be due to variability in the samples tested, which is natural for biological samples [58]. This variation may also reflect non-linearity effects, where even small

variations in material composition and microstructure can be amplified when looking at exponential stress-strain data [59]. Using a perturbation analysis, collagen fiber stiffness and collagen density were then identified as important factors for wound healing outcomes. Together, these results highlight the value of Bayesian inference for fitting constitutive models with shared parameters and variables. Additionally, they imply that next iterations of dermal scaffold design should focus on controlling tightly and independently the collagen density, stiffness, and microstructure to achieve desired wound healing outcomes.

4.5.3 Engineered Dermal Scaffolds Effectively Regulate Collagen Remodeling

Modulation of wound healing outcomes by engineered dermal scaffolds and autograft skin resulted from the complex interplay of biochemical and biomechanical signaling included in our model. We found that increasing scaffold collagen density reduced wound contraction, but also modestly slowed cellularization. These model outputs were consistent with our animal study findings. For the no-fill case, the model captured the rapid influx and proliferation of cells over the first few weeks, similar to other work in the field [27, 50, 60] and experimental studies [32]. As cells migrated and proliferated, the untreated wounds healed through a combination of cell-induced remodeling and extreme permanent contraction of surrounding skin, as expected of rodent wounds [26]. On the other hand, the autograft skin simulation showed the least contraction, not only due to the high stiffness of the autograft, but also because of its inhibition of cell migration and proliferation. Previous work describing cellularization of allograft dermis also supports these results[61]. Special attention has been given to the potential negative effects of the native dense dermal architecture on vascularization, which is necessary to maintain viability of resident graft tissue cells. It is expected that an endothelial cell density field would parallel the cellularization results from our simulations. In fact, our own animal experiments showed reduced vascularization in rat skin autografts compared to Oligomer treatment [9] and, in some cases, autograft failure owing to insufficient vascularization. Explicit modeling of endothelial cell density has been explored in other models [45], and could be incorporated in our framework in future iterations. The Oligomer treated wounds exhibited a response in between the no-fill and the autograft skin simulations. Increasing the density of the scaffold reduced contraction from approximately 85% to 60% compared to no-fill, while cellular ingrowth was only reduced slightly. Thus, we anticipate

that engineered dermal scaffolds can be tailored to regulate this trade-off, minimizing wound contraction while modulating the number and phenotype of infiltrating cell populations.

In addition to the contraction and cellularization of wounds, the remodeling of collagen fiber dispersion was also of interest. No-fill controls began as isotropic, but due to their low collagen density and stiffness, the collagen quickly aligned as the wound contracted, consistent with scar formation in rat wounds [34]. In the other extreme, the rat skin autograft began with a greater degree of alignment and underwent significantly less reorganization owing to its high density and stiffness. Simulated dermal scaffold treatment of wounds also produced insightful results. Here, the degree of alignment by 14 days was found to be nonlinearly related to scaffold parameters. For the Oligomer-4 and Oligomer-20 cases, the scaffolds underwent significant reorganization, while the Oligomer-40 scaffold retained its initial alignment. The model includes many complex mechanobiological couplings that guide this finding. The reorganization of fibers is dependent on the collagen turnover rate, initial orientation, as well as tissue elastic deformations as captured in eq. 15. Control of cell phenotype plays a role, which is effectively captured in the matrix-mediated inhibition of myofibroblast contractility in eq. 13. This finding parallels our *in vivo* experimental observations of decreased α-SMA staining in Oligomer-40 treated wounds [9].

Equipped with our computational model, a natural next step was to test new designs to develop predictions regarding optimal dermal scaffold design. To better understand the effect of initial collagen dispersion and alignment on the 14-day outcome, we ran additional simulations in which these two parameters were controlled independently. We found that increasing the dispersion of the fibers results in a lesser degree of contraction with minimal impact on cellular infiltration. Isotropic scaffolds may then be more permissive of scaffold integration while reducing permanent contraction. The initial alignment vector of collagen fibers impacted the final orientation of the wound area but not the degree of contraction.

4.5.4 Limitations and Future Work

The primary focus of this study was on permanent contraction and collagen fiber alignment outcomes of wound healing, with experimental data gathered to calibrate and inform the model focused on these mechanobiological outcomes. Future work will focus on extending the model, bringing increased definition to other relevant biochemical and cellular parameters, namely vascularization, nutrient supply, and inflammation-correlated cytokine levels. While the general

wound healing process is similar for humans and rodents, we appreciate that important differences exists. Specifically, rodent wounds heal primarily by contraction while those in humans heal primarily via granulation tissue formation [4, 26]. As such, we will explore opportunities to recalibrate the current model to match wound healing outcomes observed within other relevant preclinical wound healing models (e.g., porcine) as well as those seen clinically in humans. The model can also be modified to simulate perturbations of the normal wound healing process, extending our framework to the context of chronic wounds. Finally, this model is currently being adapted to address other wound types, including application of *in situ* scaffold-forming Oligomer formulations for surgical breast tissue voids following breast conserving surgery (lumpectomy) [11].

4.6 Conclusion

This work presents a new 3D computational model of skin wound healing to assist in the design of engineered dermal scaffolds for improved tissue restoration outcomes. Through the integration of experiments and simulations, we found that collagen density and fiber architecture of scaffolds can be used to regulate the permanent contraction and fiber alignment of simulated rodent wounds. This work is a significant improvement over state-of-the-art models by introducing a coupled theory that combines a comprehensive mechanobiological model with a 3D finite element framework of nonlinear mechanics, including growth and remodeling. The model explains contraction and fiber alignment of rodent wounds for no-fill, Oligomer scaffold, and autograft treatment cases. Equipped with this computational tool, we were then able to propose the next iteration of dermal scaffold designs. These scaffolds, in turn, will be further evaluated in follow up preclinical studies. This work represents an important initial step towards the integrated use of *in vivo* and *in silico* models to guide novel therapeutic solutions directed at patient-centric wound care.

4.7 Disclosures

This project was supported by the Indiana Clinical Translational Sciences Institute TL1 Fellowship (NIH UL1TR002529), Interdisciplinary Bioengineering Training in Diabetes Research Program (T32 DK101001), Indiana Medical Scientist/Engineering Training Program (MSTP;

NIGMS T32 GM077229), and the National Science Foundation (NSF CMMI 1911346). Dr. Voytik-Harbin has significant financial interest in GeniPhys, LLC, a small business that she founded to assist with the commercialization of tissue engineering and regenerative medicine technologies such as those described here. Collagen Oligomer and associated custom fabricated materials are the subject matter of issued and pending patents that are owned by Purdue Research Foundation and licensed to GeniPhys, LLC.

4.8 Appendix A: Supplementary Information

Parameter values for the finite element model (Tables 3 and 4). Additional information regarding the Monte Carlo Markov Chain (Figure 4.10), pair plots (Figure 4.11 and 4.12) and effective sample size of the statistical model (Figure 4.13). Simulations of wounds of different size and shape (Figure 4.14). The code for the multilevel data fitting as well as the finite element model will be made available at the repositories:

https://github.com/davidsohutskay/ACTA_2021_MCMC
https://github.com/davidsohutskay/ACTA_2021_FE

Table 3. Parameters for the local extracellular matrix model. Parameters listed as estimated were selected in this work, modified from our previous wound healing model, or selected in the previous model.

Parameter	**Value**	**Observations**	**Physical Meaning**
p_{ϕ}	2×10^{-7} [1/h]	[62]	Physiologic collagen production
$p_{\phi.c}$	2×10^{-7} [1/h]	[60]	Collagen production activated by cytokine
$p_{\phi,J}$	2×10^{-7} [1/h]	[20]	Collagen production activated by stretch
$K_{\phi,c}$	0.0001 [-]	[20]	Saturation of cytokine effect in collagen production rate
$K_{\phi,\rho}$	1.06 [-]	[20]	Saturation of collagen production by collagen fraction
d_{ϕ}	0.00097 [1/h]	[62]	Collagen degradation
$d_{\phi,c}$	0.000485 [1/h]	[62]	Enhanced collagen degradation by collagen fraction
τ_{ω}	4.85 [h]	[20]	Time constant for reorientation
τ_{κ}	0.485 [h]	[20]	Time constant for dispersion
γ_{κ}	2 [-]	[20]	Shape of dispersion rate curve
$\tau_{\lambda_p^a}$	4.85×10^{-7} [h]	Estimated	Time constant for plastic deformation
$\tau_{\lambda_p^s}$	4.85×10^{-7} [h]	Estimated	Time constant for plastic deformation
$\tau_{\lambda_p^n}$	4.85×10^{-7} [h]	Estimated	Time constant for plastic deformation

Table 4. Parameters for the global biochemical and biomechanical model. Parameters listed as estimated were selected in this work, modified from our previous wound healing model, or selected in the previous model.

Parameter	**Value**	**Observations**	**Physical Meaning**
t_ρ	2×10^{-5} [MPa]	[27]	Traction
$t_{\rho,c}$	2×10^{-4} [MPa]	[20]	Myofibroblast traction
K_t	0.4 [-]	Estimated	Traction saturation due to collagen
$K_{t,c}$	0.0001 [-]	[20]	Traction saturation due to cytokine
$D_{\rho\rho}$	0.0833 [mm^2/h]	[50, 63]	Cell diffusion coefficient
$D_{\rho c}$	1.66e-4[mm^5/mol/h]	[20, 60]	Chemotaxis coefficient
D_{cc}	0.01208 [mm^2/h]	[27, 60, 64]	Cytokine diffusion coefficient
p_ρ	0.034 [1/h]	[50]	Cell proliferation
$p_{\rho.c}$	0.034/4 [1/h]	Estimated	Cytokine-increased proliferation
$p_{\rho,\theta}$	0.034/4 [1/h]	Estimated	Mechanoregulation of proliferation
$K_{\rho,c}$	0.0001 [-]	[20]	Cytokine saturation
d_ρ	0.10*prho	[50]	Cell death rate
$K_{\rho,\rho}$	0.0001 [mol/mm^3]	[50]	Cell division saturation
$p_{c,\rho}$	90e-16/10000[1/h]	[20]	Cell secretion of cytokine
$p_{c,\theta}$	3e-18[1/h]	[20]	Mechanoregulation of cytokine
$K_{c,c}$	1 [mol/mm^3]	[20]	Cytokine saturation
d_c	0.001 [1/h]	Estimated	Cytokine degradation
ρ_0	1000 [cells/mm^3]	[32, 65]	Initial cell number
c_0	0.0001 [mol/mm^3]	[20]	Initial cytokine concentration
γ_θ	5 [-]	[20]	Shape of mechanosensing curve
ϑ^e	2 [-]	[20, 21]	Midpoint of mechanosensing curve

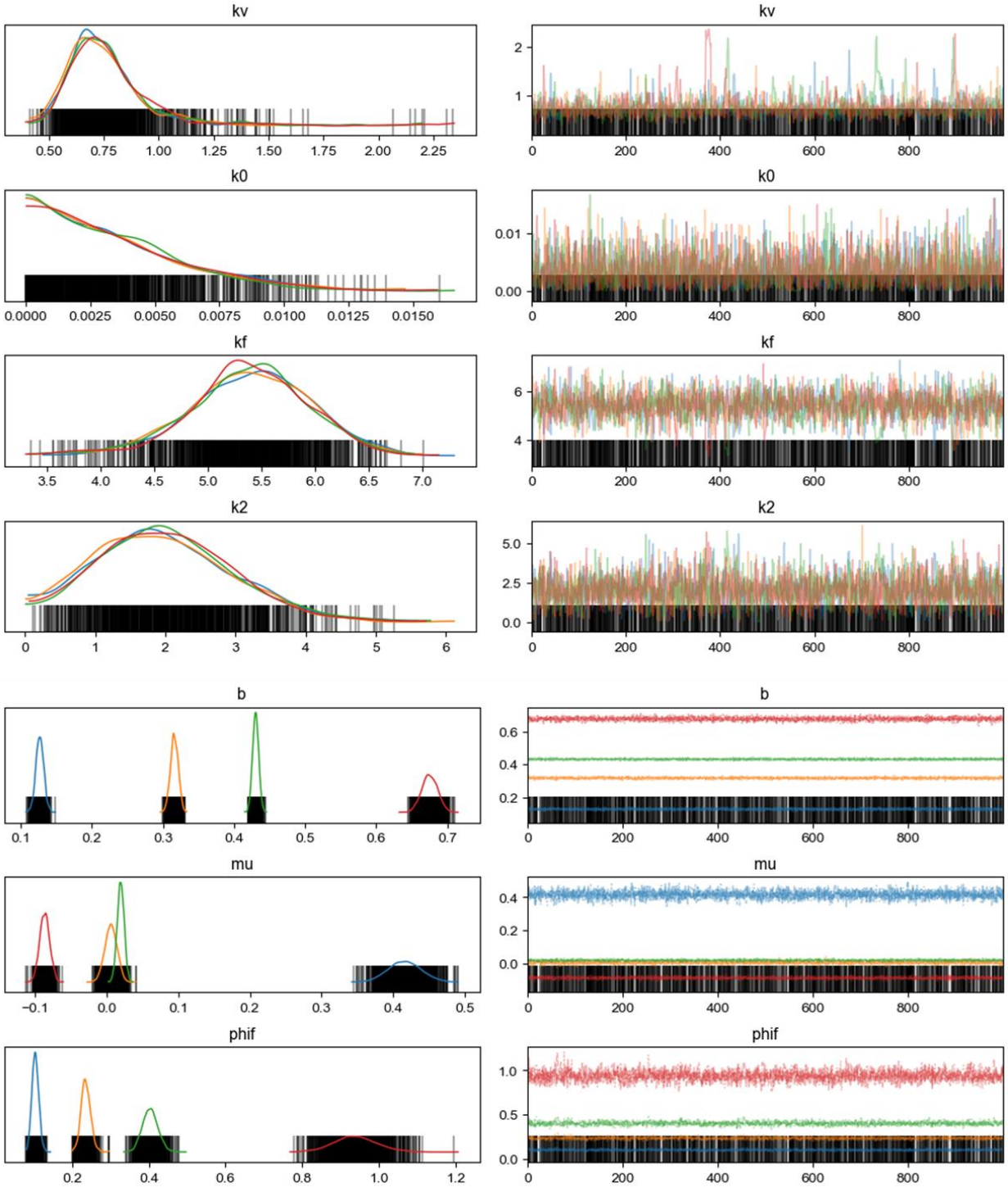

Figure 4.10. Trace plot of the Monte Carlo Markov Chain. Plots are shown for each of the shared (k_v, k_0, k_f, k_2) and unshared (b, μ, φ) parameters.

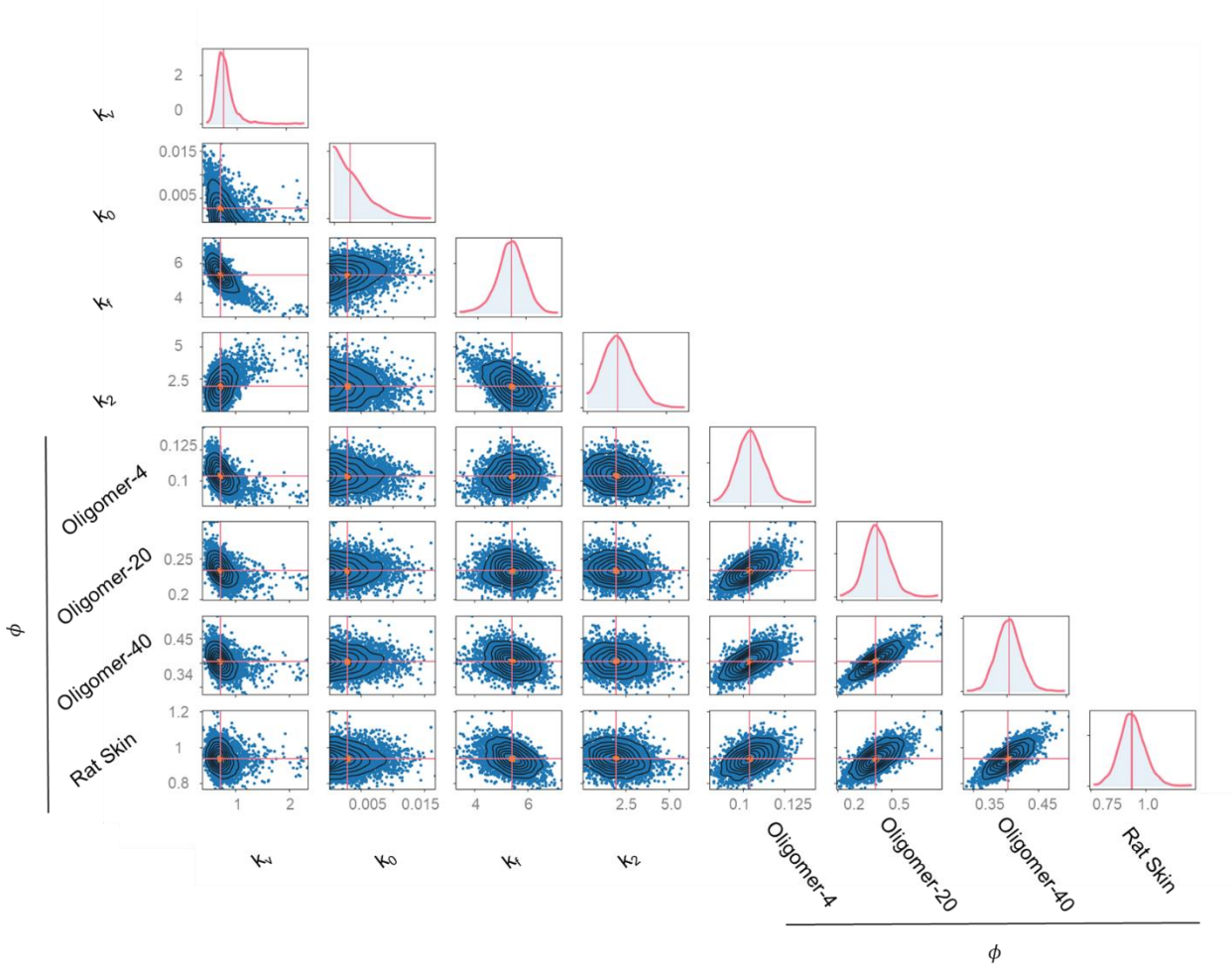

Figure 4.11. Pair plots of the stiffness parameters and collagen density for collagen scaffolds and rat skin. These parameters are directly linked together through the mechanical constitutive law and density measurements, and indirectly linked to the fiber orientation and dispersion. Covariance exists between k_v and other material parameters, as well as between the collagen Oligomer density measurements.

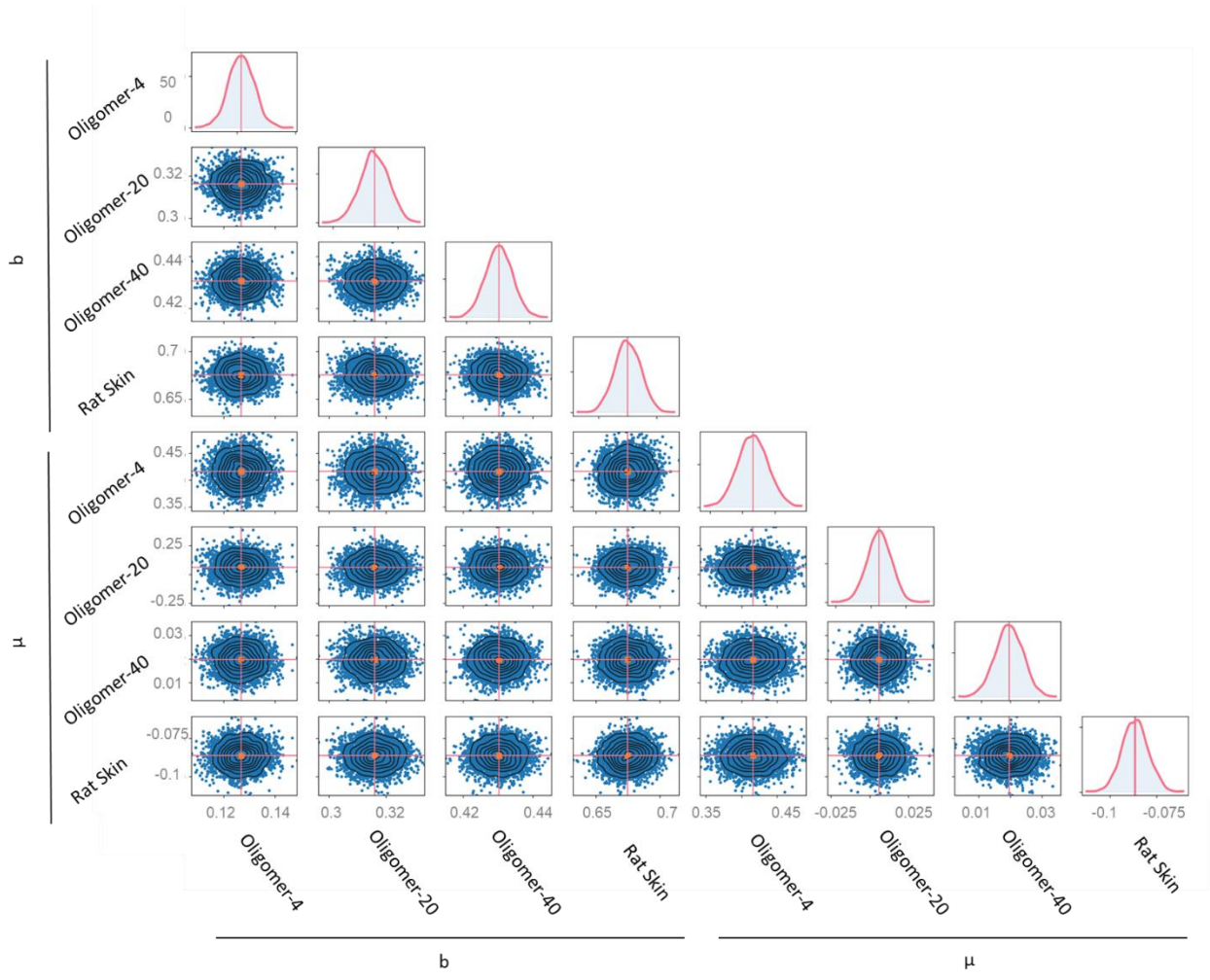

Figure 4.12. Pair plots of the fiber orientation and dispersion for collagen scaffolds and rat skin. These parameters are directly linked in the Von Mises fiber distribution and indirectly to the mechanical behavior. The plots suggest the parameters are largely independent.

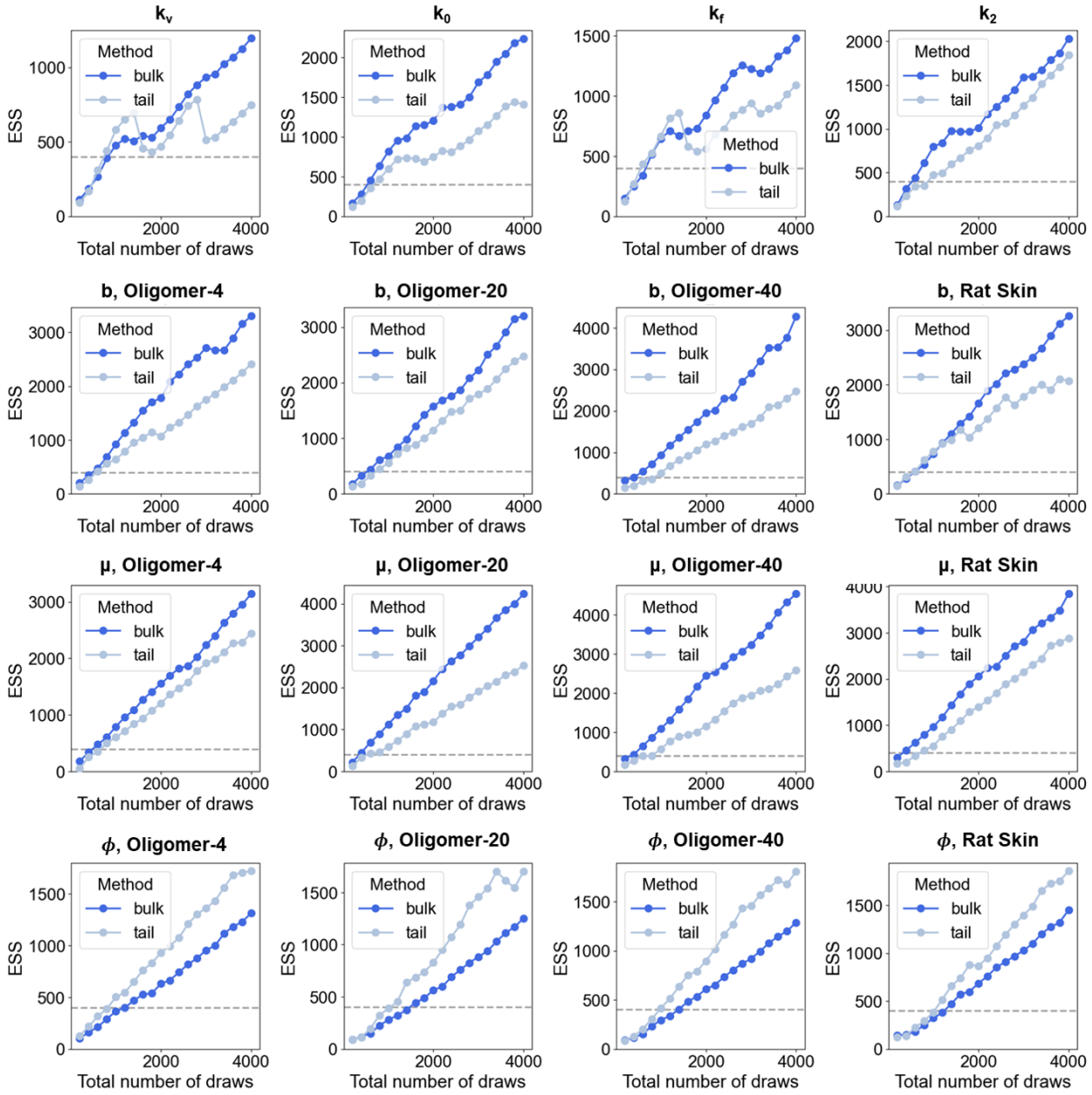

Figure 4.13. Evolution plot of the effective sample size. All parameters reach an ESS greater than 500, suggesting the chains have converged to their posterior value.

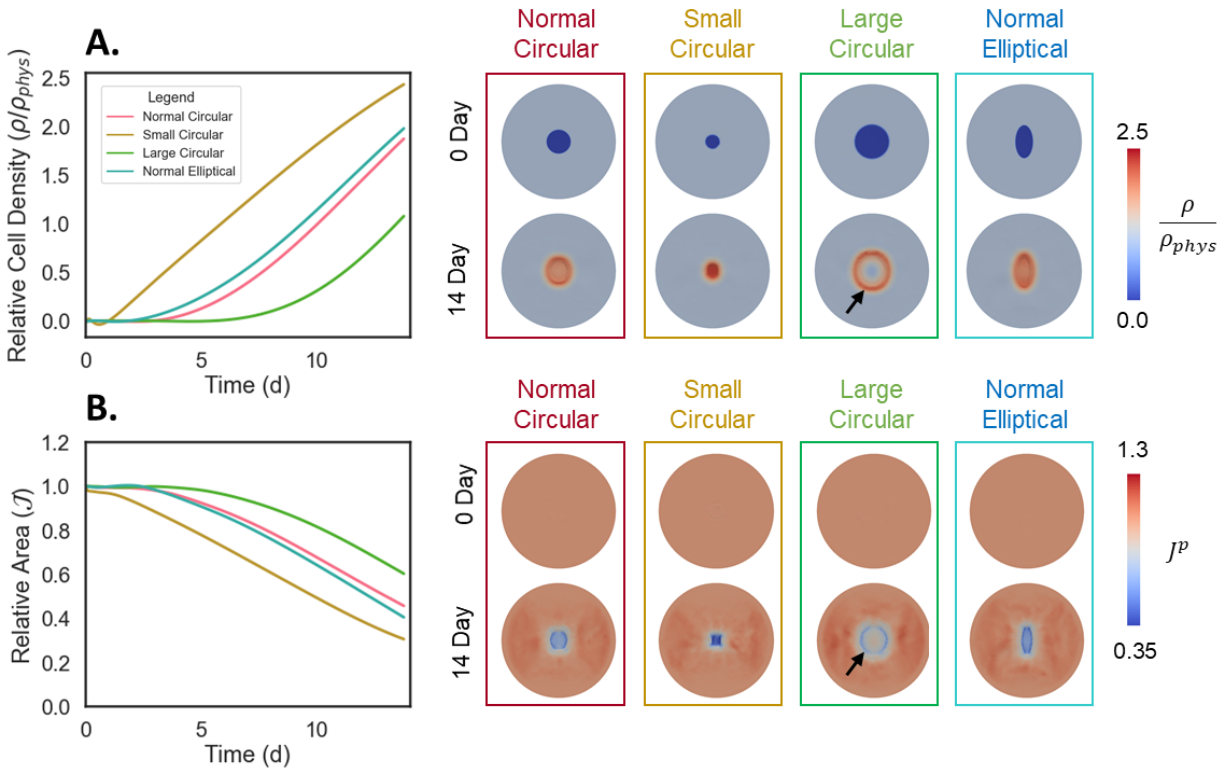

Figure 4.14. Effect of wound size and geometry on A. cellularization and B. contraction of isotropic Oligomer-40 treated wounds. Larger volume wounds undergo slower cellularization and contract moderately slower than smaller wounds. This contraction is more evident at the wound border where the cells have successfully migrated. Elliptical wounds, which have a greater surface area than their circular counterparts but the same volume, also undergo faster recellularization and contraction, but to a lesser degree.

4.9 References

1. Sen CK, Gordillo GM, Roy S, Kirsner R, Lambert L, Hunt TK, Gottrup F, Gurtner GC, Longaker MT. Human skin wounds: a major and snowballing threat to public health and the economy. Wound Repair Regen. 2009;17(6):763-71.
2. Eming SA, Martin P, Tomic-Canic M. Wound repair and regeneration: mechanisms, signaling, and translation. Sci Transl Med. 2014;6(265):265sr6.
3. Keane TJ, Horejs CM, Stevens MM. Scarring vs. functional healing: Matrix-based strategies to regulate tissue repair. Adv Drug Deliv Rev. 2018;129:407-19.
4. Reinke JM, Sorg H. Wound repair and regeneration. Eur Surg Res. 2012;49(1):35-43.
5. Kreger S, Bell B, Bailey J, Stites E, Kuske J, Waisner B, Voytik-Harbin S. Polymerization and matrix physical properties as important design considerations for soluble collagen formulations. Biopolymers. 2010;93(8):690-707.
6. Bailey J, Critser P, Whittington C, Kuske J, Yoder M, Voytik-Harbin S. Collagen oligomers modulate physical and biological properties of three-dimensional self-assembled matrices. Biopolymers. 2011;95(2):77-93.
7. Blum KM, Novak T, Watkins L, Neu CP, Wallace JM, Bart ZR, Voytik-Harbin SL. Acellular and cellular high-density, collagen-fibril constructs with suprafibrillar organization. Biomater Sci. 2016;4(4):711-23.
8. Novak T, Seelbinder B, Twitchell CM, van Donkelaar CC, Voytik-Harbin SL, Neu CP. Mechanisms and Microenvironment Investigation of Cellularized High Density Gradient Collagen Matrices via Densification. Adv Funct Mater. 2016;26(16):2617-28.
9. Sohutskay DO, Buno KP, Tholpady SS, Nier SJ, Voytik-Harbin SL. Design and biofabrication of dermal regeneration scaffolds: role of oligomeric collagen fibril density and architecture. Regen Med. 2020;15(2):1295-312.
10. Brookes S, Zhang L, Puls TJ, Kincaid J, Voytik-Harbin S, Halum S. Laryngeal Reconstruction Using Tissue-Engineered Implants in Pigs: A Pilot Study. Laryngoscope. 2020.
11. Puls TJ, Fisher CS, Cox A, Plantenga JM, McBride EL, Anderson JL, Goergen CJ, Bible M, Moller T, Voytik-Harbin SL. Regenerative tissue filler for breast conserving surgery and other soft tissue restoration and reconstruction needs. Sci Rep. 2021;11(1):2711.

12. Limbert G. Mathematical and computational modelling of skin biophysics: a review. Proc Math Phys Eng Sci. 2017;473(2203):20170257.
13. Benítez JM, Montáns FJ. The mechanical behavior of skin: Structures and models for the finite element analysis. Computers & Structures. 2017;190:75-107.
14. Gasser TC, Ogden RW, Holzapfel GA. Hyperelastic modelling of arterial layers with distributed collagen fibre orientations. J R Soc Interface. 2006;3(6):15-35.
15. Annaidh AN, Bruyère K, Destrade M, Gilchrist MD, Maurini C, Otténio M, Saccomandi G. Automated estimation of collagen fibre dispersion in the dermis and its contribution to the anisotropic behaviour of skin. Ann Biomed Eng. 2012;40(8):1666-78.
16. Jorgensen SN, Sanders JR. Mathematical models of wound healing and closure: a comprehensive review. Med Biol Eng Comput. 2016;54(9):1297-316.
17. Javierre E, Moreo P, Doblaré M, García-Aznar J. Numerical modeling of a mechano-chemical theory for wound contraction analysis. Int J Solids Struct. 2009;46(20):3597-606.
18. Buganza Tepole A, Kuhl E. Computational modeling of chemo-bio-mechanical coupling: a systems-biology approach toward wound healing. Comput Methods Biomech Biomed Engin. 2016;19(1):13-30.
19. Lee T, Holland MA, Weickenmeier J, Gosain AK, Tepole AB. The geometry of incompatibility in growing soft tissues: Theory and numerical characterization. J Mech Phys Solids. 2021;146:104177.
20. Tepole AB. Computational systems mechanobiology of wound healing. Comput Methods Biomech Biomed Engin. 2017;314:46-70.
21. Tepole AB, Ploch CJ, Wong J, Gosain AK, Kuhl E. Growing skin: A computational model for skin expansion in reconstructive surgery. J Mech Phys Solids. 2011;59(10):2177-90.
22. Takeuchi H, Ishida M, Furuya A, Todo H, Urano H, Sugibayashi K. Influence of skin thickness on the in vitro permeabilities of drugs through Sprague-Dawley rat or Yucatan micropig skin. Biol Pharm Bull. 2012;35(2):192-202.
23. Olsen L, Sherratt JA, Maini PK. A mechanochemical model for adult dermal wound contraction and the permanence of the contracted tissue displacement profile. J Theor Biol. 1995;177(2):113-28.

24. Schriefl AJ, Reinisch AJ, Sankaran S, Pierce DM, Holzapfel GA. Quantitative assessment of collagen fibre orientations from two-dimensional images of soft biological tissues. J R Soc Interface. 2012;9(76):3081-93.
25. Rappel H, Beex LA, Hale JS, Noels L, Bordas S. A tutorial on bayesian inference to identify material parameters in solid mechanics. Arch Comput Methods Eng. 2020;27(2):361-85.
26. Lorenz HP, Longaker MT. Wounds: biology, pathology, and management. Surgery: Springer; 2008. p. 191-208.
27. Koppenol DC, Vermolen FJ, Niessen FB, van Zuijlen PPM, Vuik K. A mathematical model for the simulation of the formation and the subsequent regression of hypertrophic scar tissue after dermal wounding. Biomech Model Mechanobiol. 2017;16(1):15-32.
28. Schuff MM, Gore JP, Nauman EA. A mixture theory model of fluid and solute transport in the microvasculature of normal and malignant tissues. II: Factor sensitivity analysis, calibration, and validation. J Math Biol. 2013;67(6-7):1307-37.
29. McClarren RG, McClarren, Penrose. Uncertainty Quantification and Predictive Computational Science: Springer; 2018.
30. Evans ND, Oreffo RO, Healy E, Thurner PJ, Man YH. Epithelial mechanobiology, skin wound healing, and the stem cell niche. J Mech Behav Biomed Mater. 2013;28:397-409.
31. Nagaraja S, Wallqvist A, Reifman J, Mitrophanov AY. Computational approach to characterize causative factors and molecular indicators of chronic wound inflammation. J Immunol. 2014;192(4):1824-34.
32. Rognoni E, Pisco AO, Hiratsuka T, Sipila KH, Belmonte JM, Mobasseri SA, Philippeos C, Dilao R, Watt FM. Fibroblast state switching orchestrates dermal maturation and wound healing. Mol Syst Biol. 2018;14(8):e8174.
33. McDougall S, Dallon J, Sherratt J, Maini P. Fibroblast migration and collagen deposition during dermal wound healing: mathematical modelling and clinical implications. Philos Trans A Math Phys Eng Sci. 2006;364(1843):1385-405.
34. Quinn KP, Golberg A, Broelsch GF, Khan S, Villiger M, Bouma B, Austen Jr WG, Sheridan RL, Mihm Jr MC, Yarmush ML. An automated image processing method to quantify collagen fibre organization within cutaneous scar tissue. Exp Dermatol. 2015;24(1):78-80.

35. MacNeil S. Biomaterials for tissue engineering of skin. Materials Today. 2008;11(5):26-35.
36. Sohutskay DO, Puls TJ, Voytik-Harbin SL. Collagen self-assembly: biophysics and biosignaling for advanced tissue generation. Multi-scale Extracellular Matrix Mechanics and Mechanobiology: Springer; 2020. p. 203-45.
37. Eskandari M, Kuhl E. Systems biology and mechanics of growth. Wiley Interdiscip Rev Syst Biol Med. 2015;7(6):401-12.
38. Alastrué V, Martinez M, Doblaré M, Menzel A. Anisotropic micro-sphere-based finite elasticity applied to blood vessel modelling. J Mech Phys Solids. 2009;57(1):178-203.
39. Göktepe S, Abilez OJ, Kuhl E. A generic approach towards finite growth with examples of athlete's heart, cardiac dilation, and cardiac wall thickening. J Mech Phys Solids. 2010;58(10):1661-80.
40. Xu G, Bayly PV, Taber LA. Residual stress in the adult mouse brain. Biomech Model Mechanobiol. 2009;8(4):253-62.
41. Koppenol DC, Vermolen FJ. Biomedical implications from a morphoelastic continuum model for the simulation of contracture formation in skin grafts that cover excised burns. Biomech Model Mechanobiol. 2017;16(4):1187-206.
42. Bowden LG, Byrne HM, Maini PK, Moulton DE. A morphoelastic model for dermal wound closure. Biomech Model Mechanobiol. 2016;15(3):663-81.
43. Flegg JA, Byrne HM, McElwain DL. Mathematical model of hyperbaric oxygen therapy applied to chronic diabetic wounds. Bull Math Biol. 2010;72(7):1867-91.
44. Flegg JA, Menon SN, Maini PK, McElwain D. On the mathematical modeling of wound healing angiogenesis in skin as a reaction-transport process. Front Physiol. 2015;6:262.
45. Xue C, Friedman A, Sen CK. A mathematical model of ischemic cutaneous wounds. Proc Natl Acad Sci U S A. 2009;106(39):16782-7.
46. Humphrey J, Rajagopal K. A constrained mixture model for growth and remodeling of soft tissues. Math Models Methods Appl Sci. 2002;12(03):407-30.
47. Irons L, Humphrey JD. Cell signaling model for arterial mechanobiology. PLoS Comput Biol. 2020;16(8):e1008161.

48. Wong VW, Akaishi S, Longaker MT, Gurtner GC. Pushing back: wound mechanotransduction in repair and regeneration. J Invest Dermatol. 2011;131(11):2186-96.
49. Sherratt JA, Murray JD. Models of epidermal wound healing. Proc Biol Sci. 1990;241(1300):29-36.
50. Valero C, Javierre E, Garcia-Aznar JM, Gomez-Benito MJ. A cell-regulatory mechanism involving feedback between contraction and tissue formation guides wound healing progression. PLoS One. 2014;9(3):e92774.
51. Emmert MY, Schmitt BA, Loerakker S, Sanders B, Spriestersbach H, Fioretta ES, Bruder L, Brakmann K, Motta SE, Lintas V, Dijkman PE, Frese L, Berger F, Baaijens FPT, Hoerstrup SP. Computational modeling guides tissue-engineered heart valve design for long-term in vivo performance in a translational sheep model. Sci Transl Med. 2018;10(440).
52. De Jesus AM, Aghvami M, Sander EA. A Combined In Vitro Imaging and Multi-Scale Modeling System for Studying the Role of Cell Matrix Interactions in Cutaneous Wound Healing. PLoS One. 2016;11(2):e0148254.
53. Barocas VH, Tranquillo RT. An anisotropic biphasic theory of tissue-equivalent mechanics: the interplay among cell traction, fibrillar network deformation, fibril alignment, and cell contact guidance. J Biomech Eng. 1997; 119(2):137-45.
54. Loerakker S, Obbink-Huizer C, Baaijens FP. A physically motivated constitutive model for cell-mediated compaction and collagen remodeling in soft tissues. Biomech Model Mechanobiol. 2014;13(5):985-1001.
55. Moreo P, Garcia-Aznar JM, Doblare M. Modeling mechanosensing and its effect on the migration and proliferation of adherent cells. Acta Biomater. 2008;4(3):613-21.
56. Faris O, Shuren J. An FDA Viewpoint on Unique Considerations for Medical-Device Clinical Trials. N Engl J Med. 2017;376(14):1350-7.
57. Brewick PT, Teferra K. Uncertainty quantification for constitutive model calibration of brain tissue. J Mech Behav Biomed Mater. 2018;85:237-55.

58. Meador WD, Sugerman GP, Story HM, Seifert AW, Bersi MR, Tepole AB, Rausch MK. The regional-dependent biaxial behavior of young and aged mouse skin: A detailed histomechanical characterization, residual strain analysis, and constitutive model. Acta Biomater. 2020;101:403-13.
59. Lee T, Turin SY, Gosain AK, Bilionis I, Buganza Tepole A. Propagation of material behavior uncertainty in a nonlinear finite element model of reconstructive surgery. Biomech Model Mechanobiol. 2018;17(6):1857-73.
60. Cumming BD, McElwain DL, Upton Z. A mathematical model of wound healing and subsequent scarring. J R Soc Interface. 2010;7(42):19-34.
61. Wong AK, Schonmeyer BH, Singh P, Carlson DL, Li S, Mehrara BJ. Histologic analysis of angiogenesis and lymphangiogenesis in acellular human dermis. Plast Reconstr Surg. 2008;121(4):1144-52.
62. Laurent G. Dynamic state of collagen: pathways of collagen degradation in vivo and their possible role in regulation of collagen mass. American Journal of Physiology-Cell Physiology. 1987;252(1):C1-C9.
63. Ghosh K, Pan Z, Guan E, Ge S, Liu Y, Nakamura T, Ren XD, Rafailovich M, Clark RA. Cell adaptation to a physiologically relevant ECM mimic with different viscoelastic properties. Biomaterials. 2007;28(4):671-9.
64. Murphy KE, Hall CL, Maini PK, McCue SW, McElwain DL. A fibrocontractive mechanochemical model of dermal wound closure incorporating realistic growth factor kinetics. Bull Math Biol. 2012;74(5):1143-70.
65. Miller CC, Godeau G, Lebreton-DeCoster C, Desmouliere A, Pellat B, Dubertret L, Coulomb B. Validation of a morphometric method for evaluating fibroblast numbers in normal and pathologic tissues. Exp Dermatol. 2003;12(4):403-11.

5. CONCLUSION

5.1 Summary

Wounds are a large and growing medical problem worldwide. They can lead to significant morbidity, such as hypertrophic scars, severe joint contractures which limit motion, and loss-of-limb. There is a need for therapies which can better regenerate lost tissue. Although dermal replacement scaffolds have emerged as one option, the influence of scaffold features on outcomes such as recellularization and contraction is still incompletely understood. The work presented in this thesis bridge the gap between experimental regenerative medicine and computational modeling to help define this influence. We presented results from both an *in vivo* animal model and *in silico* computational model used to evaluate dermal replacement scaffolds for improving clinical outcomes.

Our animal wound model tested collagen oligomer scaffolds with varied properties created using a plastic compression technique. We found that scaffold density and material properties (elastic modulus, tensile strength) varied according to degree of compression. The compression procedure also created more aligned microstructures as measured with microscopy. We implanted these scaffolds into full-thickness rodent wounds and found that after two weeks the collagen scaffolds facilitated wound recellularization and became well integrated. Denser scaffolds were more effective at resisting contraction and had a lower number of myofibroblasts. However, they had slower recellularization and vascularization overall. This preliminary study highlights some of the important features of collagen dermal replacement scaffolds.

Next, we developed a finite element model of wound healing. We modeled wound healing with reaction-diffusion equations for cell/cytokine interactions, and a hyperelastic constitutive scaffold material. We used a generalized structural tensor approach to encore microstructural information. First, we calibrated our model structural parameters to our experimental data with a Bayesian model. Then we simulated no-fill wounds which undergo extreme contracture and compared to the other representative groups from our animal study. We found that the model was able to capture the behavior well and reinforced our conclusion that collage fibril density is an important regulator of wound contracture and recellularization. Finally, we conducted predictive simulations for future validation.

Overall, our findings support the importance of scaffold biomechanics and mechanobiology in the design of engineered dermal replacements. We plan to conduct additional future work, both *in vivo* and *in silico*, to further elucidate the optimal design of dermal scaffolds.

5.2 Future work

5.2.1 Preclinical and clinical model validation

Our long-term goal is to develop clinically useful dermal replacements for patient care, and provide mathematical tools for optimizing scaffold design. Thus, the validation of simulation results to ensure their accuracy is of critical importance. This process can also be used to improve understanding of constitutive laws and wound pathogenesis. In Chapter 4, we presented a few predictive simulations of the model regarding fiber orientation and wound geometry. We found that initial collagen fibril orientation was important for determining the final scar orientation but did not have a significant influence on degree of contraction. We found that smaller wounds with a higher surface area to volume ratio contracted faster than larger wounds, which we believe is likely due to the more rapid influx of cells along the wound border. Each of these findings can be re-tested using our full-thickness animal model. If divergent results are obtained, the parameters or constitutive laws of the mathematical model can be adjusted to account for this. Finally, we can pursue additional tests or future iterations of the model that may correspond to disease states or clinical scenarios and compare them again with patient or animal data.

5.2.2 Additional clinical applications

The mathematical framework described in Chapter 4 of this thesis is flexible in its utility. Although we have focused here on cutaneous dermal wounds, the process of tissue regeneration will have a similar phenotype in many organ systems. Wounds progress through phases of inflammation, proliferation, granulation and remodeling regardless of cell origin. Inflammatory cytokines, cell migration, and the ever-present extracellular matrix always play a fundamental role. As an initial test of further application, we have begun applying the model to surgical lumpectomy wounds from breast cancer treatment. Breast cancer is a common illness which can lead to patient death, although early treatment by surgery and chemotherapy can lead to complete remission. Traditional mastectomy removes the entire breast and leads to poor cosmetic outcomes in the

absence of reconstruction. One alternative is the lumpectomy, which removes the tumor and surrounding margins leaving the remaining breast intact. This breast-conserving surgery generally leads to favorable cosmesis, but some patients may experience scarring and contracture which changes the shape or consistency of the breast. Accordingly, we have adapted our finite element model to simulate breast wound healing and the development of contracted scars.

5.2.3 Machine learning for design optimization

In addition, we are interested in the use of other computational tools to understand and mathematically optimize the design of scaffolds. Machine learning methods have seen explosive growth in recent years for their ability to incorporate data into dynamic models. Gaussian process regression is one such tool that can allow for inverse problem solving, rapid prototyping, and uncertainty quantification. We are applying Gaussian process regression to help understand both the biochemical and biomechanical aspects of wound healing, such as how myofibroblast mechanobiology may impact the model, as well as in our optimization of scaffold design. In addition to this, many other machine learning tools such as deep neural networks would allow further calibration, data integration, and design optimization.

5.3 Conclusions

This work represents the initial stages of model development that will contribute to the efficient engineering design of collagen dermal replacement scaffolds for improving difficult-to-heal wound outcomes. We have demonstrated the importance of features such as collagen density, microstructure, and mechanics on tissue regeneration, and shown the capability of mathematical modeling for further predictions. Future validation studies building on this thesis work will continue to improve the translational relevance and allow the testing of specific pathophysiologic hypotheses. Ultimately, our long-term goal is to see collagen oligomer and other biomaterials combined with accurate mathematical models be used to create patient- and disease- specific treatments.

VITA

David Sohutskay was born December 23, 1991 in Cleveland, Ohio, and grew up in the suburb of Solon, Ohio. After graduating from Solon High School with Honors in 2010, he attended The Ohio State University and graduated with a dual-degree Bachelor of Science Cum Laude in Biomedical Engineering and Bachelor of Science Cum Laude in Neuroscience in 2014. Work at Ohio State with Drs. Jessica Winter and Carlos Castro and a Summer Undergraduate Research Fellowship at Wake Forest with Dr. Anthony Atala and Hooman Sadri-Ardekani spurred his interest in pursuing a doctoral degree. David entered the Indiana/Purdue Medical Scientist Training Program and began his medical training in Indianapolis. David finished his first two years of medical school with many Honors. He joined the Harbin lab at the Purdue University Weldon School of Biomedical Engineering, where he completed the research described herein. David has a strong interest in the basic mechanics and biological properties of extracellular matrix, tissue engineering and regenerative medicine. Over the course of his doctoral research, he grew a deep interest in the application of computational modeling to biomedical engineering applications. He hopes to apply these tools to solve problems in aging and degenerative disease. David was awarded a T32 fellowship for Bioengineering Training in Diabetes research, a fellowship from the Indiana Clinical Translational Sciences Institute, and a Bottorf Fellowship for Innovation in Clinical Translation. He has also explored entrepreneurship through the Purdue Biomedship Program. After completing his Doctor of Philosophy degree, he will return to the Indiana University School of Medicine to complete his Medical Doctorate, with the long-term goal of holding a career as an academic physician-scientist and bioengineer at the interface of experimental and computational modeling. Using these tools, he hopes to both develop novel therapies for patients as well as provide a better understanding of disease pathogenesis.

PUBLICATIONS

Sohutskay, David O., Theodore J. Puls, and Sherry L. Voytik-Harbin. Collagen self-assembly: biophysics and biosignaling for advanced tissue generation. Multi-scale Extracellular Matrix Mechanics and Mechanobiology. Springer, Cham, 2020. 203-245.

Sohutskay, David O., Kevin P. Buno, Sunil S. Tholpady, Samantha J. Nier, and Sherry L. Voytik-Harbin. Design and biofabrication of dermal regeneration scaffolds: role of oligomeric collagen fibril density and architecture. Regenerative Medicine 15.2 (2020): 1295-1312.

Sohutskay, David O., Adrian Buganza Tepole, and Sherry L. Voytik-Harbin. Mechanobiological Wound Model for Improved Design and Testing of Collagen Dermal Replacement Scaffolds. (Submitted for Review 2021).